Eduardo Manuel Ribeiro Duarte

Licenciado em Ciências de Engenharia Física

Low-Cost Thin Film Perovskite Solar Cells

Dissertação para obtenção do Grau de Mestre em

Engenharia Física

Orientador:	Manuel João de Moura Dias Mendes, Post-Doc Fellow, FCT-UNL
Co-orientadora:	Elvira Maria Correia Fortunato, Full Professor, FCT-UNL

Júri

Presidente:	Professora Doutora Isabel Catarino, FCT, UNL
Arguente:	Doutora Alexandra Barreiros, LNEG
Vogal:	Doutor Manuel Mendes, FCT, UNL

FACULDADE DE CIÊNCIAS E TECNOLOGIA
UNIVERSIDADE NOVA DE LISBOA

July, 2018

Low-Cost Thin Film Perovskite Solar Cells

Este documento foi gerado utilizando o processador (pdf)LaTeX, com base no template "novathesis" [1] desenvolvido no Dep. Informática da FCT-NOVA [2].
[1] https://github.com/joaomlourenco/novathesis [2] http://www.di.fct.unl.pt

Acknowledgements

Gostaria de agradecer em primeiro lugar à Prof. Dra. Elvira Fortunato e ao Prof. Dr. Rodrigo Martins, que continuam a proporcionar a tantos alunos, os recursos para que estes possam perseguir os seus sonhos académicos. Um agradecimento especial aos meus orientadores, Prof. Elvira Fortunato e Prof. Manuel Mendes pela oportunidade de trabalhar e explorar um tema interessante e importante para a nossa sociedade, e pelo apoio prestado ao longo deste trabalho.

Um grande agradecimento vai também para a mestre Carolina Fidalgo por me ter aturado em momentos de desespero e pelos conselhos de um Perovskito para outro. Outro grande agradecimento vai também para o mestre Alexandre Fonseca por me mostrar muito do que apliquei e me aconselhar e aturar muito depois do seu trabalho estar concluído. Quero deixar igualmente o meu agradecimento à Beatriz Esteves pela sua valiosa ajuda na fabricação de muitos dos dispositivos deste trabalho. A special English thank you goes to Deneb, for advising me and helping me in the beginning of my thesis, when I was feeling lost the most.

Quero agradecer à equipa do Cenimat: Alexandra Gonçalves, Sónia Pereira, Rita Branquinho, Joana Pinto, Andreia Araújo, Carolina Marques, Sofia Ferreira, Emanuel Carlos, Olalla Sanchez e Daniela Gomes, por toda a paciência que tiveram comigo e pela sua ajuda e competência em tarefas que em muito contribuíram para o trabalho desta tese.

Quero agradecer a todos a quem me orgulho de chamar amigos, alguns de longa data, outros adquiridos neste precurso académico, mas todos estes deixaram a sua marca e que me ajudaram a chegar onde estou hoje. A todos voçês um muito obrigado do fundo do coração por todos os momentos e que seja até aos 100!

Um agradecimento especial vai também para a Vó Sofia por todo o apoio e paciência na nossa convivência de avó e neto. Um enorme Obrigado terá claro de ir para os meus pais, Cristina Duarte e Francisco Duarte, de que tanto me orgulho e que sei que sempre deram e sempre darão tudo por mim, com apoio incondicional nas melhores e piores alturas.

Um enorme Obrigado a Todos!

Abstract

Perovskite is a class of materials named after their characteristic crystal structure, presenting excellent optoelectronic properties. These properties (particularly, ambipolar charge transport) allow these materials to integrate solar cells with and without the addition of selective layers, like Electron-Transport-Layer and Hole-Transport-Layer, possessing also the ability to be fabricated using simple, non-expensive, solution processing techniques, like Spin-Coating. Coupled with its facile production, the steep rise in SC efficiency over the last years, makes these materials a strong candidate to replace Silicon in the photovoltaic market, both in solid-state and flexible devices.

Despite its many advantages, Perovskite SC still face considerable costs regarding processing conditions and HTL materials. By fabricating these devices under ambient air conditions and using Copper(I) Thiocyanate as the material for the HTL, the fabrication costs are significantly reduced. To further lower fabrication cost, Methylammonium Chloride is studied as a replacement for Methylammonium Iodide in Perovskite precursor solution fabrication. Using this solution, crystalline films were obtained, studying several deposition parameters, and the best reported ones, should provide a starting point for further optimization under similar fabrication conditions.

The main goal for this work was the optimization of SC, using Spin-Coating technique, keeping the devices as low-cost as possible. Improving Perovskite film quality is detrimental to enhance SC performance, which is why efforts were made to minimize film degradation during Perovskite film fabrication and HTL deposition steps.

Due to the hygroscopic nature of the organic component in Perovskite films, the influence of humidity levels was tested, and methods to reduce thin film degradation via humidity exposure were also evaluated.

Overall, device optimization was successful, with Perovskite films reaching >95% bulk density and the champion device presenting PCE of 2.65%, with J_{sc} of 15.11 mA/cm^2 and V_{oc} of 0.701V.

Keywords: Perovskite Photovoltaics; Thin film solar cells; Spin-Coating; MACl; Solar cell contacts; CuSCN HTL; Humidity influence on Perovskite.

Resumo

A Perovskite é uma classe de materiais assim denominada devido à sua estrutura cristalina, possuindo excelentes propriedades optoeletrónicas. Estas propriedades (em especial, transporte ambipolar) permitem que estes materiais sejam aplicados em células solares, com e sem a adição de camadas, como *Hole-Transport-Layer* e *Electron-Transport-Layer*. A possibilidade de serem fabricadas através de técnicas simples e de baixo custo, aliado à rápida subida na eficiência destes dispositivos nos últimos anos, faz da Perovskite uma forte candidata a substituir o Silício, tanto em dispositivos de estado-sólido, como flexíveis.

Apesar das vantagens, estes dispositivos enfrentam elevados custos de produção devido não só ao seu processamento, mas também à escolha de materiais, em particular para a *Hole-Transport-Layer*. A fabricação destas células em condições atmosféricas normais, através de Spi-coating e usando Tiocianato de Cobre como material para a HTL, torna os custos de produção significativamente reduzidos. No entanto, de forma a reduzir ainda mais o custo, foi estudado Cloreto de Metilamónio como substituto para o Iodeto de Metilamónio na fabricação da solução precursora de Perovskite, uma vez que este é significativamente menos dispendioso. Embora não tenha sido possível obter dispositivos altamente eficientes, obtiveram-se filmes cristalinos, usando esta solução.

O principal objetivo deste trabalho consistiu na otimização de células solares, mantendo um reduzido custo de fabricação. Melhorar a qualidade da Perovskite é essencial para aumentar a eficiência, tendo sido por isso feitos esforços para minimizar a degradação da camada ativa, durante a fabricação do filme de Perovskite e deposição da HTL.

Devido à natureza higroscópica da componente orgânica da Perovskite, foi testada a influência da humidade na formação de filmes, bem como também diferentes métodos para reduzir a degradação do filme devido à exposição à humidade.

Com base nos diferentes testes, a otimização dos dispositivos solares foi bem sucedida, obtendo-se filmes de Perovskite com densidades em volume superiores a 95%, uma eficiência de 2,65%, J_{sc} de 15,11 mA/cm^2 e um V_{oc} de 0,701 V para o melhor dispositivo.

Palavras-chave: Perovskite fotovoltaicas; Células solares de filmes finos; Spin-Coating; MACl; Contactos para células solares de filmes finos; CuSCN HTL; Influência da humidade na qualidade da Perovskite.

Contents

List of Figures

List of Tables

Acronyms

CuSCN	Copper(I) Thiocyanate.
DMF	N,N-dimethylformamide.
DMSO	Dimethyl Sulfoxide.
ETL	Electron Transport Layer.
FA	Formamidinium.
FDC	Fast Deposition-Crystallization.
FTO	Fluorine-doped Tin Oxide.
GBL	γ-butyrolactone.
HTL	Hole Transport Layer.
MA	Methylammonium.
MACl	Methylammonium Choloride.
MAI	Methylammonium Iodide.
$MAPbI_3$	Methylammonium Lead Iodide.
PCE	Power Conversion Efficiency.
PSC	Perovskite Solar Cell.

rpm	Rotations per Minute.
SC	Solar Cell.
SEM	Scanning Electron Microscopy.
spiro-OMeTAD	2,2',7,7'-Tetrakis-(N,N-di-p-meth-oxyphenylamine)-9',9'-spirobifluerene.
TMM	Transfer-Matrix Method.
TTIP	Titanium Isopropoxide.
UV-Vis	Ultraviolet-Visible.
XRD	X-Ray Diffraction.

Chapter 1

Goals and motivation

The continuous and growing energetic needs, the challenges regarding traditional energy resources, and the ever growing concern with sustainable development, has led Humanity in search of what is known as renewable energies.

The Sun is a excellent energy source that will not disappear anytime soon, delivering to the surface of the earth in one hour the same amount of energy consumed by humans in a year [1]. For these reasons, it constitutes a superb renewable energy source.

Although it delivers such an incredible amount of energy, the processes for collecting and using this energy are far from perfect. The conversion of this energy into electrical energy is done through the use of photovoltaic materials, incorporated in devices designated as solar cells (SC). In the last years, Perovskite SC's have attracted attention mainly due to the rapid increase in Power Conversion Efficiency (PCE), increasingly approaching those of Silicon, material that to this day, still dominates the solar cell market.

The attention given to these materials comes also due to its remarkable characteristics as a photovoltaic material, coupled with the ability to be processed by simple and relatively cheaper techniques, such as spin-coating, without the use of excessive temperatures or high vacuum environment.

This work aims at improving the solar cell devices fabricated until this stage, striving to improve device performance, through the understanding of fabrication parameters vital for better device quality, while keeping the fabrication process as simple and as low-cost as possible, hoping to achieve comparable PCE as to those found in Silicon based devices. Besides device optimization, an effort is made in lowering the fabrication costs by studying a different material(MACl) as a replacement for MAI in Perovskite precursor solution.

Chapter 2

Introduction

Perovskite solar cells (PSC) have been gathering an increasing amount of attention, mainly due to the rapid increase of device efficiency in a short time period over the last years [2, 3].

In 2009 it was reported a device efficiency just shy of 4% [4], on a dye-sensitized SC. 2012 was the year that sparkled an increase in attention for PSC, as it was the year that a 9.7% solid-state PSC efficiency was reported, with 500 hours of confirmed stability [5]. The rise of attention towards this type of SC sparkled a race for better performing devices, and in 2015 a device efficiency of 20.2% was reported by W. Jang *et al.*, using Formamidinium (FA) as a cation. As of late 2017 a certified efficiency of 22.7% has been achieved [6, 7]. The reported efficiency of PSC keeps getting closer to those reported in Silicon based devices [8].

The continuous interest in these materials stems not only from its attractive optoelectronic properties such as adequate and tunable band-gap, high absorption coefficient and high life-time and mobility of the carriers [9, 10], but also due to its innate ability to be fabricated using simple and low-cost processing techniques, namely spin-coating [2, 3].

Low-processing temperatures is a key requirement when fabricating flexible SC devices, which is also the reason why Perovskite materials, having met this condition (processing temperatures under 150°C) [2], have also made a huge contribution in this field, where a 2.6% device efficiency was reported in 2013 [11] for a device built on a flexible substrate. The efficiency skyrocketed, and in 2015, a PCE of 15.3% was reported by S. Shin *et al.* [12]. As of late 2017, the record efficiency for a Perovskite SC device built onto a flexible substrate is reported to be 18.1% PCE [13].

Although there has been remarkable advance in solar cells using Perovskite materials, the top reported devices still do not meet all the requirements for a possible commercialization, such as low fabrication cost, mainly due to the materials used, but also due

to high processing temperatures (preventing these devices from being used in flexible substrates) and highly controlled fabrication environments. Even for solid-state devices, the PCE still falls behind that of top Silicon devices.

Currently, efforts are being made to further increase device efficiency through a number of different ways, while also keeping in mind the fabrication costs, so that Perovskite based devices can one day compete in the SC market, currently dominated by Silicon, with the goal of one day becoming the material of choice for both solid-state (single junction and tandem) and flexible devices.

2.1 Solar Cell

Solar cell is a device that uses the photovoltaic effect in order to convert solar to electrical energy. As demonstrated in figure 2.1, this energy conversion is achieved through the use of semiconductor materials with an appropriate band gap (E_g), so that photon energy (E_{ph}) is high enough ($E_{ph} > E_g$) to create an electron-hole pair within the material, by exciting a valence electron into the conduction band of the material. After this excitation process, the charges are separated due to the electrical field created by the p-n junction and can then be collected in an external circuit.

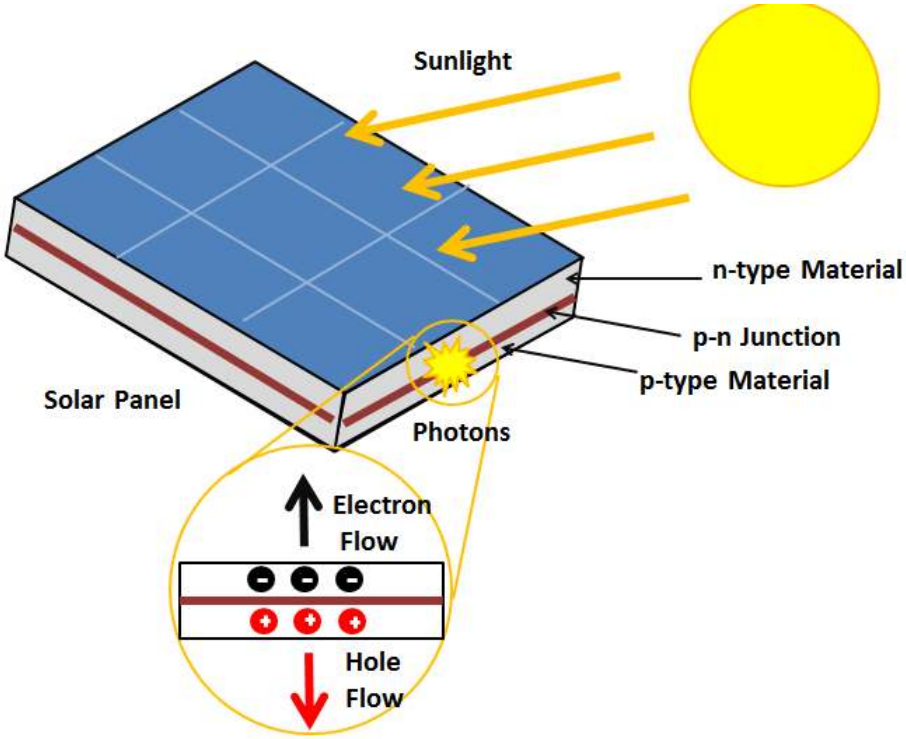

Figure 2.1: General working principle of a solar cell [14].

The efficiency of the different processes for the energy conversion and collection, will determine the device efficiency, and is greatly dependent on the choice of materials and its optoelectronic properties, such as an adequate band-gap (as close to the ideal 1.34

eV as possible [8]), absorption coefficient, carrier life-time and mobility and others. The solar cell efficiency is calculated through different parameters that can be obtained with the I-V and P-V measurements (further details in Appendix A).

There are two major configurations when fabricating a Perovskite SC, designated as conventional configuration (which is the most common and was the one employed in this work), which can be planar or meso-structured, and inverted configuration. The difference in these structures lies in the stacking of the different layers (as demonstrated by figure 2.2).

The typical solar cell structure is a conventional type and consists of 5/6 different layers, deposited usually on top of a glass substrate. This solar cell has a frontal contact of FTO (FTO), on top of which a layer designated as Electron-Transport-Layer (ETL), is deposited, consisting of just a compact TiO_2 film, in the case of the planar structure, or a mesoporous TiO_2 film deposited on top of the compact TiO_2 film, if it is a meso-structured device. Following the ETL deposition, the active layer of Perovskite is deposited, Methylammonium Lead Iodide ($MAPbI_3$) being the most common material for this layer. The Hole-Transport-Layer (HTL) is usually the last layer to be deposited, and the most used material is 2,2',7,7'-Tetrakis-(N,N-di-p-meth-oxyphenylamine)-9',9'-spirobifluerene (spiro-OMeTAD) [2]. On top of these films, gold, aluminum or silver back contacts are also deposited.

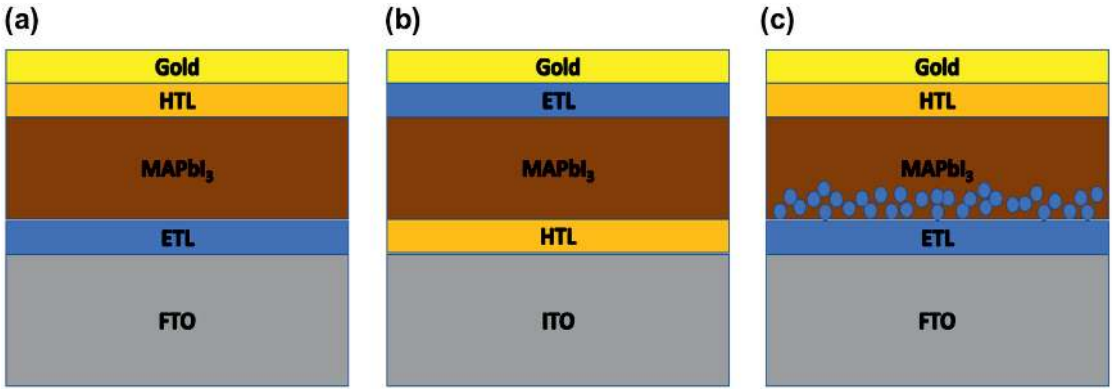

Figure 2.2: Different Solar Cell arquitectures [15]. a) Planar Structure; b) Inverted Structure; c) Mesoscopic Structure.

2.2 Perovskite Materials

Thin film solar cells, can be made from a variety of materials such as Si (amorphous and crystalline), Compound semiconductors (GaAs, GaInP and others), CdTe, CuInSe2 and organic semiconductors [16], but many of these materials are toxic (CdTe), expensive to obtain/manufacture (most compound semiconductors), therefore preventing them from being considered for commercialization. This is where organic-inorganic Perovskite

materials shine, as they are relatively cheaper and can be fabricated using simple and low-cost techniques.

2.2.1 Crystalline Structure

Perovskite used to be the name for the crystalline structure of $CaTiO_3$, but now refers to any material that presents the same crystalline structure of ABX_3, exemplified in figure 2.3, where X is an anion simultaneously connecting to the two cation, A and B. In most cases, A is an organic molecule, such as Methylammonium (MA) or Formamidinium (FA), B can be either Pb or Sn and X is an halogen, such as I, Cl, Br or a mix of these, since it is possible to tune the material properties by mixing the different integrating elements [17].

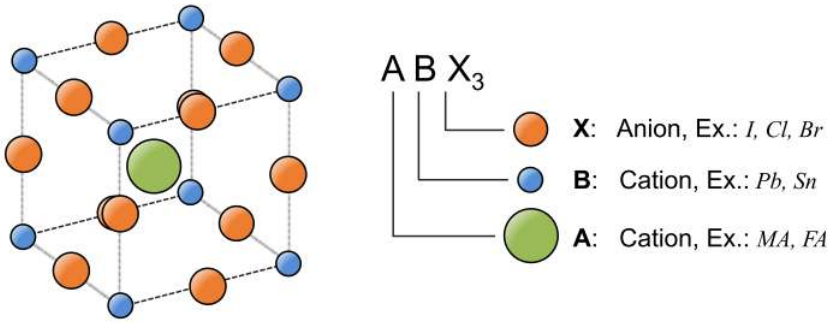

a

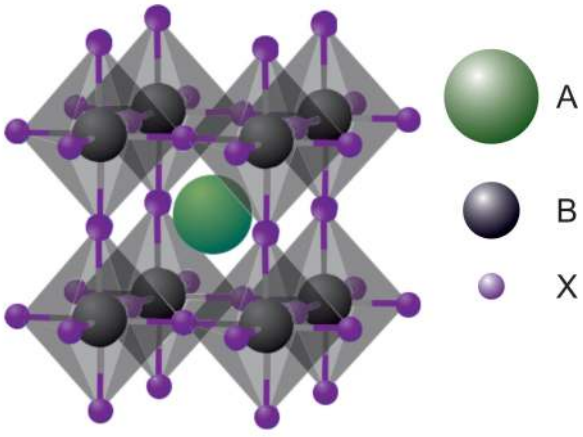

b

Figure 2.3: Perovskite Crystal Structure; a)Perovskite unit cell [17]; b) Crystal Structure of cubic metal halide Perovskite (ABX_3) [18].

As mentioned, these materials possess unique properties such as tunable band-gap, high absorption coefficient, bipolar charge transport ability, high carrier mobility and life-time, long charge diffusion lengths, and sollution processability [2, 19], without being extremely costly, making it a very attractive material for thin film solar cells.

2.2.2 Perovskite - Thin Film fabrication

Perovskite thin films can be processed from a variety of techniques like spin-coating (one and two-step methods), dip-coating, doctor blade coating, spray pyrolysis, chemical and thermal evaporation and others, and even mixing different techniques [20–27]. The spin-coating technique is a relatively simpler and cheaper technique, compared to most, which are the main reasons to keep researching and developing Perovskite SC devices using this technique.

When fabricating thin films, high uniformity, good surface coverage and overall film quality, are essential for better performing solar cells. Many efforts have been made to achieve these qualities using spin-coating technique, whether through material choices or even fabrication processes.

To achieve crystalline Perovskite thin films, it is important to first understand the influence of the fabrication parameters on film deposition and crystallinity, and a large amount of research is dedicated in order to understand each individual fabrication parameter [28]. Giles E. Eperon *et al.* studied the importance of film morphology and surface coverage by varying processing conditions such as annealing temperature and time, fabrication environment (controlled humidity levels), and also material related parameters like film thickness (both of Perovskite layer and TiO_2 compact layer) and solution solvents. This group reported a loss in surface coverage with increasing annealing temperature, increasing annealing time and lower film thickness (varied individually), translating in lower device efficiency. Increasing annealing temperature had an interesting effect on the films, where a transition from a continous layer to large Perovskite islands is reported, this way reducing surface coverage and suggesting that lower temperatures equal better surface coverage [29].

A. Dualeh *et al.* also studied the effect of annealing temperature on film morphology, and reported incomplete film crystallization for annealing temperatures below 80° C, regardless of annealing time. For high annealing temperatures (>150° C), the crystallization is almost instantaneous and for extreme temperatures (200° C) it was reported a quick formation of a yellowish film, indicating the presence of PbI_2 [30]. Indeed, for an annealing temperature of 200° C, the absorption spectra resembles that of pure PbI_2 and for annealing temperatures above 120° C, XRD diffractogram reveals a peak associated to PbI_2, indicating Perovskite degradation.

In order to achieve highly uniform films, while still using spin-coating technique, M. Xiao *et al.* devised a new approach regarding the deposition/spinning step of Perovskite films. This research group devised an efficient, reproducible and simple method for reaching good morphology and high surface coverage, designated as Fast Deposition-Crystallization (FDC) method, specific for one-step spin-coating procedure. FDC method consists of spin-coating a precursor solution onto the substrate, make it spin and during the spinning-step, drop an anti-solvent agent, like chlorobenzene, toluene and others, in which the Perovskite as low solubility. This anti-solvent agent dropping step has the

role of promoting rapid nucleation and crystal growth, by removing excess of precursor solution solvents [19]. Using this deposition method, M.Xiao and coworkers reported full surface coverage and micrometer-size grains, while being able to control film thickness.

In order to also promote rapid nucleation, W. Nie *et al.*, reported the use of what is named as "hot-casting method", in which both precursor solution and substrate are heated, prior to Perovskite deposition. Using this method yielded Perovskite thin films with millimeter-size grains, which is atributted to a prolonged growth of crystals due to excess of solvent present at temperatures above crystallization temperature [31].

Regarding deposition procedures, Z. Xiao and coworkers reported an interesting deposition method, in which a layer of PbI_2 is first spin-coated onto the substrate, followed by deposition of a Methylammonium Iodide (MAI) layer. During the annealing and drying step, the two layers undergo an interdiffusion process and the end result is a pin-hole free Perovskite film, with full substrate coverage, reporting better uniformities than when using a precursor solution with both PbI_2 and MAI [32]. This research group also reported being able to control crystallization and grain size, by varying annealing time.

J.H. Im *et al.* reported a similar process denoted "two-step spin-coating", leading to the formation Perovskite cuboids that are reportedly influenced by MAI concentration [33].

As expected, the different parameters of Perovskite precursor solutions play a big part in film formation, specifically concentration, influencing film thickness, surface coverage, current density and such [28, 33, 34].

Perovskite solvents also play a role in film fabrication and, as such, have also been the target of research. Solvent engineering is reported to help achieve highly uniform films. N. Jeon *et al.* and B. Cai *et al.*, both investigated different precursor solution solvents (GBL, DMF and DMSO), reporting in both cases significant improvement on film coverage and crystallinity when using a mixed solvent for the precursor solution, whether that be DMF:DMSO or GBL:DMSO. This improvement has been attributed to the fact that DMSO acts as solvent and also a coordination agent, allowing the formation of an intermediate phase complex denoted "MAI-PbI_2-DMSO"[35], delaying the rapid interaction between MAI and PbI_2 during evaporation of DMF/GBL (in which $MAPbI_3$ has high solubility) [21]. Both research groups used the FDC method developed by M. Xiao *et al.* which is reported to help remove excess of solvents and allow a quick formation of the intermediate phase film [21].

Also regarding Perovskite precursor solutions, H. Tsai *et al.* studied different solution aging times, meaning the solution was prepared and left to stir at 70° C for various times before film deposition. This technique is reported to drastically affect film formation and crystallinity and overall device performance [36]. This research group correlates the film improvement with aging time due to the formation of larger nucleation seeds, therefore increasing grain-size with increasing aging time.

These studies give an idea of the different possibilities that exist in order to further

improve thin film formation and corresponding device performance, while also demonstrating the sensibility of the fabrication process for good Perovskite thin films.

2.3 Electron and Hole Transport Layers

As already mentioned, one of the big advantages of Perovskite materials is their bipolar charge transport ability. For this reason it is possible to fabricate ETL and HTL-free Perovskite solar cells, which is also an effective way of reducing the cost of fabrication [37]. Despite this fact, Perovskite solar cells benefit from the addition of said layers, which help improve charge collection and prevent short-circuit on bad film coverage areas of the Perovskite layer.

The material choice for a specific layer (ETL and HTL) is not made at random, considering different factors like absorption coefficient (since most likely one of these layers will have to allow radiation to pass through), band-gap, carrier mobility, fabrication parameters, how it affects layer interface, etc. But perhaps, the most important thing to consider is the proper energy level alignment with the active (Perovskite) layer [37]. As exemplified by figure 2.4, proper band alignment is critical, not only to facilitate charge collection, but also to block opposing charges [37].

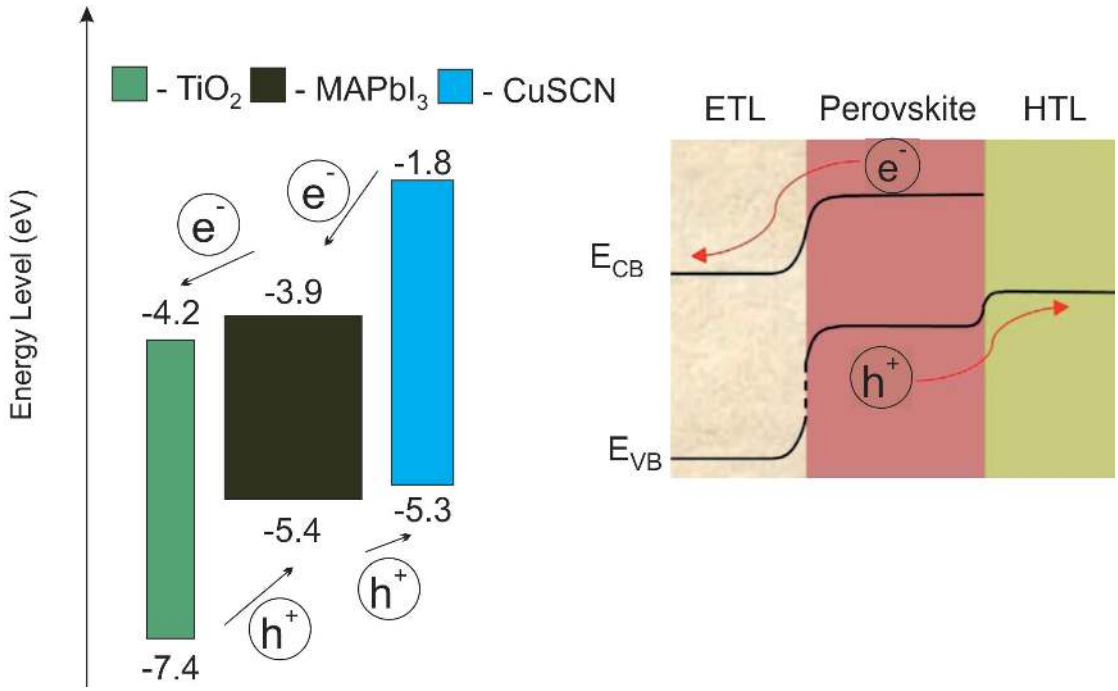

Figure 2.4: Energy level alignment for some of the materials used in this work; Schematic band-bending of energy levels [37–40]

2.3.1 Electron Transport Layer - ETL

This layer has the main goal of helping charge extraction after electron-hole pair formation in the Perovskite layer. In the specific case of the ETL, it deals with electron extraction, facilitating the transport of these carriers to the respective electrical contact. When fabricating conventional structure solar cells, the most common material for this layer is TiO_2 [41]. Depending on whether the architecture is planar or mesoscopic (figure 2.2), ETL is composed of one or two layers. The planar architecture implies that only a compact-layer of TiO_2 will be deposited on top of the FTO. This compact film will act mainly as a blocking layer, reducing charge recombination [42]. Mesoscopic device architecture means that, on top of the compact film, a mesoporous layer will be deposited (also from TiO_2 in this specific case), which is reported to have a profound impact in reducing hysteresis behavior, acting as a scaffold for the Perovskite layer and immensely increasing charge collection [18, 41, 42].

2.3.2 Hole Transport Layer - HTL

Similar to the behavior of the ETL, HTL has the purpose of increasing charge collection, in this case, holes, helping transport them to the respective electrical contact. In the organic HTL department, spiro-OMeTAD is the material of choice for most devices reported in the literature [2]. However, it presents some clear disadvantages like its high cost, low hole-mobility and conductivity [37].

Inorganic HTL, mainly due to its significant lower cost, have gathered increasing interest, appearing to be an effective alternative to organic HTL's by reportedly having high hole-conductivity and being easy to fabricate inexpensively (simple solution-processing techniques and low fabrication temperatures), while also being more thermally stable (less degradation in comparison), therefore acting as an insulating layer protecting the Perovskite film from enviromental humidity [37, 43–45].

Copper(I) Thiocyanate (CuSCN) appears to be a excellent candidate for HTL fabrication due to its lower production cost, appropriate energy levels, and good optoelectronic properties, without the need for high processing temperatures nor expensive techniques. Devices with high efficiency have been reported with CuSCN as the material for the HTL layer [43], hence making this as the material of choice for the HTL of the devices fabricated during this work.

2.4 Film deposition techniques

Although Perovskite can be fabricated from a variety of techniques, one of the goals for this work was to keep fabrication costs to a minimum, and as such, the main deposition technique was kept as simple and as low cost as possible.

2.4.1 Spin-coating technique

One of the techniques that can be used to fabricate a thin film of Perovskite is Spin-coating. This technique presents advantages in respect to others in its simplicity and low-cost, making it ideal for this work. Many researchers, using this technique, have focused their resources into improving Perovskite thin film crystallinity (and by extent, SC efficiency), with successful results [19, 21, 35].

Spin-coating is a fairly simple technique (as demonstrated in figure 2.5) but effective in thin film production. The solution, containing the material that will form the film, is deposited in the center of the substrate which is then made to spin at typically around 3000rpm [46]. It can be a single step spin in which the substrate is made to spin with one speed and acceleration for the spin duration, or like in the case for the Perovskite film deposition step, have first a slower spinning step, intended to aid spreading the film on the substrate, followed by a faster second step which serves the purpose of removing excess solvents and further spreading the film. Speed, acceleration, and time are all factors that might influence film formation and can be tuned according to the needs of the user.

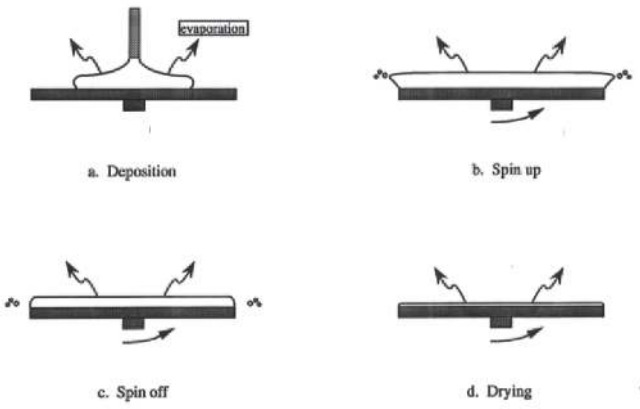

Figure 2.5: Schematic of film fabrication via Spin-coating method [47].

2.4.2 Electron-beam evaporation technique

The gold contacts were the only film to be deposited with a different technique, which was e-beam evaporation.

E-beam evaporation technique uses highly accelerated electrons that are emitted from a filament (usually tungsten) due to the passing of current through the filament. The highly accelerated electrons are forced, via magnetic field, into a trajectory culminating at the crucible (which is water cooled so as to also reduce contamination). The accelerated electrons transfer their energy into the material in the crucible, which vaporizes and deposits onto the substrate. Since the whole process is done inside a chamber at very low

pressure, this process is capable of producing highly pure thin films. [48, 49]. Figure 2.6 schematically represents this deposition technique.

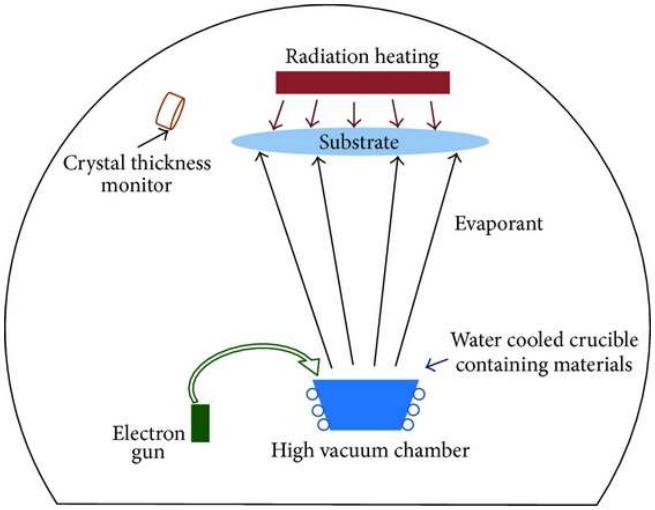

Figure 2.6: Schematic thin film deposition via E-beam technique [48].

2.5 Characterization Techniques

To evaluate film crystallinity different techniques were used and device performance characterization was mainly done through electrical measurements in order to reach device efficiency.

2.5.1 SEM - Scanning Electron Microscopy

Scanning Electron Microscopy (SEM) is a technique in which highly accelerated electrons are focused and made to collide with the sample. A number of different "products"result from this interaction, as electrons decelerate upon impact (as illustrated by figure 2.7). To obtain images of the film surface, the electron-sample interactions that matter are the ones where the resulting products are also electrons (secondary and backscattered electrons). Forcing the beam to scan a determined area of the sample, it is possible to obtain images with a scale as small as a few nanometers [50]. From these images one can evaluate film qualities like film spreading, impurities, and even check if the film presents grain-like features.

2.5.2 XRD - X-Ray Diffraction

X-Ray Diffraction (XRD) is a technique that allows to obtain information about composition and crystal structure of a material, and is very helpful to understand film crystallinity variations due to a change in fabrication procedure, for example.

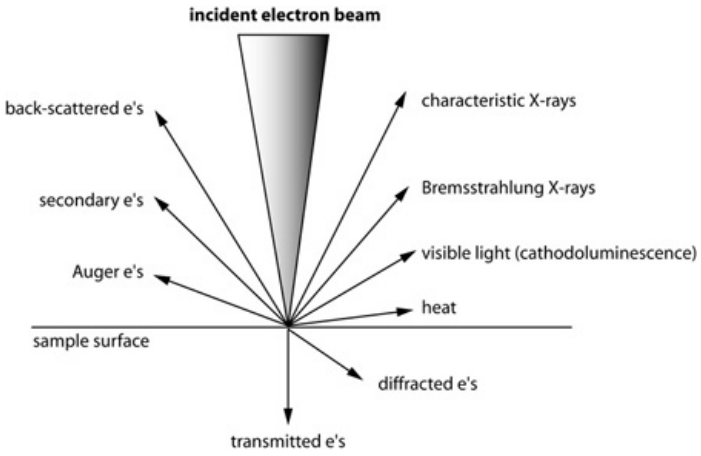

a

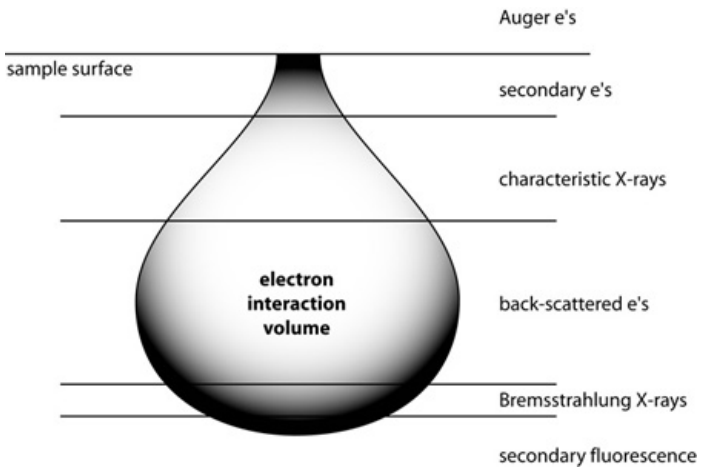

b

Figure 2.7: a) Electron-Sample interaction schematic; b) Electron-Sample interaction volume [51].

It is based on the interaction of a monochromatic x-ray beam with the sample. Due to the crystallographic plains of the material, it will only produce constructive interference (diffraction) in certain directions, according to Bragg's Law.

$$2d\sin(\theta) = n\lambda \tag{2.1}$$

From Bragg's Law comes Bragg's equation (2.1), where d refers to interplanar distance, θ is the sample orientation relative to the incident beam, n a positive integer and λ is the wavelength of the incident beam. In this law, and according to the interplanar distance, it is possible to observe that, only in some orientations, there will be constructive interference, translated into XRD peaks in the diffractogram. Peak position in a XRD diffractogram is therefore characteristic of the material's crystal structure, since each material will have unique d-spacing [52]. Figure 2.8 illustrates a constructive interference (waves in the same phase) according to Bragg's law, which is the base principle for the

XRD technique.

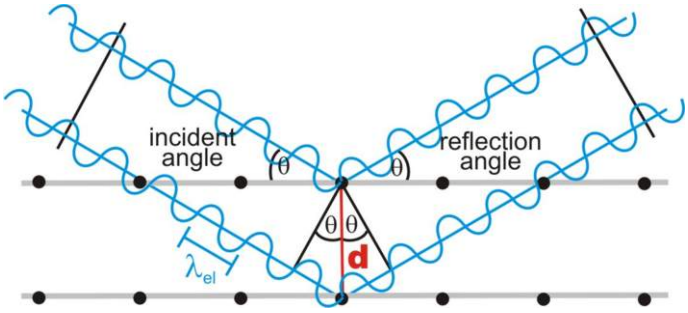

Figure 2.8: Constructive interference of reflected waves according to Bragg's Law [53].

2.5.3 Ultraviolet-Visible Spectroscopy

Ultraviolet-Visible (UV-Vis) Spectroscopy allows to obtain information about absorbance, transmittance, and reflectance of each composing layer of the solar devices. This technique uses a spectrophotometer to measure transmittance and reflectance (direct and total, with different setups). From this two measurements it is possible to extrapolate the sample absorption via: $1 = A + T + R$, where A refers to sample absorbance, T its transmittance and R its reflectance. Although it is not simple, it is also possible to estimate film thickness using Beer-Lambert's equation (2.2), where I_0 corresponds to initial beam intensity, I the intensity of the beam that reaches the detector (after traveling through the sample), α the absorption associated to the material, and l film thickness.

$$I = I_0.e^{(\alpha.l)} \tag{2.2}$$

In this work, it was estimated the thickness for the ETL by fitting the experimental transmittance and reflectance spectra with simulated ones, using the analytic Transfer-Matrix Method (TMM), implemented via Mathematica software.

Chapter 3

Experimental Procedure

This chapter will describe in detail the experimental processes used to achieve complete solar cell devices.

The solar cells' fabrication process can be divided into three main categories: Substrate Preparation, Film Deposition and Contact Deposition. All the cell layers (except for the electrodes) were deposited using spin-coating technique. Figure 3.1 schematically represents the most crucial steps for the solar cell fabrication procedure.

3.1 Substrate Preparation

Fluorine doped tin oxide (FTO) coated glass (100 mm x 100 mm x 2.2 mm, 13 Ω/sq, 82-84.5% transmittance), was first cut into 2.5 x 2.5 cm substrates. These substrates were then covered in Kapton tape (on the FTO side), leaving two stripes, of 3-4 mm in width, on opposite sides, to prepare for the etching. The etching procedure is described in topics below, and was adapted from Ossila website [54].

1. Prepare a 2M HCl solution;
2. Place mask onto the FTO glass substrates;
3. Apply Zinc powder onto the areas of interest;
4. Remove excess powder;
5. Place the substrate in a glass container (petri dish);
6. Coat the substrate with the 2M HCl solution;
7. Wait around 3 minutes for the reaction to finish;

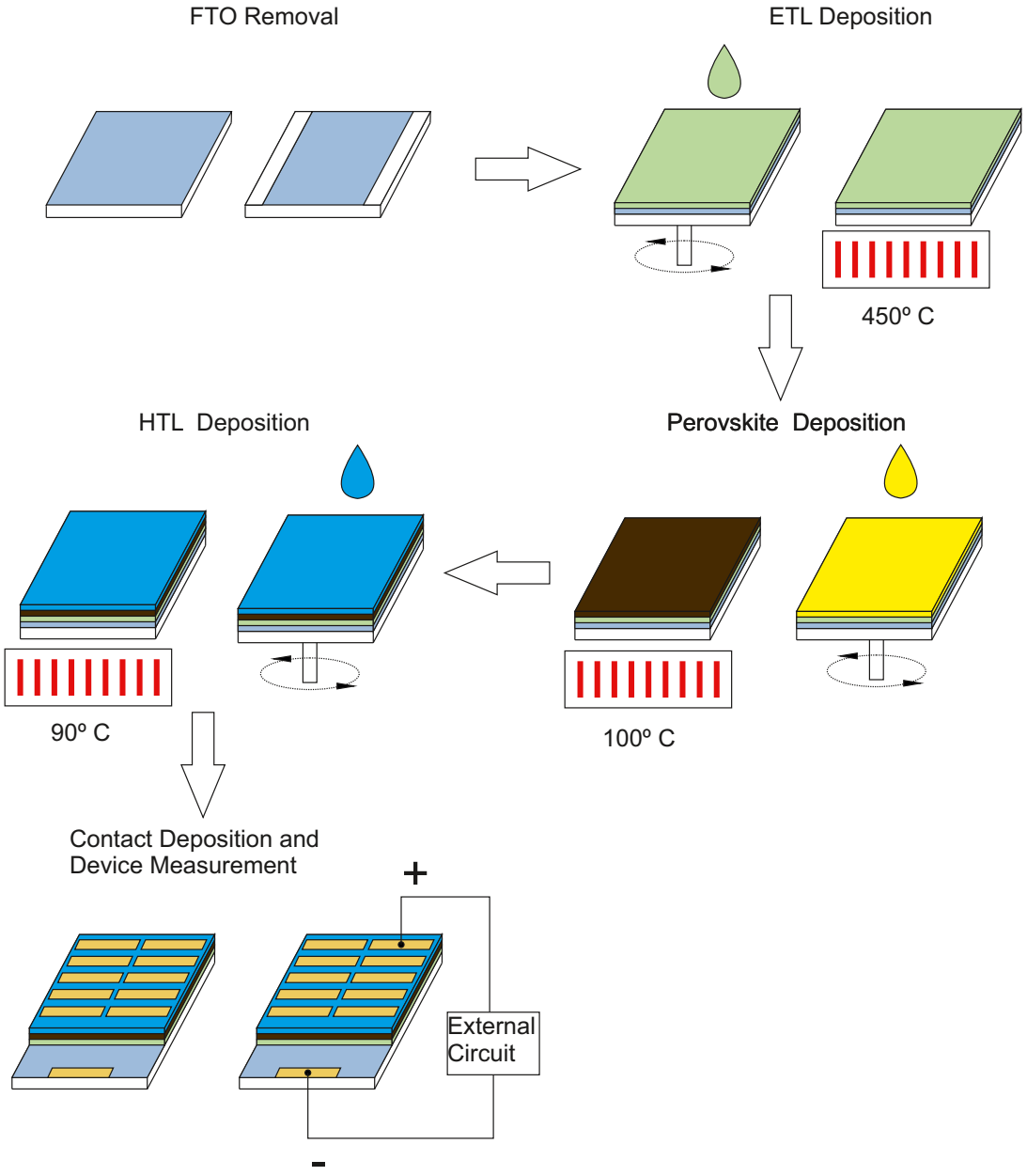

Figure 3.1: Schematic representation of the SC fabrication process and I-V measurement.

8. With an cotton bud, wipe the etched area;
9. Remove mask;
10. Clean substrate with a cotton bud soaked in IPA.

The end result of this procedure is represented in figure 3.2.

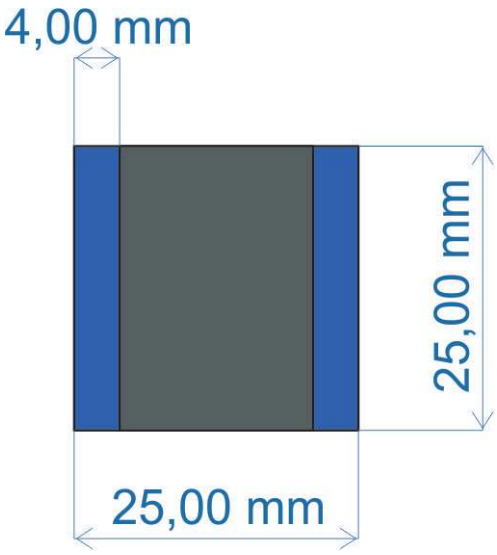

Figure 3.2: Glass substrate after FTO removal - In grey: un-etched FTO film; In blue: etched areas(glass only).

Prior to the ETL deposition, the substrates were cleaned using ultrasonic baths. The first bath contained DI water and detergent and lasted for 15 minutes at 50° C. After, the substrates were rinsed in a DI water bath for 15 minutes at 50° C. The substrates were then transferred onto an Acetone bath, followed by an IPA bath, both at 50°C for 15 minutes. The glass substrates were rinsed in DI water and dried using a nitrogen gun, before being submitted to UV treatment for 15 minutes as the final cleaning step, improving at the same time the wettability of the substrate.

3.2 Film deposition

This section will report, in order of deposition, the processes related to the fabrication of each film/layer of the solar cells.

3.2.1 ETL deposition

For the ETL deposition the material of choice was TiO_2 and two different solutions were used to make the compact layer, which are described in full detail in appendix B. It was dropped a controlled volume (150 µl) of the precursor solution onto the substrate, which was then spun at 3000 rpm (2000 rpm/s ramp) for 1 minute, for the solution using TTIP, and 5000 rpm (with a 4000 rpm/s ramp) when using the $TiCl_4$ solution, as

to obtain similar thickness [55]. After the spin-step, the substrates were dried for 10 minutes, at 120° C and then annealed at 450° C for 30 minutes on a hot-plate, in ambient air conditions.

It was also tested the use of a mesoporous layer to see if it would improve the device performance. The solution is described as well in appendix B, and the spin-step, dry-step and annealing conditions were the same as for the compact layer using the TTIP.

3.2.2 Perovskite deposition

For the active layer, a few different solutions were tested, varying from different concentrations, to different solvents and reagents. For the MACl study, various concentrations were used, but for MAI only two were tested, and for full solar cell devices only the 1M solution was used. All the details for the used solutions are in appendix B.

For this work it was employed a technique called "Solution aging", where the precursor solution is prepared in advance to the deposition, with precise timing. For this work a 24 hour aging was used, meaning the solution was prepared and left to stir at 70° C for 24 hours. Prior to the spin-step, the substrates were also heated to 70°C (Hot-casting method). Higher temperatures were tested using the MACl precursor solution (90° C and 100° C), but the solution would evaporate too quickly on the substrate before the substrate was made to spin, especially at 100° C and as such, they were eliminated from following studies.

A precursor solution volume of 150 µl when using the MACl solution, and 120 µl for the MAI solution, was spin-coated onto the substrate using a two-step spinning program. For the MACl solution the spinning program consisted of a first step of 2500 rpm for 15 s (2000 rpm/s ramp) followed by a 5000 rpm for 25 s (4000 rpm/s) step. In the case of the MAI solution it was first used a spinning step of 1000 rpm for 10 s (500 rpm/s ramp) followed by 6000 rpm for 20 s (5000 rpm/s ramp) step. During the second stage of the spinning process, different anti-solvent agents were dispersed onto the substrate. It was also tested using an anti-solvent on the first stage of the spinning step. This will be described in further detail on chapter 4.

The final step for the active layer is the annealing, which was done at 100° C for 10 minutes in the MACl case and it was tested 15 and 60 minutes using MAI solution.

3.2.3 HTL deposition

CuSCN was used as the material for the HTL. Two different solutions were tested and their respective details are in appendix B. The main HTL solution used is the one where the solvent is Di-n-propyl sulfide. This solution has to be done at least 48 hours prior to HTL deposition in order for the solution to become transparent. A volume of 100 µl was spun-cast onto the substrate with a spin-step of 4000 rpm (3000 rpm/s ramp) for 1 min in the beginning and it was then changed to 30 s. It was also tested a method which will be referred as "Drop-Cast", in which the defined volume of solution is only dropped onto

the substrate after the first 5 s of spinning, where the parameters are: 5000 rpms (4500 rpm/s ramp) for 30 s. Annealing of this layer is done at 90° C for 30 minutes in ambient air conditions.

3.3 Contact deposition

The final step in order to complete the solar cells is to deposit the gold contacts. Acetate masks illustrated in figure 3.3, designed using CorelDRAW software, were cut using a CO_2 LASER (from Universal Systems) and placed onto the devices prior to gold deposition. The deposition was achieved through electron-beam evaporation in working pressure of 10^{-5} mbar and it was deposited 80-100 nm of gold for the back and front contacts. The end result of the devices is represented in figure 3.4. As the contacts were also one of the key tasks for this work, further details of the contact process will be presented and analyzed in chapter 4.

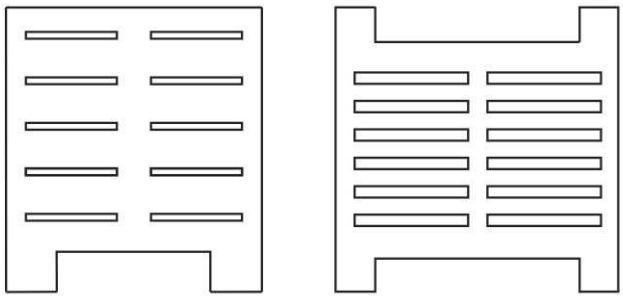

Figure 3.3: a) Masks used in the original version of the contacts (opening for contacts: 8x0.6 mm^2); b) Masks used for the new contact version (opening for contacts: 10x1 mm^2).

3.4 Characterization

In this section it is presented the characterization techniques and the respective equipment, used throughout this work.

3.4.1 SEM analysis

Cross section measurements of complete SC devices was accomplished using a Carl Zeiss Auriga crossbeam (SEM-FIB) workstation instrument equipped with an Oxford Instruments Aztec X-ray energy dispersive spectrometer. Surface morphology of Perovskite films was mainly evaluated using a Tabletop Microscope TM3030 Plus + Quantax 70 SEM.

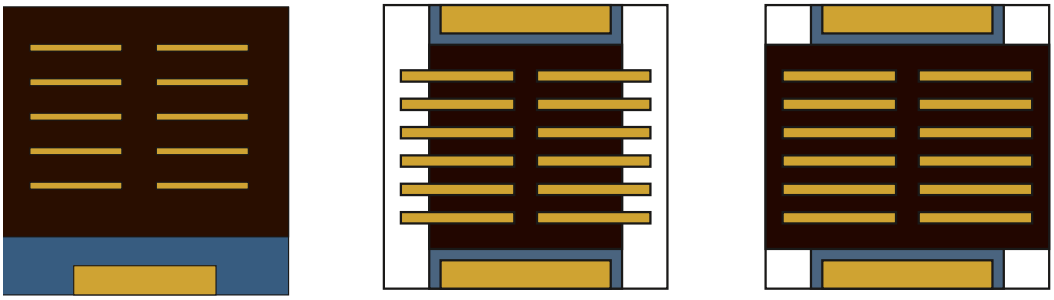

a b c

Figure 3.4: a) SC device using original contact version; b) SC device using etching/perimeter-mask version; c) SC device using final version; In white are the areas that remain film-free; In grayish-blue FTO-only areas; In dark-brown is represented the effective device area (area where all the layers are deposited; In gold are represented the different deposited contacts.

3.4.2 UV-Vis Spectroscopy

The optical characterization of the films was achieved using a Shimadzu UV 3101PC. To obtain absorbance spectra, an ISR-260 Integrating Sphere was used in order to obtain Total Transmittance and Reflectance spectra within a 300-830 nm range. The thickness estimation for the TiO_2 compact layer was obtained through optical simulations with TMM, using Mathematica software, developed by Professor Manuel Mendes.

3.4.3 XRD analysis

Structural analysis of Perovskite films was achieved through X-ray Difraction (XRD) using a PANalytical X'Pert Pro X-ray diffractometer in Bragg-Brentano geometry, with a monochromatic Cu-Kα radiation source (1.5406 Å). The resulting diffractogram was acquired using the High Score Plus software (PANalytical).

3.4.4 Electrical characterization

I-V measurements (and consequently P-V measures) were obtained using a SS150 Reflective Solar Simulator from Sciencetech coupled with LabView software. The measurements were carried out at room temperature under AM 1.5 conditions.

Chapter 4

Results and Discussion

This chapter will be divided into three main sections, as these were the main goals throughout the thesis. In each section it will be presented the corresponding results, as well as these being interpreted and discussed, terminating with a few conclusions about the results.

The first section will address the processes of fabrication of the front and back contacts, as this was thought to be one of the key reasons as to why the devices developed until this stage were not achieving the desired performance.

The middle section focuses on the study of MACl as a possible viable replacement of MAI, in Perovskite synthesis for future devices.

The third section will report the efforts on one of the major objectives of this master thesis: the optimization of the devices obtained in the previous work.

The results presented in this chapter will not be chronologically in order, and as such, the results from each section can be correlated only to an extent.

4.1 Solar Cell Contacts

As it was already mentioned, the contacts were thought to be hurting the performance of the devices, particularly, the back contacts. The measuring tips, with which the I-V measures were taken, could have been penetrating the gold contacts and thus, damaging the underlying films, ultimately reaching the FTO film, causing a short-circuit and invalidating the measurement. In order to prevent this from happening, a new type of contacts needed to be thought of, one that could deal with the fact that the measuring tips could penetrate the films.

The first step was to remove the FTO in the areas where the tips for the I-V measurements were to be placed, meaning part of the back contacts was placed on a FTO-free

zone of the device. A few trials were made in that sense, using different processes [56, 57], until there was success removing the FTO through the process described in full detail in 3.1. The resulting substrate is illustrated in figure 3.2.

Following the successful removal of the FTO stripes, after a few test versions diverging mainly on number and position of contacts, a new mask design was created (3.3b) to replace the one used for the previous type of contacts (3.3a). This new mask incorporates a second front contact, to help reduce the distance between the measuring tips during the measurement, hoping to improve it.

4.1.1 Etching-Method Contacts

Initially it was used a fabrication process, reliant on keeping the stripes (areas where the FTO had been removed) film-free. This was first done by selectively removing, on the zones of interest, the film that was just spin-casted onto the substrate. This meant that, after the deposition of an individual layer and prior to the dry-step or annealing step, an etching of a "perimeter area"was done, using a cotton bud soaked in different materials, depending on the film being removed at the time. For the TiO_2 and CuSCN layers, the respective solution solvents were used for the etching of the desired area, while for the Perovskite layer, acetone was used for the etching. The resulting substrate is shown in figure 4.1, where the blue color refers to the film-free areas, grey color referring to an area with only FTO film (front contact) and the dark-brown color referring to the effective device area (all films present). This method shall be referred as the "Etching contact method"in this document.

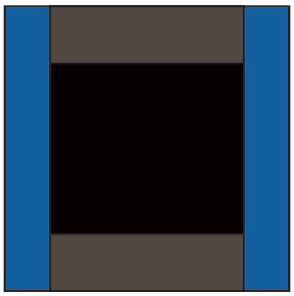

Figure 4.1: Substrate resulting from the etching method, prior to gold contact deposition, with dimensions as the ones in figure 3.2. Blue color refers to film-free areas of the substrate; Grey color refers to the FTO front contacts; Dark-brown color refers to effective device area.

After a few batches using this contact method, a problem with controlling the etched area became apparent: the etching process was not extremely precise, sometimes leading to an under etching of the area, or sometimes an over-etching of the desired areas, exposing underlying layers (ultimately exposing the FTO film), compromising the device performance since exposing the FTO film on undesired areas leads to Voc loss and a

short-circuiting. Another problem that surfaced while doing this type of contact procedure was the clear degradation of the SC films (particularly the Perovskite film) on the film edges due to the etching, which can be observed in figure 4.2. In order to test the types of contacts, a few batches were dedicated only to testing the different processes of fabricating the contacts.

a b

Figure 4.2: Effects of the Etching contact method on film quality, presenting degradation on film edges.

The I-V and P-V measurements for the first batch of SC devices dedicated solely to the contact testing is presented in figure 4.3, with the details of each measurement being presented in table 4.1. There seems to occur some abnormalities, such as a sudden drop or small rise and stabilization, in the current values towards the end of the measurements. It is believed (although it was not tested during this work) to be due to the electronic measurement unit, as upon measuring low currents, it automatically enters in a limiting range of current, giving out, from that point forward, the same value of current, independently on the real value. This is verified in more devices, especially in those of lower performance, as these naturally present low currents, therefore entering the limiting range of the measurement unit sooner.

The difference of the devices is very clear, pointing towards the original contact procedure being the correct one. The measurements for the device with original contacts falls within the expected values according to previous work [34], but the difference with using the etching version was not expected to be so pronounced. Only a slight variation in I-V measurements was expected before these devices were fabricated, and coupled with the fact that from the entire batch only one sample of each contact type was possible to measure (all other devices were not working), it was not possible to be concluded, using solely this batch, which contact type was best suited for the SC devices and as such, a new batch was made in order to repeat this test. The results are shown in figure 4.4 with the corresponding values of interest in table 4.2.

On this batch the trend was inverted, meaning the better performance was exhibited on the devices fabricated using the Etching-Method, which seems to contradict the previous batch where the contrary was observed. Another aspect making these results peculiar,

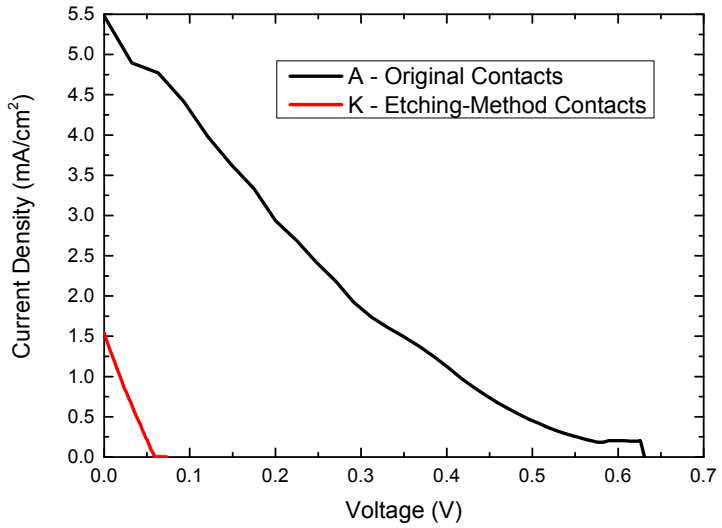

a

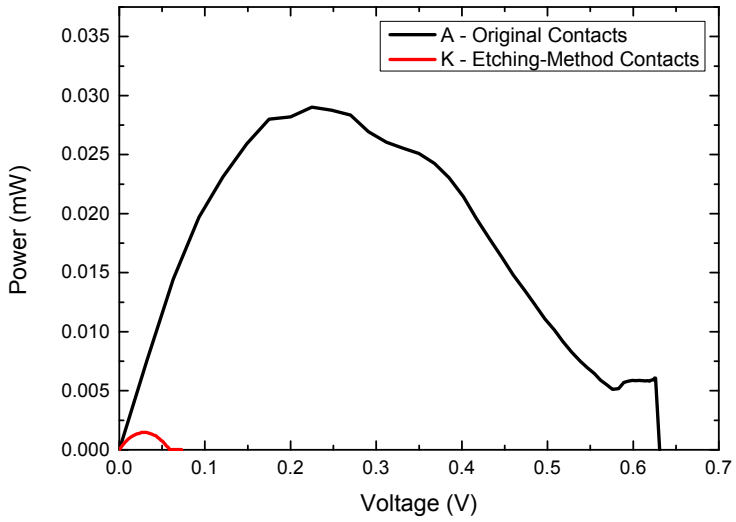

b

Figure 4.3: I-V a) and P-V b) measurements for solar devices differentiating on the contact type (Etching vs Original). Devices fabricated using a compact TiO_2 using TTIP Solution; Perovskite layer using 1 M Solution (MAI:PbI_2 1:1), with 100 µl chlorobenzene droping, annealed for 60 mins at 100°; CuSCN layer annealed at 90° for 30 mins.

Table 4.1: Performance values for the data presented in figure 4.3

SC Devices	Voc(V)	Jsc(mA/cm^2)	FF	Rsh(kΩ)	Rs(kΩ)	PCE(%)
Original contacts	0.631	5.48	0.175	1.86	3.204	0.604
Etching-Method contacts	0.073	1.54	0.187	0.511	0.910	0.021

Table 4.2: Performance values for the data presented in figure 4.4

SC Devices	Voc(V)	Jsc(mA/cm^2)	FF	Rsh(kΩ)	Rs(kΩ)	PCE(%)
Original contacts	0.674	0.338	0.439	265	11.3	0.1
Etching-Method contacts	0.416	5.186	0.202	0.988	1.31	0.435

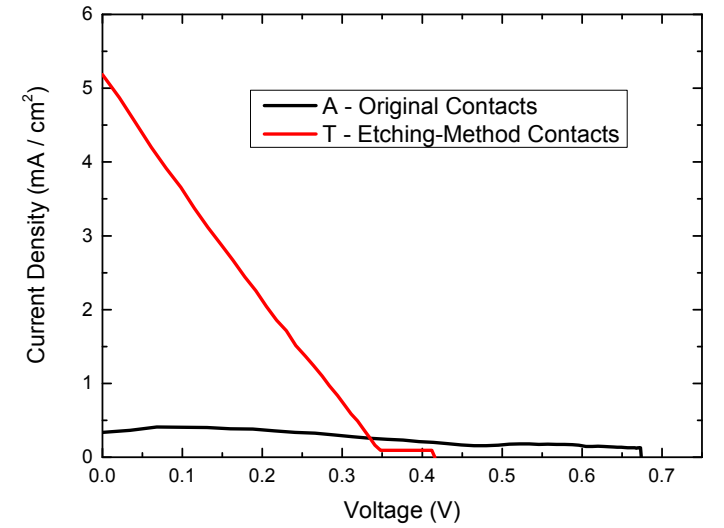

a

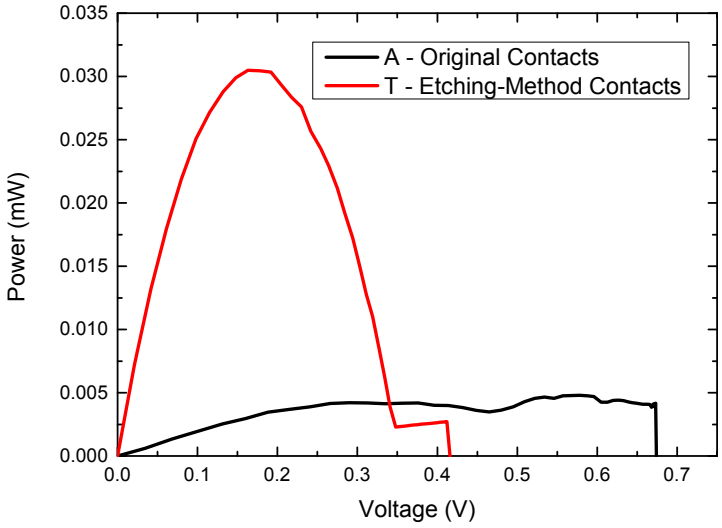

b

Figure 4.4: I-V a) and P-V b) measures for SC devices differentiating on contact type (Etching vs Original - second attempt). Devices fabricated using a compact TiO_2 using TTIP Solution; Perovskite layer using 1 M Solution (MAI:PbI_2 1:1), with 100 µl chlorobenzene droping, annealed for 60 minutes at 100° C; CuSCN layer annealed at 90° C for 30 minutes.

is the fact that from the SEM images shown in figure 4.5, the film quality appears to be better on the device made using the original contact method, where it is possible to see grain-like structures on 4.5a) versus no grains on the device with the etching-method 4.5b). In figure 4.6 it is possible to see again the difference between the device fabricated using the original procedure(on the right) and the one made with the etching-method(on the left).

The devices were also characterized using XRD (figure 4.7) where it is possible to observe the peaks corresponding to the tetragonal phase of $MAPbI_3$, marked with full rhombus, the PbI_2 peak, marked with an asterisk, and also peaks regarding the CuSCN and FTO layer (marked with cardinal and full circle, respectively)[1] [21, 24, 34]. These diffractograms demonstrate a higher PbI_2 peak for the device fabricated using the etching-method, indicating a higher degree of organic degradation on the perovskite film, translating in a formation of a PbI_2 film. This could in fact be related to the etching step necessary for this method because, as demonstrated previously with figure 4.2, the film quality tends to be inferior on the film edges due to the etching procedure. The fact that the main perovskite peaks are more intense and narrow for the device fabricated using original method contacts (values in tables 4.3 and 4.4) helps corroborate the assumption that, using the etching-method results in films of lower quality.

Another problem with using the etching-method is the actual etching-step itself. Etching the films on the designated area meant that the substrates after spinning, were not immediately submitted to their heating treatment (that being a dry-step or annealing step). This is especially concerning with the Perovskite films, being that it is desired a fast crystallization of the perovskite film [19, 34]. Although in this work, the FDC (Fast Crystallization-Deposition) method developed by M.Xiao *et al.* was employed, the fact that the substrates were not placed on the hot-plate right after the spinning step was done, could be delaying the crystallization of the films.

These results demonstrate that the contact procedure does in fact play a significant role in the quality of the device while also pointing to the fact that, although tackling the issue of damaging the films with the measuring tips during I-V measures, the new type of contacts (using the etching method) was in fact hurting the devices.

Table 4.3: Perovskite Peak Parameters of the diffractograms in 4.7 - Original Method device.

2θ (◦)	Intensity (a.u.)	FWHM (◦)
14.07	22117.6	0.127
28.3	9065.1	0.149

[1] The XRD peak symbol system remains the same throughout the document.

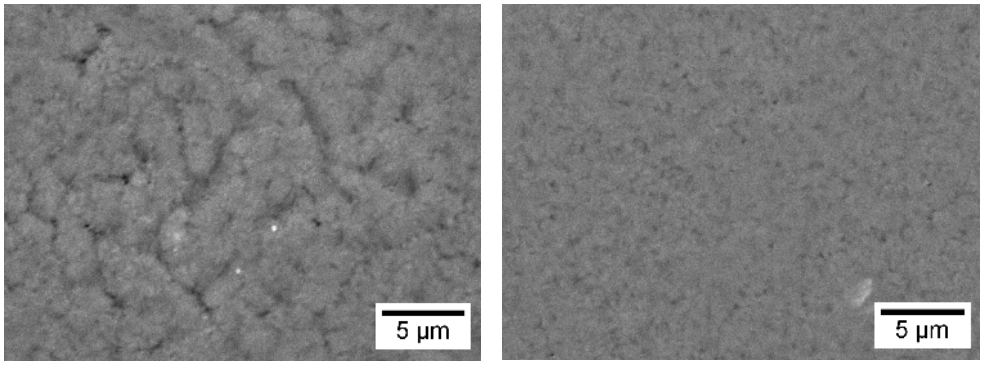

a b

Figure 4.5: Surface morphology influence with contact type. a) Original-Method; b) Etching-Method

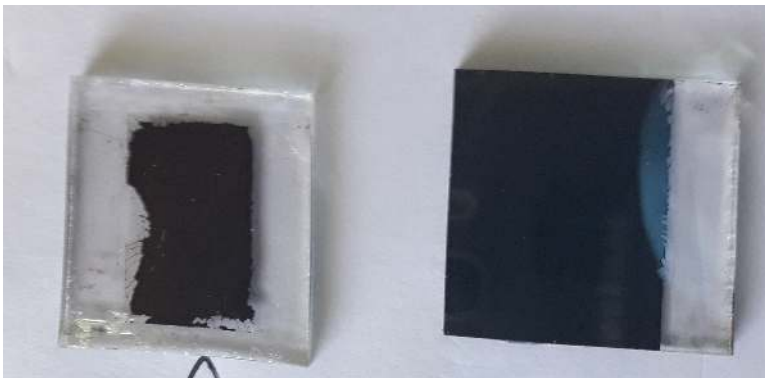

Figure 4.6: Difference between devices using the etching-method (on the left) and the original contact process (on the right).

Table 4.4: Perovskite Peak Parameters of the diffractograms in 4.7 - Etching Method device.

2θ (∘)	Intensity (a.u.)	FWHM (∘)
14.07	17164.6	0.130
28.3	8929.3	0.177

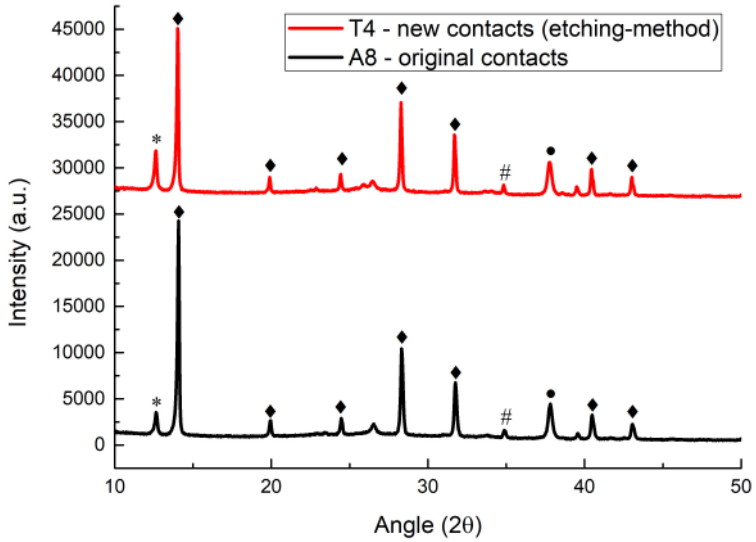

Figure 4.7: XRD diffractograms - Contact Study: Etching-Method vs Original Method. Peaks corresponding to the tetragonal phase of $MAPbI_3$, marked with full rhombus, the PbI_2 peak, marked with an asterisk and also peaks regarding the CuSCN and FTO layer (marked with cardinal and full circle, respectively).

4.1.2 Perimeter-Mask-Method Contacts

The results from 4.1.1 made it clear that the etching-method was not the correct procedure for the contacts on the SC devices and as such, a different approach was needed, one that still tackled the issue of the possible film damage during the I-V measurements, while avoiding the film degradation that resulted from the etching-method.

As discussed previously, the actual etching step was the main problem with that specific contact procedure and as such, the new approach for the contacts envisioned removing all together this step.

The solution found was instead of removing (etching) the films after each deposition, the areas of interest (lateral stripes of glass only and FTO areas for the front contact) would remain film-free throughout the entire film deposition process. This was done by taping Kapton masks on the designated areas, removing them only before the gold contact deposition step. The resulting substrate is represented in figure 4.8, where in yellow color is represented the Kapton mask and in dark-brown the SC films. This particular contact method shall be referred as "Perimeter-Mask-Method". This method allows for a more controlled film-free area and it does not introduce a intermediate step between the spinning and the annealing treatments of each film (the substrate is moved directly to the hot-plate after the spin step).

From this SC batch resulted the I-V measurements present in figure 4.9 with the respective performance values in table 4.5, where again the unusual I-V behavior, most likely due to the electronic measurement unit, is verified. These results, indicate a higher

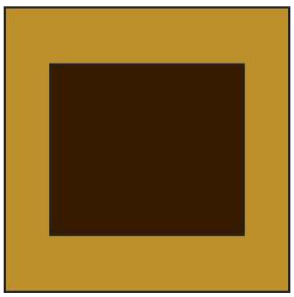

Figure 4.8: Substrate resulting from Perimeter-Mask Contact Method of fabrication. Dark-brown area is the effective device area; Gold color area represents the Kapton mask placed on the substrates before ETL deposition, with the same dimensions as in figure 3.2.

performance for the devices fabricated using the original contact method. On a first approach this could be related with the fact that the Kapton masks leave behind a glue residue (due to the high annealing temperatures used for TiO_2), possibly undermining the I-V measurements. The XRD measurements (figure 4.10) also point towards a higher film quality on the device fabricated using the original contact method, since the diffractograms for that device shows narrower and more intense peaks, as demonstrated when comparing tables 4.6 and 4.7. These results point towards the original contact procedure translating in a better SC device. For this reason, the Perimeter-Mask method was no longer used in future batches.

Table 4.5: Performance values for the data presented in figure 4.9

SC Devices	Voc(V)	Jsc(mA/cm^2)	FF	Rsh(kΩ)	Rs(kΩ)	PCE(%)
Original contacts	0.55	0.33	0.45	0	8.9	0.08
Perimeter-Mask contacts	0.25	0.23	0.73	0	0.11	0.041

Table 4.6: Perovskite peak parameters of the diffractograms in 4.10 - Original Method device.

2θ (◦)	Intensity (a.u.)	FWHM (◦)
14	18138.2	0.148
28.28	7058.5	0.170

Table 4.7: Perovskite peak parameters of the diffractograms in 4.10 - Perimeter-Mask Method device.

2θ (◦)	Intensity (a.u.)	FWHM (◦)
14	8953.0	0.166
28.27	4119.7	0.171

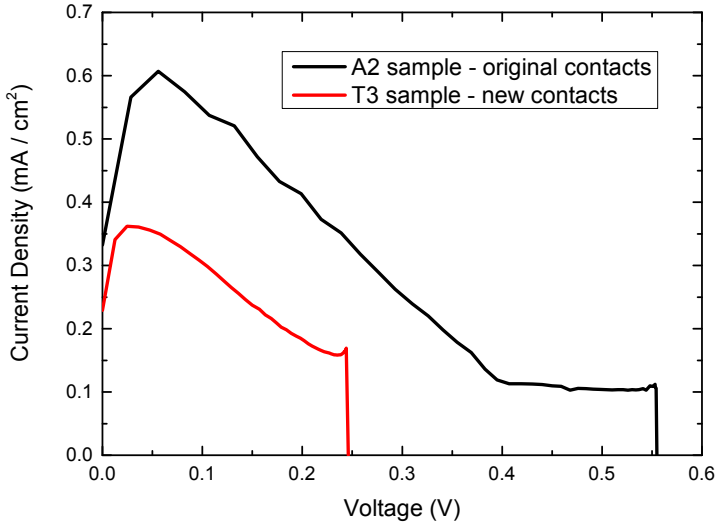

a

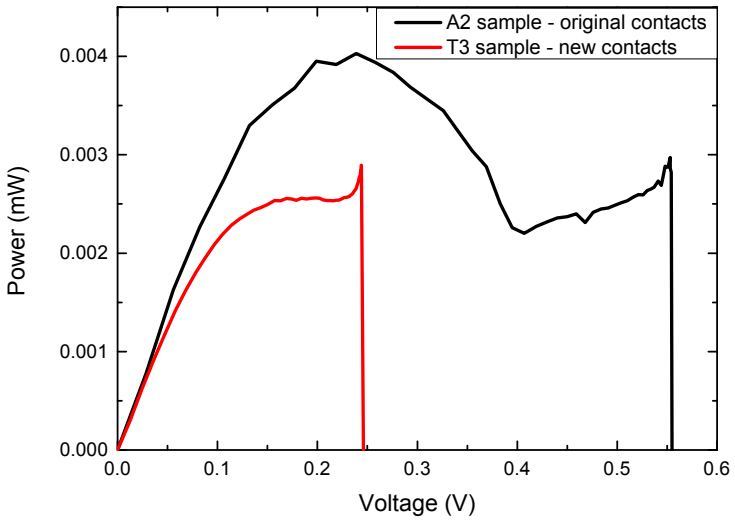

b

Figure 4.9: I-V a) and P-V b) measurements for SC devices differentiating on contact type (Perimeter-Mask vs Original).Devices fabricated using a compact TiO_2 using TTIP Solution; Perovskite layer using 1 M Solution (MAI:PbI_2 1:1), with 100 µl chlorobenzene droping, annealed for 60 minutes at 100° C; CuSCN layer annealed at 90° C for 30 minutes.

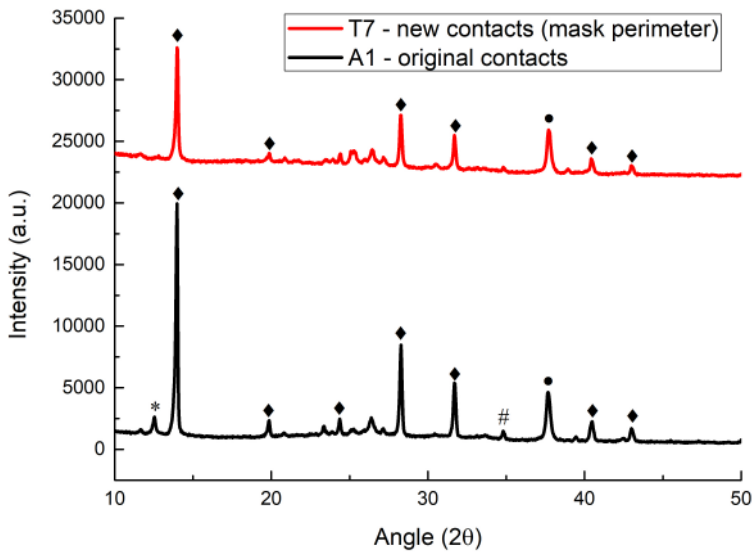

Figure 4.10: XRD diffractograms - Perimeter-Mask-Method vs Original Method. Peaks corresponding to the tetragonal phase of $MAPbI_3$, marked with full rhombus, the PbI_2 peak, marked with an asterisk and also peaks regarding the CuSCN and FTO layer (marked with cardinal and full circle, respectively)

4.1.3 Conclusions

The results presented previously clearly demonstrate the importance of having good contacts for the SC measurements. It also shows the impact that the different contact procedures have on the device performance, highlighting the sensitivity of the fabrication process of this kind of devices.

Although the above tested methods proved to do more harm than good to the SC devices, the issue remained: the tips could be damaging the films during I-V measures, undermining the device performance. As this issue was of critical importance to a better device performance, the solution found in order to tackle the issue of the film damage during I-V measures, without compromising the device performance (example: bad film quality due to the special contact procedures), was to combine the original contact procedure with the premise of the other contact types, that being fact that the devices should be prepared to deal with possible film damage caused by the tips during I-V measurements. In a sense, the solution found is a simplification of the contact procedures, where the substrates are still being striped of FTO on the designated areas (two lateral stripes), but these areas do not remain film-free as was done in the other contact procedures.

Given that this tackles the main issue while keeping the fabrication procedure simple, in comparison, there was no need to devote anymore batches to studying the contacts, being that this procedure is essentially the same as the original, only with the addition of the FTO removal step and an extra front-contact. The resulting substrate is represented in figure 3.4c), and this contact procedure is designated as Final-contact-method.

4.2 MACl as replacement for MAI in Perovskite precursor solution

This section reports the efforts on the study of MACl as a replacement for MAI in the Perovskite precursor solution. The main reason for this study is the fact that MACl is a significantly cheaper material when compared to MAI. As already mentioned, a low-cost device is one of the main goals to achieve, so that in the future this kind of devices are able to commercially compete with the dominant Silicon based solar devices. Another reason is the actual benefit of Cl incorporation in SC devices, which has been reported as a way to enhance the material properties by improving the carriers transport within the active Perovskite layer [28, 58, 59]. Devices fabricated using MACl as a precursor in Perovskite solution have been reported to have high film quality and integrate SC devices with high PCE [31, 36].

4.2.1 First batch of SC using MACl as a Perovskite solution precursor

As a starting point for the MACl study, the same solution reported by Hsinhan Tsai *et al.* was used for the fabrication of the first SC devices using the MACl precursor solution, meaning: a 0.217 M solution in DMF, with the spinning and annealing parameters described in 3.2.2 for MACl solutions. The Perovskite solution was deposited on top of a compact TiO_2 film using the TTIP solution. In the final seconds of the spinning step, 80 µl of toluene were dropped on the substrates. The resulting substrates are present in figure 4.11.

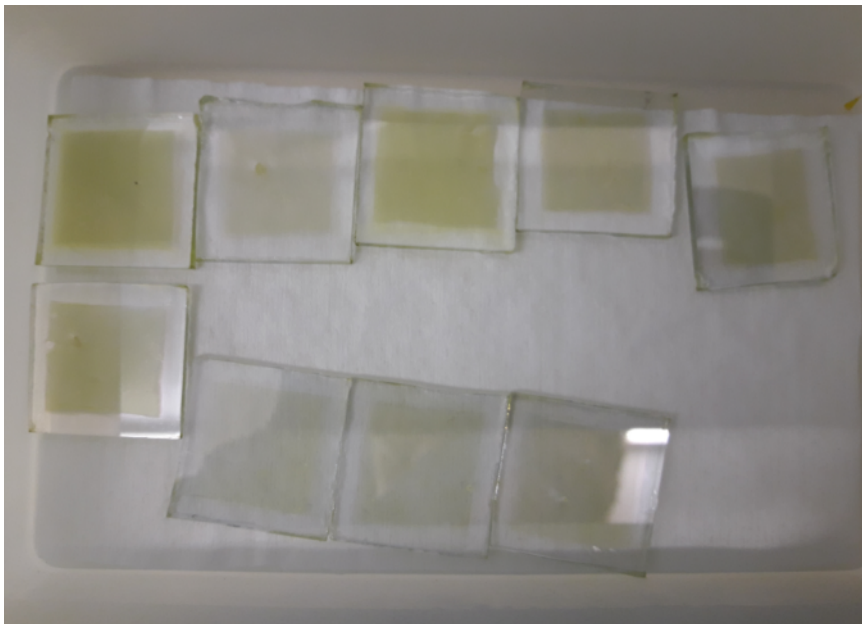

Figure 4.11: Substrates with compact TiO_2 and Perovskite layer using 0.217 M MACl solution in DMF. The difference in color tone is most likely related to small differences in the anti-solvent dropping step such as timing, distance to the substrate, or disperse flow.

As it can be seen in figure 4.11, the resulting samples present an almost transparent yellow color, indicating the formation of a PbI_2 film instead of the desired Perovskite. This is most likely related to the fact that the solution possessed low quantities of solutes compared to the solvent, which was pure DMF. Despite the fact that using an almost identical procedure, Hshihan Tsai and coworkers obtained good quality films, these unsatisfying results here obtained were, to some extent, expected, according to the work by B.Cai *et al.*, where it is explained that the use of a pure DMF Perovskite solution results in films of lower quality, due to the difference in solubility of the two solutes in the Perovskite solution, causing them to separate from one another during the DMF evaporation [35]. Considering the resulting substrates, no HTL was deposited on top.

4.2.2 Perovskite solvent variation

Taking into account the previous results, it was necessary to test Perovskite solutions with different solvents, before remaking a SC batch. This test was conducted in glass substrates as they were not intended to be full solar devices.

Three solutions were tested: pure DMF, pure DMSO and a mixture of DMF:DMSO (1:1 ratio). The concentration used for this test was 0.434 M with 80µl of toluene dropped in the final seconds of spinning. Figure 4.12 shows the resulting substrates.

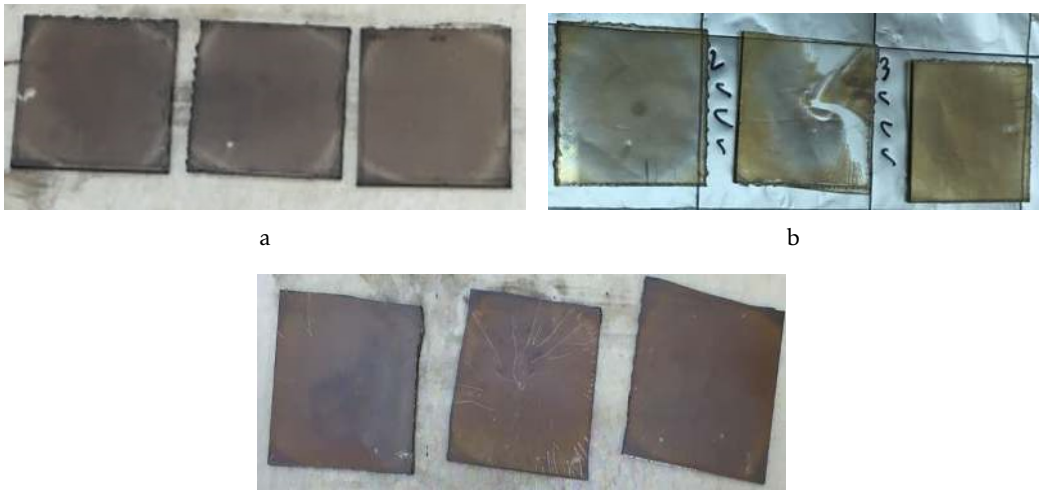

a b

c

Figure 4.12: Perovskite layer, from different solutions, deposited over glass - a) pure DMF; b) pure DMSO; c) DMF:DMSO (1:1).

From figure 4.12 a) it is possible to see an improvement on the films, by simply increasing the concentration from 0.217 M to 0.434 M. On the middle sample in 4.12b) the toluene dropping step suffered an accident, causing that non-uniform film. The middle sample in 4.12c) presents some streaks/flares which could be due to particles sitting on the substrate prior to the fluid dispense, solution sitting on the substrate for too long prior to spinning, or particles existing on the fluid being dispersed [46]. Some other

substrates also present some bubbles/holes which can also be attributed to the dispense tip being unevenly cut.

Although the substrates that were prepared using a pure DMF solution presented a better film color (closer to the desired dark-brown) when compared to the films produced with a lower concentration (4.11), these films still appear to be somewhat transparent indicating that this type of precursor solution is not ideal for SC fabrication.

The substrates where a pure DMSO solution was spin-coated, presented a transparent yellowish color, which is not ideal, indicating the formation of a PbI_2 film instead of the desired Perovskite. The sub-optimal surface coverage could be related to the low evaporation rate and high viscosity of DMSO.

The samples appearing to have better quality films are the samples where a mixed solvent of DMF:DMSO was used, showing a more desirable color, comparing to a pure DMF or DMSO substrate, while also having the least transparent films of this test. It also appears to produce an evenly spread and uniform film, especially on the sample on the right in 4.12c), quality that has been attributed to the formation of an intermediate complex (PbI_2-MAI-DMSO)[35].

It has been demonstrated that depositing perovskite on different substrates influences the material, and since the main goal is to develop SC devices, no further test were conducted in glass substrates. This test served only as an indication of the direction to follow after the first try, regarding concentration and solvents for the perovskite solution.

4.2.3 Second attempt at SC fabrication using MACl solution

Considering the results from the glass-substrate test, for this SC batch, a concentration of 0.642 M on DMF:DMSO (1:1) solvent mix was used for this solution. Only one out of three samples was possible to measure. The resulting I-V and P-V measurements, for some contacts of the sample, are represented in figure 4.13, with the respective values of interest for the best contact (contact 7 - reverse bias) are displayed in table 4.8, where it is both represented the forward and reverse bias numbers. The disparity when comparing contacts of the same substrate demonstrates the difficulty in obtaining a evenly spread and uniform film. The overall results are well below the desired values, even for the contact 7-rev. It is also possible to observe some form of hysteresis, since for the same contact using a forward bias results in slightly lower values than when a reverse bias is used for the I-V measures as shown in figure 4.13 for contacts 2, 5 and 7. This hysteresis effect could be simply due to the intrinsic properties of the perovskite material [60, 61], but also due to the interface between TiO_2 layer and perovskite layer as reported by P. Vivo *et al.*

These sub-optimal results are most likely due the film quality on the perovskite layer and the contact procedure (which had not yet been optimized). Although the perovskite film conditions chosen were the ones that presented the better results on the glass substrates, they still present a non-ideal color, and are still somewhat transparent. The fact

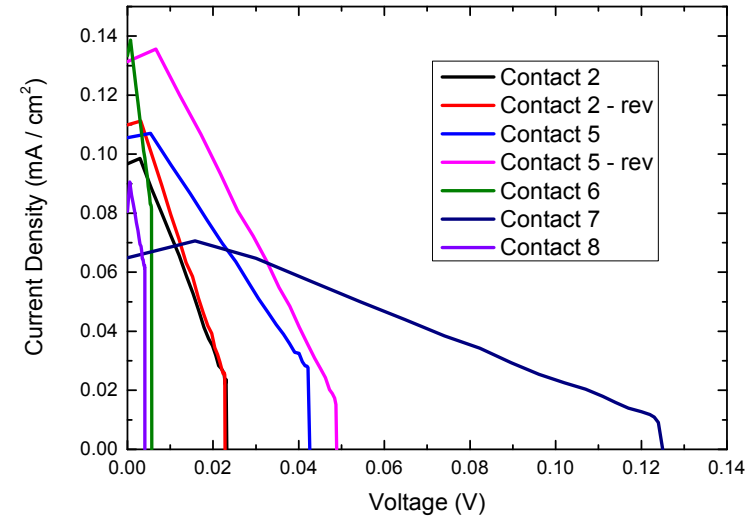

a

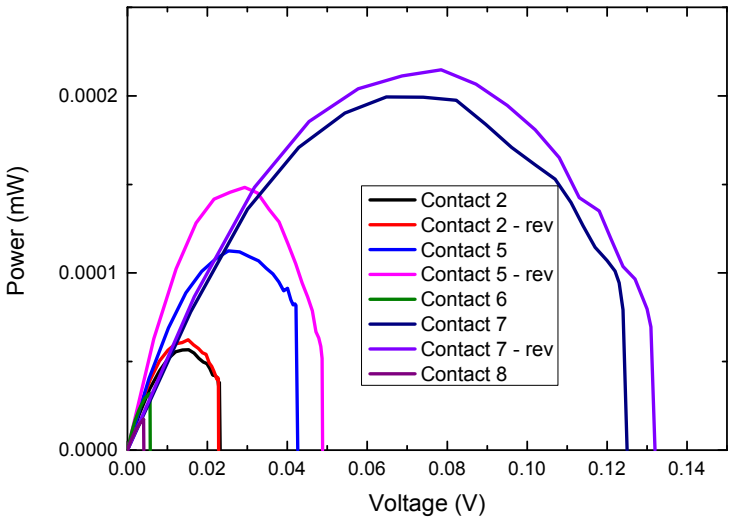

b

Figure 4.13: I-V a) and P-V b) measurements for SC devices using MACl solution. Devices fabricated using a compact TiO_2 using TTIP Solution; Perovskite layer using 0.642 M Solution (MACl:PbI_2 1:1), with 80 µl toluene droping, annealed for 10 minutes at 100° C; CuSCN layer annealed at 90° for 30 minutes.

Table 4.8: Performance values for the best curve present in 4.13 (contact 7 - rev)

SC Devices	Voc(V)	Jsc(mA/cm^2)	FF	Rsh(kΩ)	Rs(kΩ)	PCE(%)
Contact 7 - reverse bias	0.132	0.07	0.33	99.6	17.7	0.0031
Contact 7 - forward bias	0.125	0.065	0.35	69.6	14.4	0.0029

that no further samples could be measured, coupled with the fact that these kind of devices tend to suffer an extremely fast degradation, prevented from reaching a clear conclusion.

4.2.4 $TiCl_4$ as a precursor for the TiO_2 solution

Following the results from the last batch, given that the sample exhibited a small hysteresis behavior and overall low performance values, it was decided to test an aqueous TiO_2 precursor solution using $TiCl_4$, as this solution as been reported to slightly increase device performance, while at the same time countering the effects of hysteresis due to the formation of large crystals that help reduce the trap states induced from grain boundaries [55]. From the optical analysis in appendix C, using $TiCl_4$ for the TiO_2 layer, results in a compact layer with overall lower transmittance than for the compact layer produced via TTIP solution. Nonetheless, the difference is not significant and is worth to consider this new solution.

This batch was the first time that the etching-method for the contacts was thought to be hurting the devices and as such, a few SC were fabricated without the addition of the HTL (as it was observed that the solvent for the CuSCN solution has the ability do dissolve the Perovskite film). The I-V and P-V measurements for the best samples for each condition in this batch are present in figure 4.14 with the respective values of interest in table 4.9.

Table 4.9: Performance values for the I-V and P-V measures present in 4.14.

SC Devices	Voc(V)	Jsc(mA/cm^2)	FF	Rsh(kΩ)	Rs(kΩ)	PCE(%)
A	0.943E-2	0.99	0.294	0.17	0.11	0.003
K	0.311	1.61	0.135	1.52	4.20	0.068
L	0.88E-2	2.357	0.302	1.06	4.05	0.063
T	0.238	1.929	0.286	2.06	1.41	0.131

Analyzing figure 4.14 together with table 4.9, two tendencies seem to emerge: using $TiCl_4$ for the TiO_2 seems to result in devices with slightly higher Voc and Jsc with also an increase in PCE; devices without an HTL present a higher Jsc but lower Voc, with a small increase in PCE.

The increase in efficiency when using the c-TiO_2 layer produced with the $TiCl_4$ solution could not only result from a better interface between TiO_2 and the perovskite layer, but also to a more dense film, despite both not showing the desired grain-like features, as can be confirmed when observing image 4.15. Despite the fact that the c-TiO_2 fabricated using the $TiCl_4$ seems to improve the overall efficiency of the device, it was not the deciding factor to boost these devices to values close to the ones in literature, demonstrating that the main issue is most likely on the actual active layer of the SC (Perovskite).

Removing the HTL deposition step from the fabrication procedure results in devices with higher efficiency, corroborating the assumption that the contact procedure was not

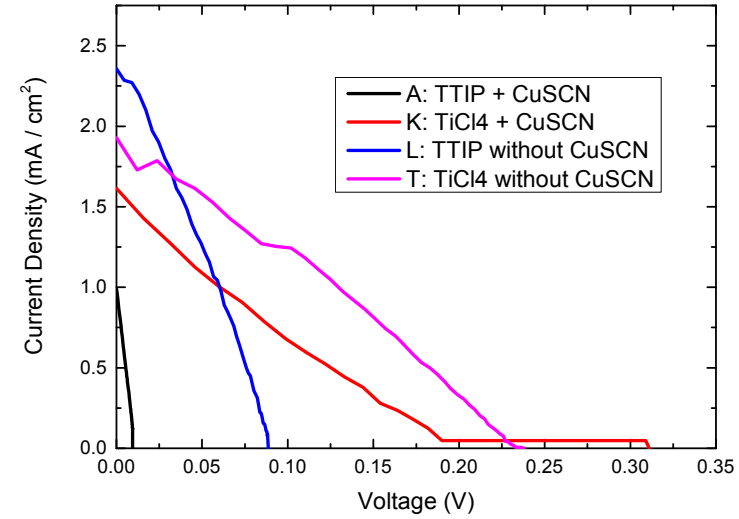

a

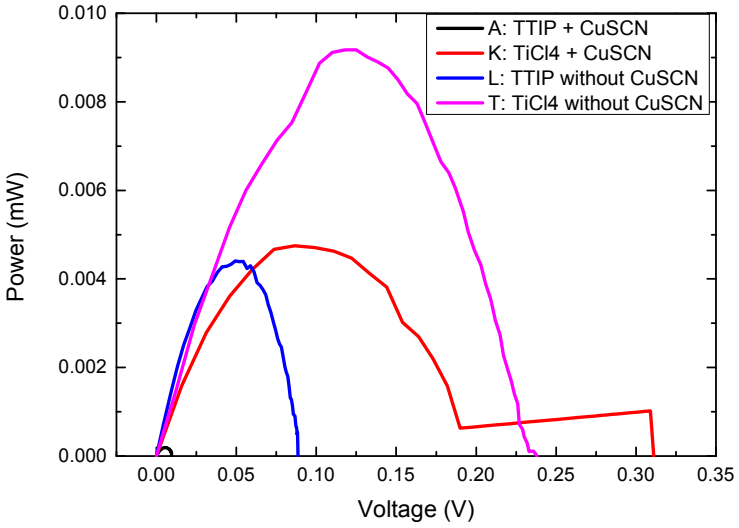

b

Figure 4.14: I-V a) and P-V b) measurements for SC devices using MACl solution. Devices fabricated using a compact TiO_2 using TTIP solution or $TiCl_4$ solution; Perovskite layer using 0.642 M Solution (MACl:PbI_2 1:1), with 80 µl toluene droping, annealed for 10 minutes at 100° C; CuSCN layer annealed at 90° C for 30 minutes.

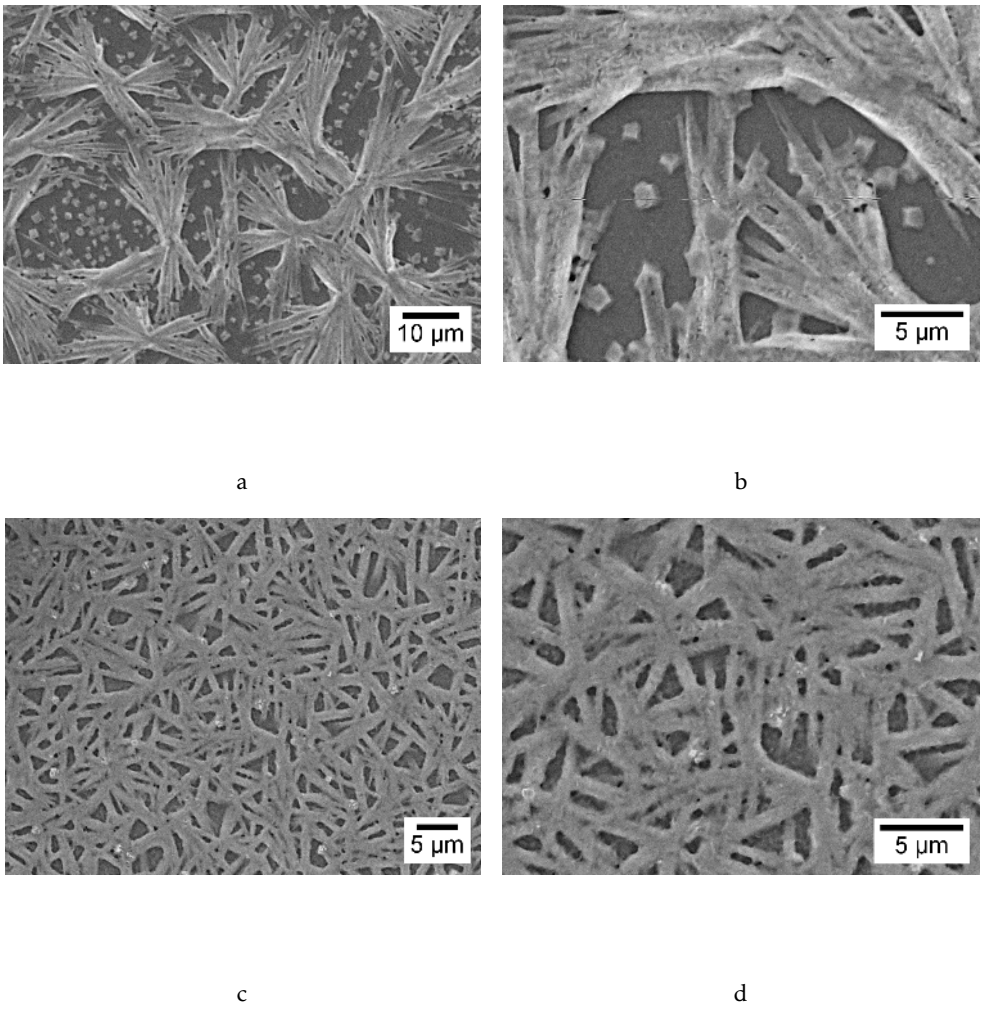

Figure 4.15: Topological SEM images: influence of different TiO_2 precursor solutions on perovskite film morphology. a) and b) images refer to a sample prepared using TTIP solution for the ETL layer, while c) and d) images refer to a sample prepared using $TiCl_4$ solution for the ETL.

improving the device performance. Although the devices without HTL present better results, they degraded much faster than the devices with an HTL, which is expected, as this layer also helps protect the Perovskite layer from degradation. This means that simply removing the HTL is not ideal.

Both conclusions that were drawn, point in one direction: the main parameter to improve these devices lies within the Perovskite layer.

4.2.5 Solvent ratio variation and anti-solvent test

As demonstrated previously, the Perovskite layer is the main focus in obtaining fully functional SC devices. Following the test from 4.2.2, where it was found that a mixture of DMF:DMSO works better than pure DMF or DMSO, it was tested different ratios for this mixture, namely 1:1, 2:1 and 1:2 ratios of DMF:DMSO, in order to understand what

type of ratio benefits these devices the most.

Together with the solvent ratio test, an anti-solvent agent test was performed, using toluene and chlorobenzene, as the anti-solvent droping is a critical step for good quality perovskite film formation.

During the fabrication of these samples, immediately there was a substantial difference when using the different anti-solvents, seen with the naked eye in figure 4.16.

Figure 4.16: Film variation when using toluene(3 left samples) and chlorobenzene (3 right samples) as anti-solvent agents. Perovskite film using a 0.642 M MACl:PbI_2 in 1:1 DMF:DMSO solution with 80 µl droping of anti-solvent agent, deposited over c-TiO_2.

Analyzing figure 4.16, it is clear that using chlorobenzene as an anti-solvent agent produces better quality films, as the chlorobenzene samples show a darker color along with a mirror-like effect. Although none of the samples present the grain-like features that are desired in these films, the chlorobeneze samples show a more dense film and no spike features as shown in figure 4.17.

Comparing the samples produced with a 2:1 DMF:DMSO solvent ratio (figure 4.18) with the samples using the 1:1 ratio, the samples with the 2:1 solvent ratio (both with toluene and cholorobenzene) display films of better quality when compared to the 1:1 solvent ratio samples. Despite the toluene samples still presenting spike/needle structures, the film appears to be more compact and dense when compared with the toluene sample from the 1:1 solvent ratio (a) and b) of figure 4.17). The Perovksite film fabricated using chlorobenzene as an anti-solvent agent shows virtually no holes on the film, despite the fact that it is still not possible to observe the desired grain-like features.

The overall quality of the films appears to improve when the DMF fraction of the solvent mix is increased, both with the toluene and chlorobenzene samples.

When compared to the 2:1 solvent ratio samples, the samples fabricated using a 1:2 DMF:DMSO solvent ratio (4.19) seem to present lower quality films, more noticeably when comparing the toluene samples of both ratios. Using the 1:2 ratio results in films with more spikes on the toluene sample, and more holes on the sample with chlorobenzene as an anti-solvent agent.

The overall result seems to point to better quality films when using a 2:1 DMF:DMSO solvent ratio, which is in agreement with the previous work [34], where the best results were obtained when using a ratio with more DMF than DMSO. This fact might be related to the high viscosity and low evaporation rate of DMSO, making the production of a

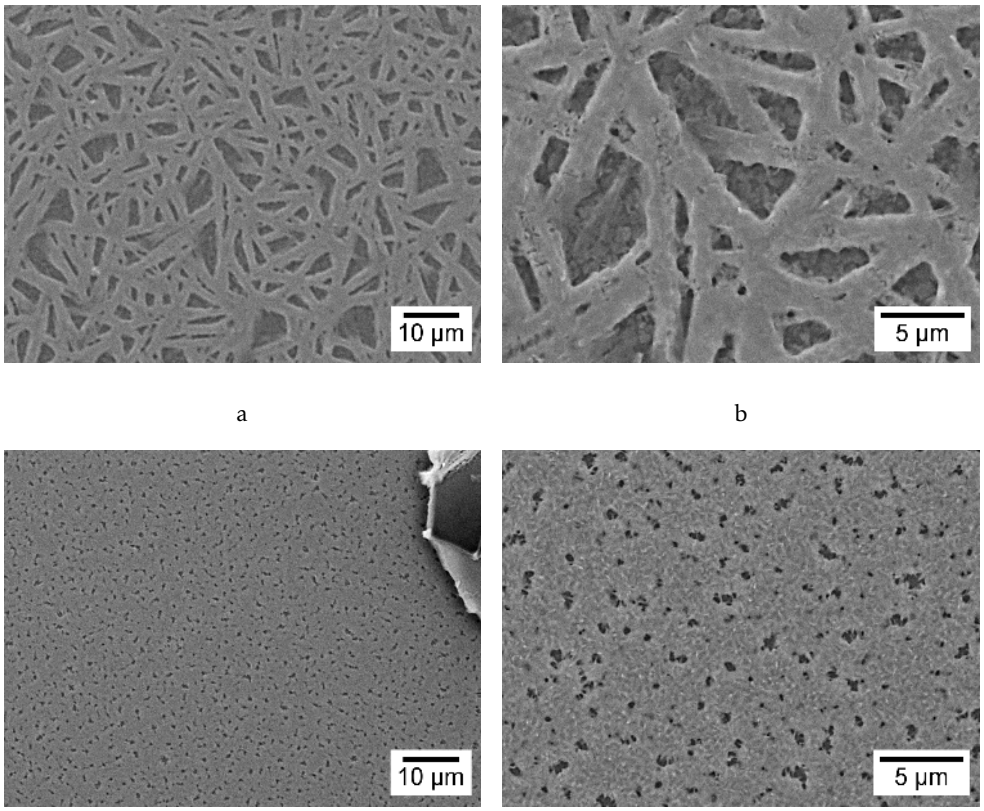

Figure 4.17: Perovskite film using a 0.642M in a 1:1 DMF:DMSO ratio precursor solution with 80 µl of anti-solvent agent, deposited over compact TiO_2. a) and b) refer to the sample with 80 µl of toluene; c) and d) refer to the sample with 80 µl of chlorobenzene.

uniform and homogeneous film more difficult. DMSO acts as solvent, but also as a coordination agent, through the formation of the PbI_2-MAI-DMSO complex, retarding the rapid reaction of MAI and PbI_2 during DMF evaporation stage, as it was already mentioned. After DMF evaporation, it is desirable a fast crystallization into a crystalline film in order to avoid humidity degradation [34], which might be delayed when there is an agent with a low evaporation rate (DMSO) in too high quantities as in the 1:2 DMF:DMSO solvent ratio solution.

Across the samples with different ratios, it is clear that using chlorobenzene as an anti-solvent agent produces Perovskite films of better quality, making it the anti-solvent of choice for the following tests.

4.2.6 Perovskite solution concentration variation

It has been reported that concentration of the Perovksite solution is a critical parameter that influences device performance [37], and given that most likely the cause for the poor performance of the devices in this study lies within the perovskite layer, testing difference concentrations could help reach a better device performance.

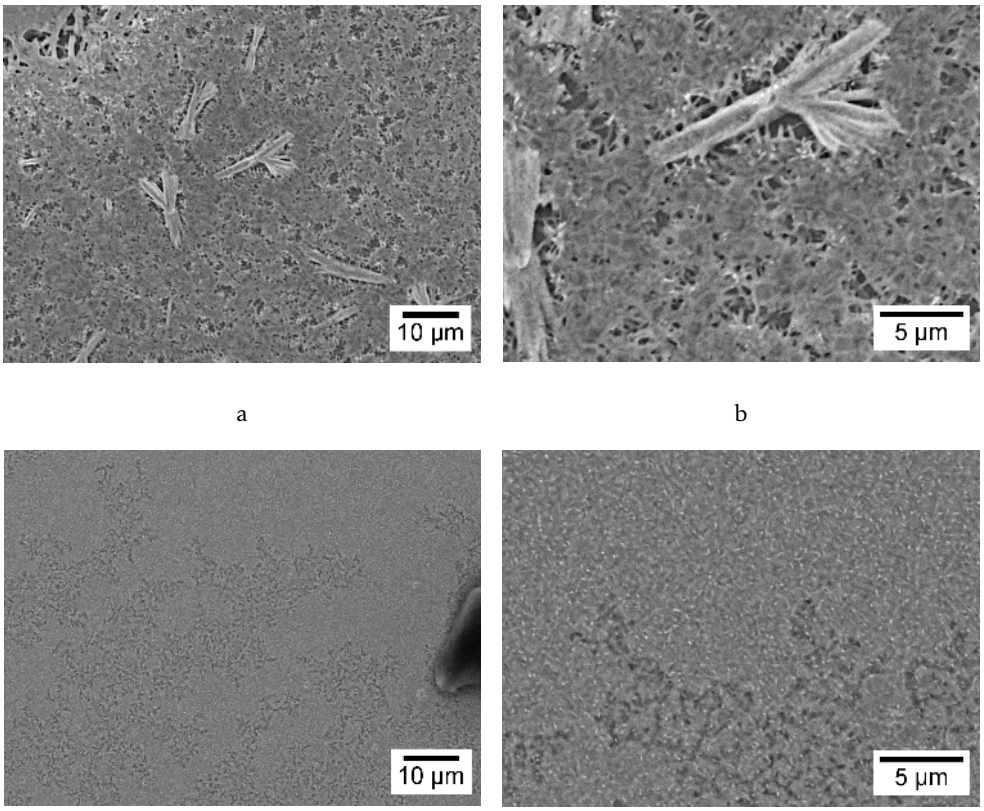

Figure 4.18: Perovskite film using a 0.642M in a 2:1 DMF:DMSO ratio precursor solution with 80 µl of anti-solvent agent, deposited over compact TiO_2. a) and b) refer to the sample with 80 µl of toluene; c) and d) refer to the sample with 80 µl of chlorobenzene.

Table 4.10: Perovskite peak parameters of the diffractogram in 4.23 - Sample A2. $MAPbI_3$ peaks at 14.08° and 28.45°; $MAPbCl_3$ peaks at 15.52° and 31.39° [24, 59].

2θ (◦)	Intensity (a.u.)	FWHM (◦)
14.08	86180.2	0.122
15.52	28418.6	0.142
28.45	30009.2	0.181
31.39	5192.0	0.205

Three different concentrations were used for this test: 0.642 M, 0.868 M and 1.085 M. These solutions were spin-coated on top of a compact TiO_2 layer using the TTIP solution, with normal deposition and annealing parameters. For this test, chlorobenzene was used as anti-solvent.

The influence of solution concentration is evaluated through the SEM images in figures 4.20, 4.21 and 4.22, coupled with the XRD diffractograms of figure 4.23, where the empty rhombus marks the $MAPbCl_3$ peaks. The respective values of interest for the Perovskite peaks of the XRD diffractograms of each sample can be found in tables 4.10, 4.11 and 4.12.

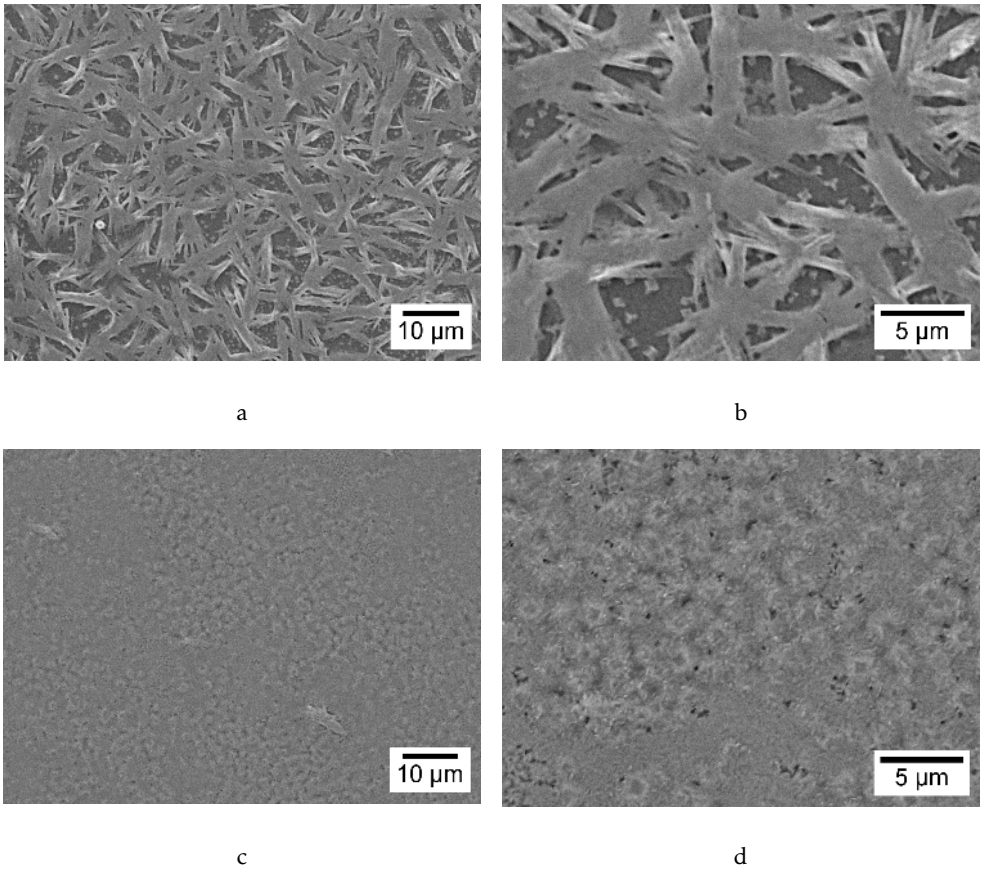

Figure 4.19: Perovskite film using a 0.642 M in a 1:2 DMF:DMSO ratio precursor solution with 80 µl of anti-solvent agent, deposited over compact TiO_2. a) and b) refer to the sample with 80 µl of toluene; c) and d) refer to the sample with 80 µl of chlorobenzene.

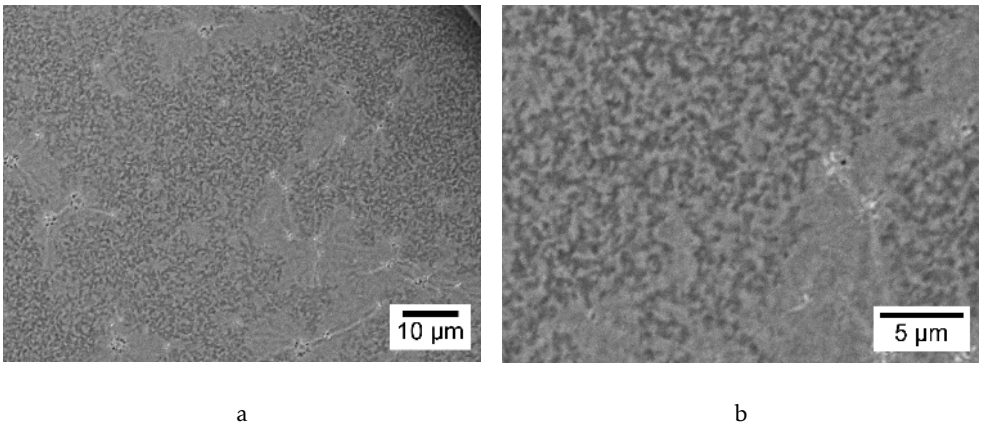

Figure 4.20: Perovskite film using a 0.642 M in a 2:1 DMF:DMSO ratio precursor solution with 80 µl of chlorobenzene, deposited over compact TiO_2.

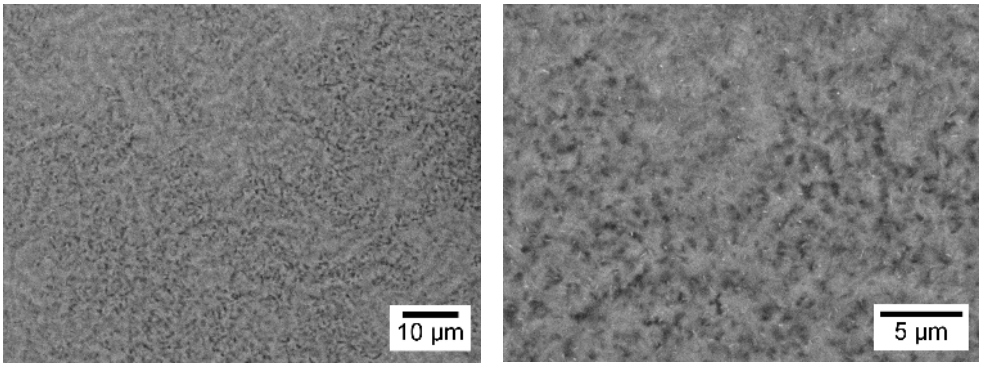

a b

Figure 4.21: Perovskite film using a 0.868 M in a 2:1 DMF:DMSO ratio precursor solution with 80 µl of chlorobenzene, deposited over compact TiO_2.

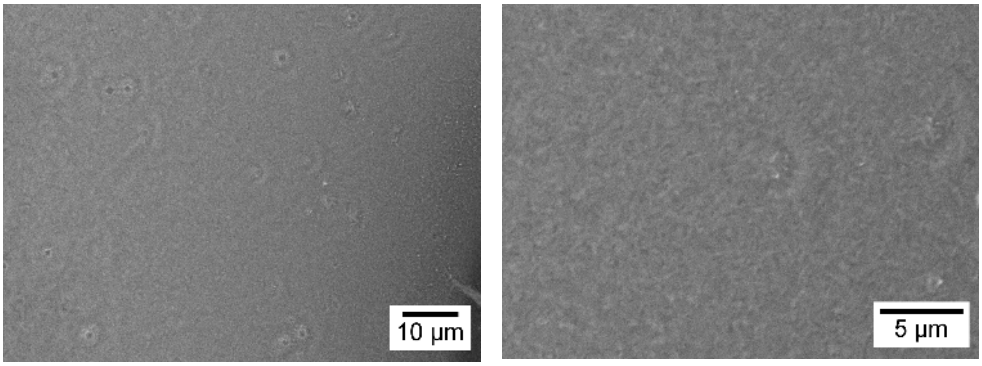

a b

Figure 4.22: Perovskite film using a 1.085 M in a 2:1 DMF:DMSO ratio precursor solution with 80 µl of chlorobenzene, deposited over compact TiO_2.

Table 4.11: Perovskite peak parameters of the diffractogram in 4.23 - Sample K2. $MAPbI_3$ peaks at 14.08° and 28.45°; $MAPbCl_3$ peaks at 15.52° and 31.39° [24, 59].

2θ (◦)	Intensity (a.u.)	FWHM (◦)
14.08	81472.6	0.250
15.52	19339.7	0.253
28.45	66971.9	0.177
31.39	7917.5	0.194

Table 4.12: Perovskite peak parameters of the diffractogram in 4.23 - Sample T2. $MAPbI_3$ peaks at 14.08° and 28.45°; $MAPbCl_3$ peaks at 15.52° and 31.39° [24, 59].

2θ (◦)	Intensity (a.u.)	FWHM (◦)
14.08	90581.1	0.254
15.52	33948.4	0.251
28.45	80806.6	0.176
31.39	15047.3	0.188

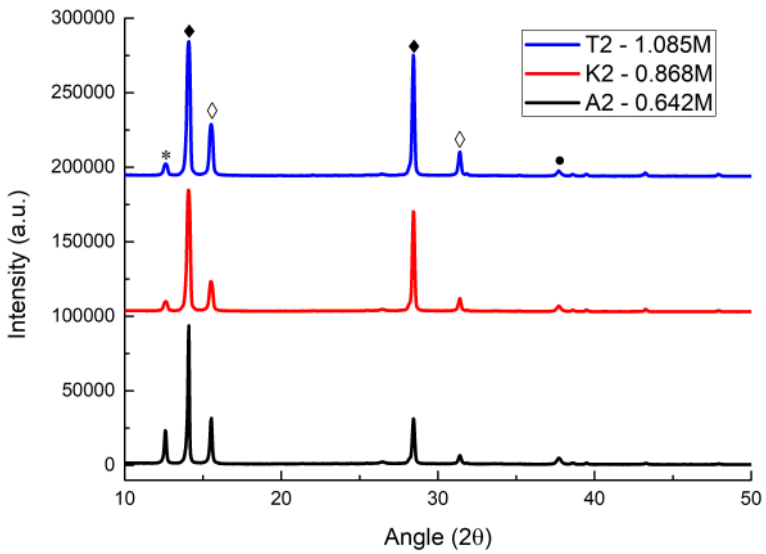

Figure 4.23: XRD diffractograms of samples of fabricated using 3 Perovskite solutions with different concentrations. Peaks corresponding to the tetragonal phase of $MAPbI_3$, marked with full rhombus, $MApBCl_3$ peaks marked with empty rhombus, the PbI_2 peak, marked with an asterisk and also peaks regarding FTO layer marked with full circle.

Table 4.13: PbI_2 peak parameters of the diffractogram in 4.23, across all 3 samples.

Sample	Intensity (a.u.)	FWHM (∘)
0.642M	21610	0.159
0.868M	6141.6	0.288
1.085M	7528.3	0.292

Increasing the concentration of the solution appears to progressively produce a smoother and more compact film, as expected. Despite the seemingly increase in film quality, as the concentration increases no grain-like features were found.

The XRD diffractograms confirms that the produced films were indeed crystalline, although no grain-like features were observed during SEM analysis. There is no sign of the desired $MAPbI_3 - xCl_x$ phase, only the undesirable high band-gap semiconductor $MAPbCl_3$ phase.

Comparing the peak values displayed in tables 4.10, 4.11 and 4.12, the $MAPbI_3$ peak at 14.08°(110) and the $MAPbCl_3$ peak at 15.52°(100), seem to broaden as the concentration of the perovskite solution increases, possibly indicating an increase in strain [62].

As it was not possible to obtain $MAPbI_3{-}xCl_x$, it is desirable to minimize the $MAPbCl_3$ phase as much as possible, which as been correlated to solution aging [36]. The sample fabricated using the 0.868 M solution shows a higher $MAPbI_3/MAPbCl_3$ peak ratio (aprox. 19.19% $MAPbCl_3$ phase), while also presenting a less pronounced PbI_2 peak (4.13). These two facts make the 0.868M solution, the best solution (out of the three concentrations tested) for the production of Perovskite thin films, using a MACl:PbI_2 solution.

4.2.7 Conclusions

Although it was not possible to obtain record-breaking solar cell devices, MACl still shows promise as a replacement for MAI, due to its lower cost and proven ability to produce good quality films [36] and the ability to obtain the $MAPbI_3$ Perovskite phase. The SC devices produced using the MACl solution still had an inferior contact procedure and as such, to some extend, this fact might have affected the device performance.

The best conditions for Perovskite film fabrication in the lab using the MACl solution are summarized in table 4.14 . These conditions are not meant to be taken as the ideal fabrication conditions for the setup, but as the starting point for future tests using this Perovskite solution.

Table 4.14: Best fabrication conditions for Perovskite films, using a MACl:PbI_2 solution.

Concentration(M)	DMF:DMSO ratio	Hot-Casting(∘C)	Anneal parameters
0.868	2:1	90	10 minutes at 100°C

4.3 Optimization of SC devices

This section reports the efforts in optimizing the SC devices developed in the previous work [34], which was the main objective for this master thesis. The focus is to understand and improve device performance.

The main issue with the previously developed devices was the low current density and low FF. These characteristics were attributed to the low bulk density of the active Perovskite layer, combined with high series resistance and low shunt resistance.

All the SC devices fabricated from this point forth, use the Final-contact-method procedure.

4.3.1 Concentration and Annealing time

As a starting point for the device optimization study, two solution concentrations were tested with different annealing times, 60 and 15 minutes. The fabrication of each solution only varied in concentration (1 M and 1.5 M), both using a 4:1 DMF:DMSO ratio as previously reported [34]. For both cases, the solutions were stirred at 70° C for 24 hours and deposited with the same spinning parameters (as described in 3.2 for MAI precursor solutions). A fixed amount of 100 µl of anti-solvent agent (cholorobenzene) was used with both solutions. Regarding annealing temperatures, for the Perovskite film deposited from the 1 M solution, it was annealed at 100° C, while for a film produced from the 1.5 M solution, an annealing temperature of 120° C was used [34].

The motivation for testing a shorter annealing time was not only as a way to reduce production costs and time, but mainly due to the fact that the prolonged exposure to heat

from the hot-plate could actually, coupled with a prolonged exposure to ambient air, have been degrading the film, which could explain the observed bulk density (figure 4.24).

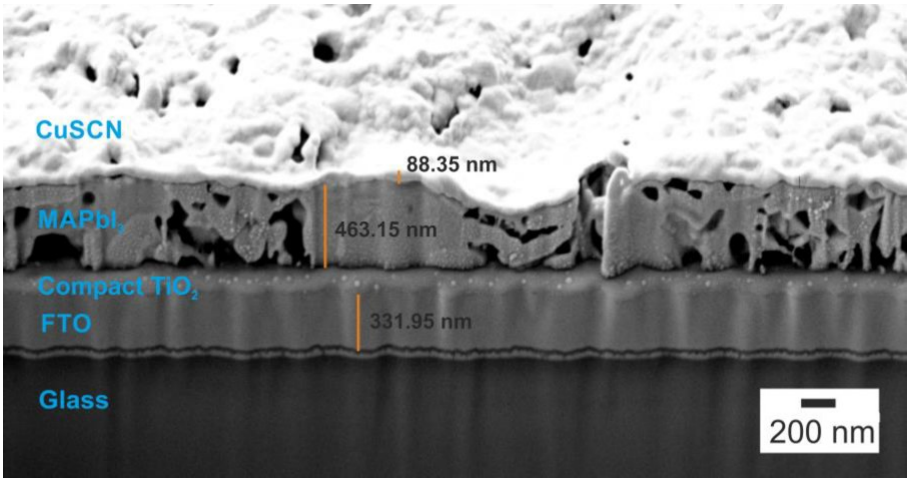

Figure 4.24: Cross section SEM image of full SC structure of previously developed devices. Perovskite film using 1M solution deposited over compact TiO_2 [34].

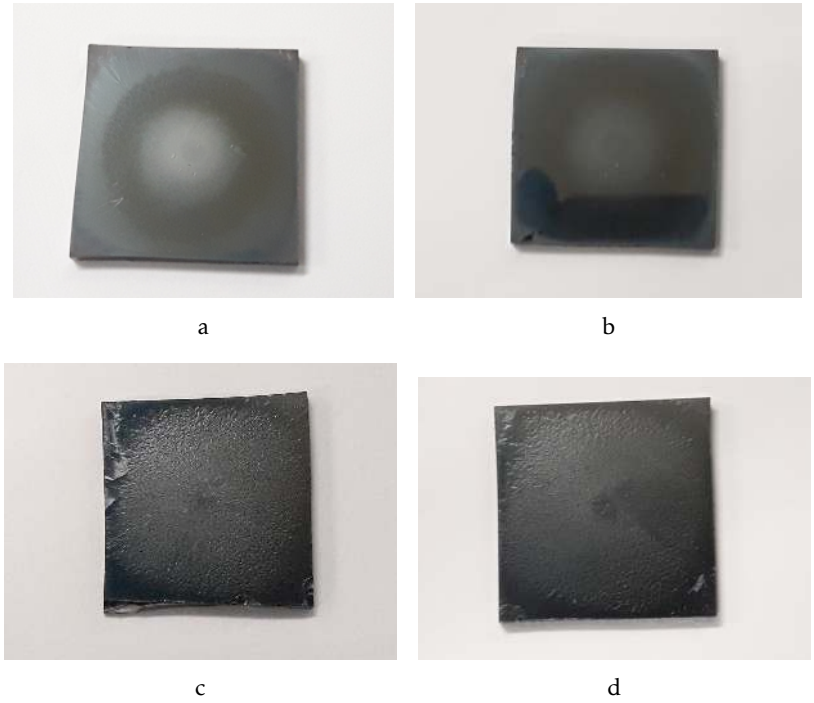

Figure 4.25: Perovskite films produced over compact TiO_2, using different solution concentration and annealing time; 1 M samples: a) 15 minutes, b) 60 minutes; 1.5 M samples: c) 15 minutes, d) 60 minutes.

In figure 4.25 it is possible to observe the resulting films, where the samples with a film produced with a 1 M solution exhibit a dark color with a mirror-like effect. The samples exhibit a ring/circle mark, which is probably due the spin chuck of the spinner.

The samples with a Perovskite film produced from a 1.5 M solution indeed show a dark film but no mirror-like feature, actually seemingly exhibiting a rough surface. This morphology of the films from the 1.5 M solution could be related to the deposition step, as it was observed during fabrication, that 1.5M solution had more difficulty spreading on the substrate (prior to spin) when compared to the 1 M solution.

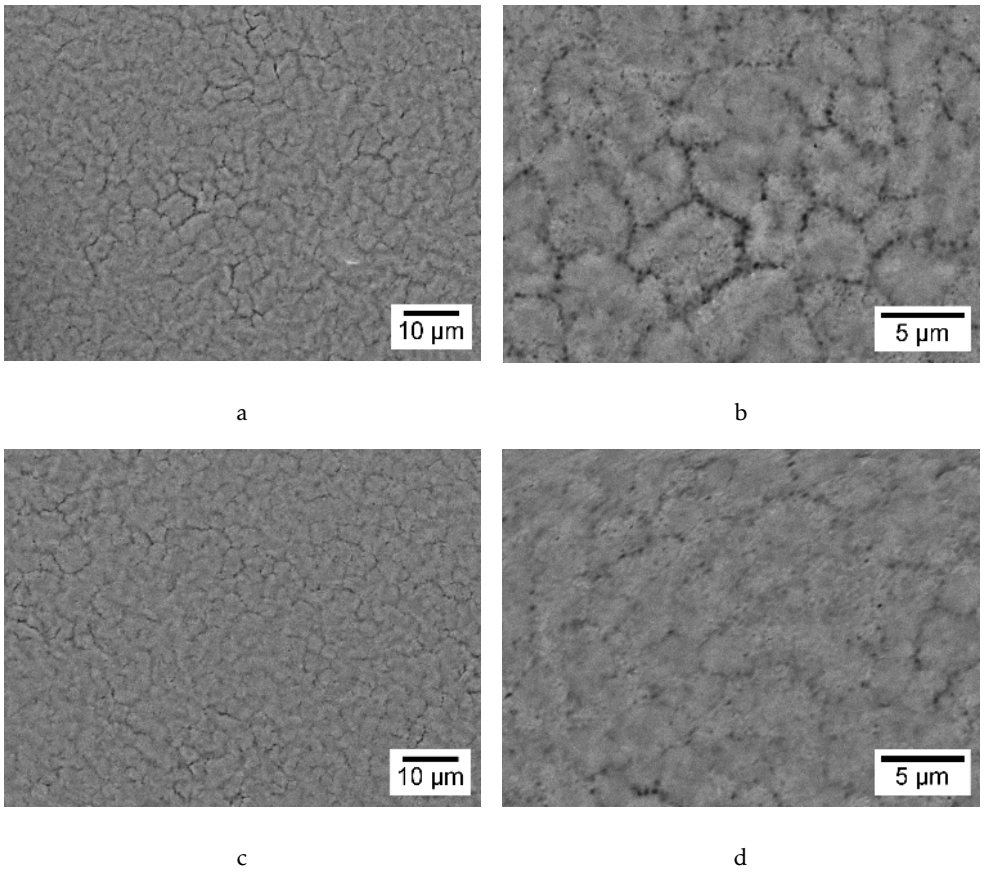

Figure 4.26: Perovskite films produced over compact TiO_2, using 1 M solution; a) and b): 15 minutes annealing at 100° C; c) and d) 60 minutes annealing at 100°C.

Annealing time does not seem to affect much the films (when examined with the naked eye), although a slight difference is noticeable when analyzing the SEM images in figures 4.26 and 4.27, where the sample annealed for 15 minutes appears to have more defined grain boundaries. Nevertheless, both annealing times result in a crystalline film with visible micrometer grains, for the case of the 1 M solution samples.

Both annealing times on the samples fabricated by 1.5 M solution, show no visible grains as was expect from what can been seen with the naked eye on figure 4.25.

From this test it is clear that the best solution concentration is 1 M, when all other parameters are fixed. 1M Perovskite solution has been demonstrated to produce slightly thinner films when compared to the 1.5 M solution, as expected [34].

Since no major differences were observed in the SEM images, regarding the different annealing times, 15 minutes of annealing is the time chosen for the fabrication process,

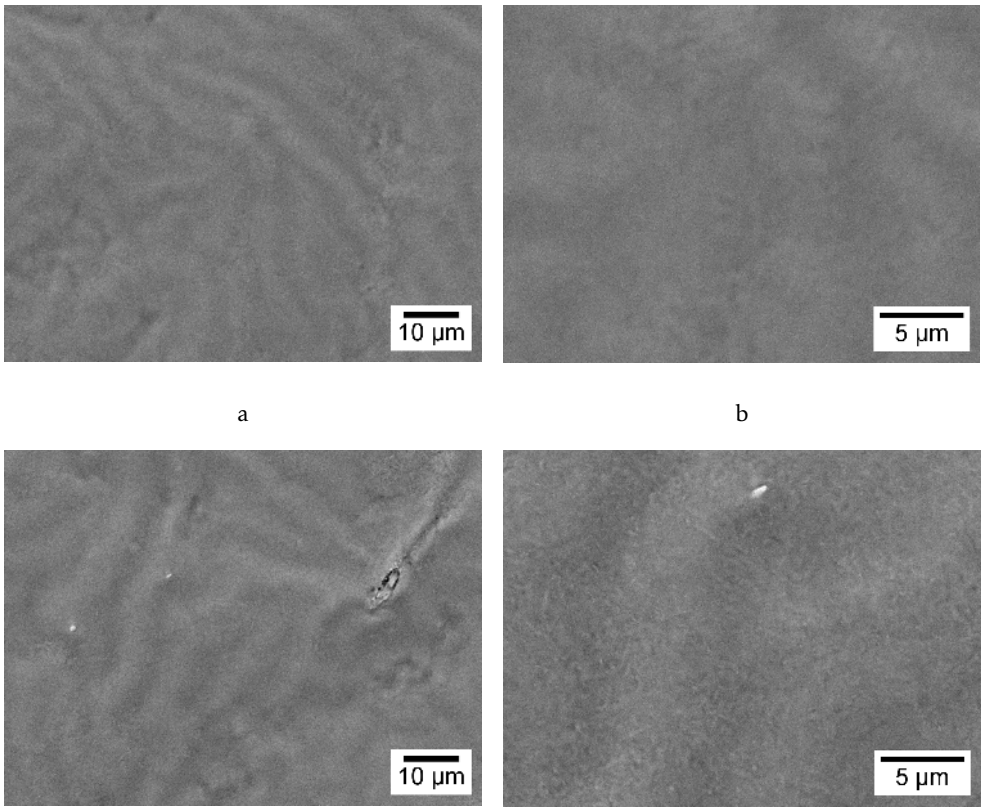

Figure 4.27: Perovskite films produced over compact TiO_2, using 1.5 M solution; a) and b): 15 minutes annealing at 120° C; c) and d) 60 minutes annealing at 120° C.

as this time reduction implies lower production costs.

4.3.2 TiO_2 Mesoporous layer

As already stated, the main issue of the devices fabricated until now, is the low current density and FF, preventing the devices from reaching higher efficiency, which has been attributed to low bulk density. The devices also suffered from high series resistance couple with low shunt resistance.

The incorporation of a mesoporous layer has been reported to increase device performance, due to an improved interface between active layer, acting as a scaffold for the Perovskite film and helping with the carrier transport, while also helping to reduce hysteresis sometimes observed in these devices [41, 42].

The I-V and P-V measurements for the best devices with and without a mesoporous layer are presented in figure 4.28 with the corresponding performance values in table 4.15.

When compared to the best device from the previous work, there is a significant increase in device performance, where the best performing device until now had a PCE

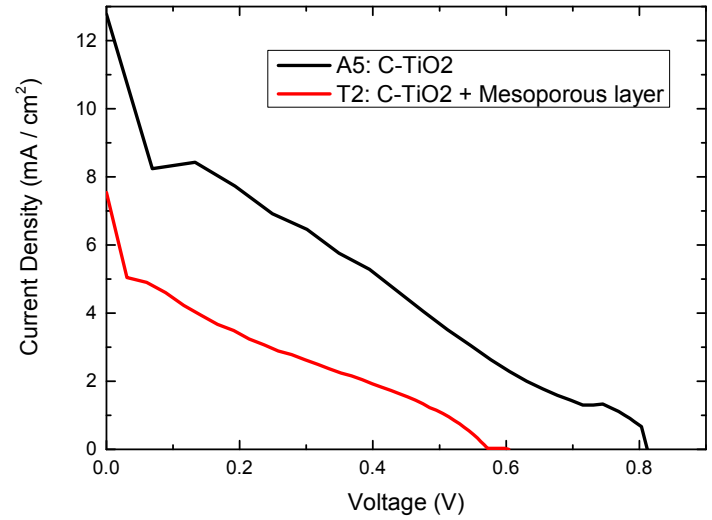

a

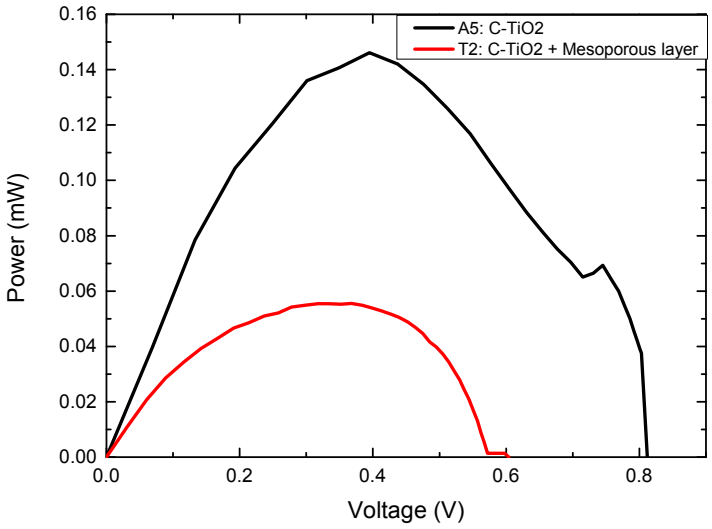

b

Figure 4.28: I-V a) and P-V b) measurements of best SC devices with and without mesoporous layer. Perovskite films produced over compact TiO_2 or compact plus Mesoporous TiO_2, using 1 M solution annealed for 15 minutes at 100° C; CuSCN deposited as HTL on top.

Table 4.15: Performance values for the samples in 4.28

SC Devices	Voc(V)	Jsc(mA/cm^2)	FF	Rsh(kΩ)	Rs(kΩ)	PCE(%)
Compact TiO_2	0.812	12.77	0.201	0.53	1.36	2.09
With Mesoporous TiO_2	0.604	7.54	0.174	0.61	2.57	0.79

Table 4.16: Perovskite peak parameters of the diffractogram in 4.30, c-TiO_2 sample.

Peak(◦)	Intensity (a.u.)	FWHM (◦)
14.03	16609.5	0.147
28.3	7140.4	0.168

Table 4.17: Perovskite peak parameters of the diffractogram in 4.30, mp-TiO_2 sample.

Peak(◦)	Intensity (a.u.)	FWHM (◦)
14.03	16302.1	0.151
28.3	7254.1	0.166

of 0.414%, versus the now obtained 2.09% PCE with these devices, with current density, open-circuit voltage and fill-factor also reaching higher values [34].

This significant increase in performance is attributed mainly to an increase in bulk density of the Perovskite film, as it is possible to confirm when comparing the cross-section images in figures 4.24 and 4.29 a).

The increased bulk density is most likely related to the solution aging, as this method has been related to crystallinity and film quality improvement in general [36]. It can also be related to the reduced annealing time, as this reduction implies less heat exposure as well reducing the exposure time to ambient air before HTL deposition. The improved contact-method procedure is most likely playing a key role as well, as this was the first batch where it was possible to measure every sample.

Although most devices present in the literature employ a mp-TiO_2 layer, here the device with the mesoporous layer has a lower performance when compared with the device without the addition of said layer. Figure 4.29 b) shows that, despite the visible improvement of the TiO_2-$MAPbI_3$ interface due to the addition of the mesoporous layer acting as a scaffold for the Perovskite, the combined thickness of the TiO_2 layers (compact and mesoporous) is substantially larger than a single c-TiO_2 layer. The Perovskite layer also seems to suffer from an increased thickness when deposited on top of the mesoporous layer of TiO_2. An increase of thickness in both the TiO_2 layer (compact and mesoporous) coupled with an increase of the Perovskite layer might explain the lower performance of these devices.

The XRD diffractograms in figure 4.30 reveals for both samples the presence of (110), (112), (202), (220), (310), (224), and (314) planes in positions 14.03°, 19.9°, 24.45°, 28.3°, 31.7°, 40.46° and 43.03°, respectively [34]. The XRD diffractograms coupled with tables 4.17 and 4.16, where the peak values for the most prominent Perovskite peaks are detailed, show no clear difference in the films deposited on compact TiO_2 or with the addition of a mesoporous layer.

Due to the higher performance of the SC composed without the addition of the mesoporous layer, all future devices are built without this layer.

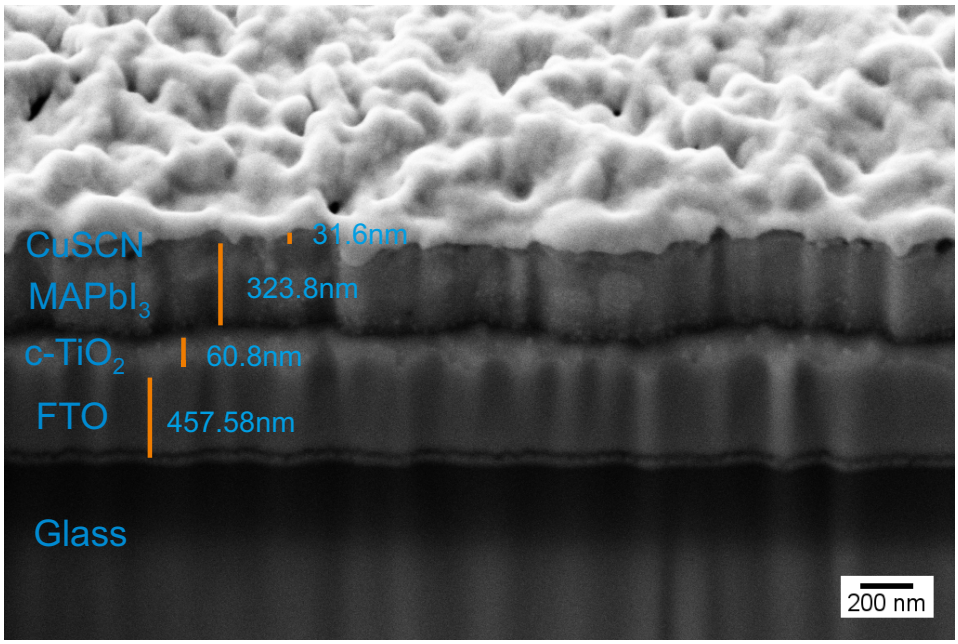

a

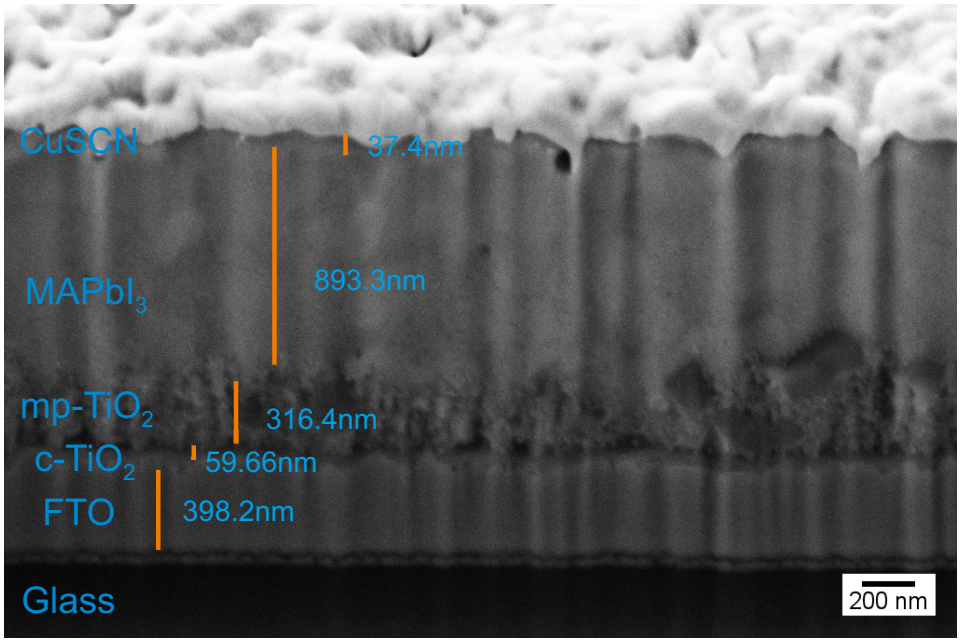

b

Figure 4.29: Cross-Section SEM images of full SC structure without a) and with b) addition of a mesoporous TiO_2 layer on top of compact TiO_2 layer.

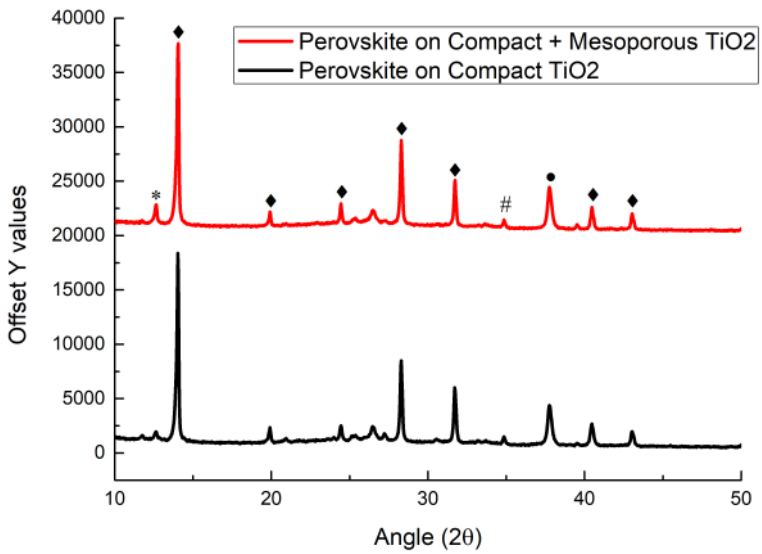

Figure 4.30: XRD diffractograms of Perovskite films deposited on top of c-TiO_2 and mp-TiO_2. Peaks corresponding to the tetragonal phase of $MAPbI_3$, marked with full rhombus, the PbI_2 peak, marked with an asterisk and also peaks regarding the CuSCN and FTO layer (marked with cardinal and full circle, respectively).

4.3.3 CuSCN as HTL

As it was already mentioned, during the fabrication of some of the SC devices, while using the etching-method contact procedure, it was observed that the solvent for the CuSCN solution actually had the ability of dissolving the Perovskite film and as such, it was thought to actually degrade the film. This film degradation was thought to be one of the causes for the low FF observed in the devices. During the spin step of the HTL layer, the samples actually turn transparent, losing their characteristic dark color, only to regain said characteristic during the annealing of the HTL, which is indicative of some sort of reaction between the deposited HTL solution and the Perovskite film.

This problem has been reported by N. Ahora *et al.*, where it was used a different approach to the deposition step of the CuSCN HTL. This research group uses a dynamic deposition method, that shall be referred in this document has "Drop-Cast method".

This method helps to minimize Perovskite degradation through a faster evaporation of the solvent of the HTL solution. The faster evaporation happens when the solution is dropped on a spinning substrate [43], as oppose to the traditional deposition procedure where the solution is first dropped onto the substrate and then the substrate is made to spin, as described in more detail in chapter 3.

Through the analysis of figure 4.31, where the I-V and P-V curves for the best devices (for each condition) of the batch are displayed, using the Drop-Cast method results in a device with overall better performance, as it can be confirmed through the values in table 4.18.

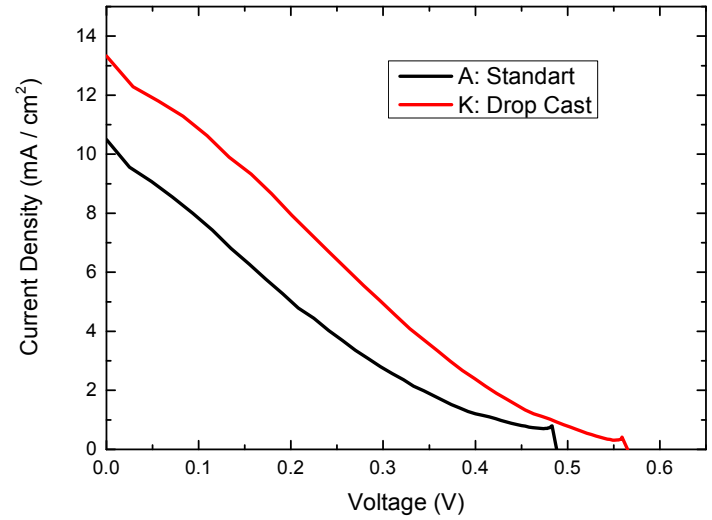

a

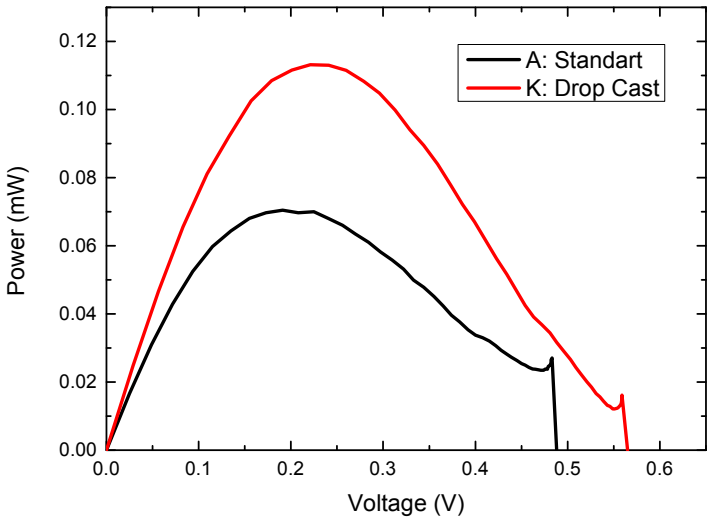

b

Figure 4.31: I-V a) and P-V b) measurements of best SC devices with different deposition methods for HTL. Perovskite films produced over compact TiO_2, using 1 M solution annealed for 15 minutes at 100° C; CuSCN deposited as HTL on top.

Table 4.18: Performance values for the samples in figure 4.31.

SC Devices	Voc(V)	Jsc(mA/cm^2)	FF	Rsh(kΩ)	Rs(kΩ)	PCE(%)
Standart deposition	0.488	10.50	0.197	0.53	0.8	1.01
Drop-Cast method	0.565	13.33	0.215	0.55	0.61	1.62

The increase in device performance, with improvement in all the performance values (table 4.18) is attributed to a reduced Perovskite degradation, induced by the deposition of the HTL using the Drop-Cast method. This assumption is corroborated when analyzing the Cross-Section images of figure 4.32, where the HTL appears to be more easily discerned, when comparing to the device in figure 4.29a), where the HTL although visible, seems to have merged with the Perovskite layer.

Another effort was made to counteract the Perovskite degradation during HTL deposition. Since the problem lies with the actual solvent and not the CuSCN, a new CuSCN solution was made using aqueous ammonia as reported by N.Wijeyasinghe *et al.* [44].

This new solution proved unsuccessful in solving the degradation problem, in fact elevating the problem even further as it can be seen from figure 4.33, as using this solution removes all together the Perovskite film from the substrate. As such, no further CuSCN was deposited using this solution.

As mentioned, this test aims to improve device performance through minimization of the HTL-induced Perovskite degradation, hoping to increase the FF of the SC devices. Table 4.19 reveals in fact a clear improvement when using this HTL deposition method. Analyzing these numbers it is safe to say that the Drop-Cast method indeed reduces Perovskite degradation, which in turn is translated into an overall performance enhancement of the device.

Table 4.19: FF values taken from the batch devoted to testing Diethyl Ether as anti-solvent agent, obtained using three samples for each sample type.

SC Devices	Highest FF	Lowest FF	Average FF
Standard deposition	0.204	0.066	0.119
Drop-Cast deposition	0.270	0.126	0.183

4.3.4 Diethyl Ether as an anti-solvent agent

Much like the intent behind the previous study of a new deposition method for the HTL, using Diethyl Ether as an anti-solvent agent serves the purpose of trying to improve the device performance, more specifically, to increase the FF, as this is seen as the major contributor to the optimization of these devices.

Y.Gao and coworkers, reported an increase in almost 50% FF when using Diethyl Ether as anti-solvent agent [63].

Given this fact, it was here tested the difference between using chlorobenzene or Diethyl Ether as anti-solvent agents.

The resulting I-V and P-V measurements for the best devices using chlorobenzene or Diethyl Ether are present in figure 4.34 with corresponding performance values in table 4.20.

Using Diethyl Ether as the anti-solvent seems to improve all performance parameters

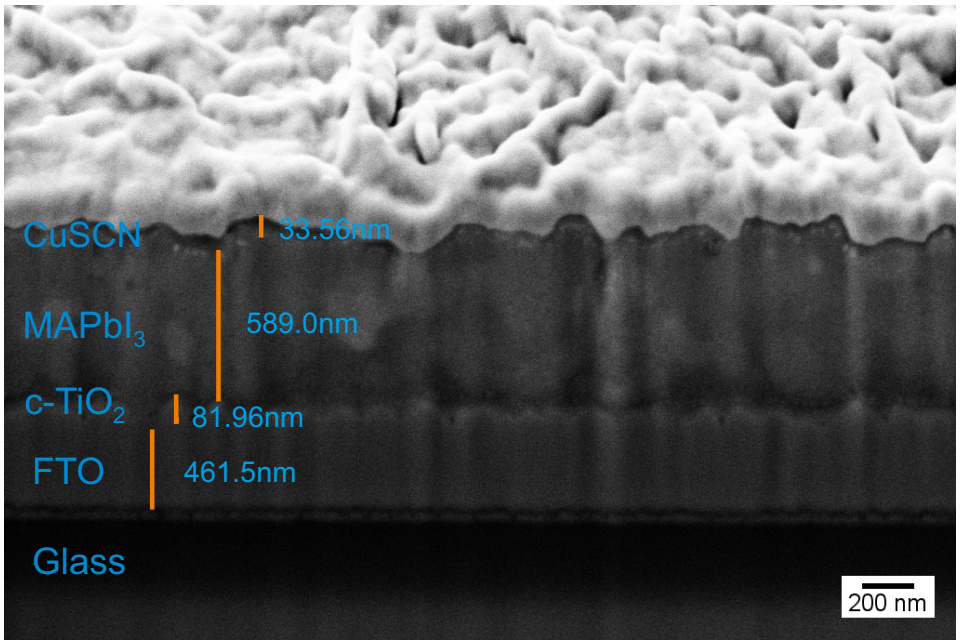

a

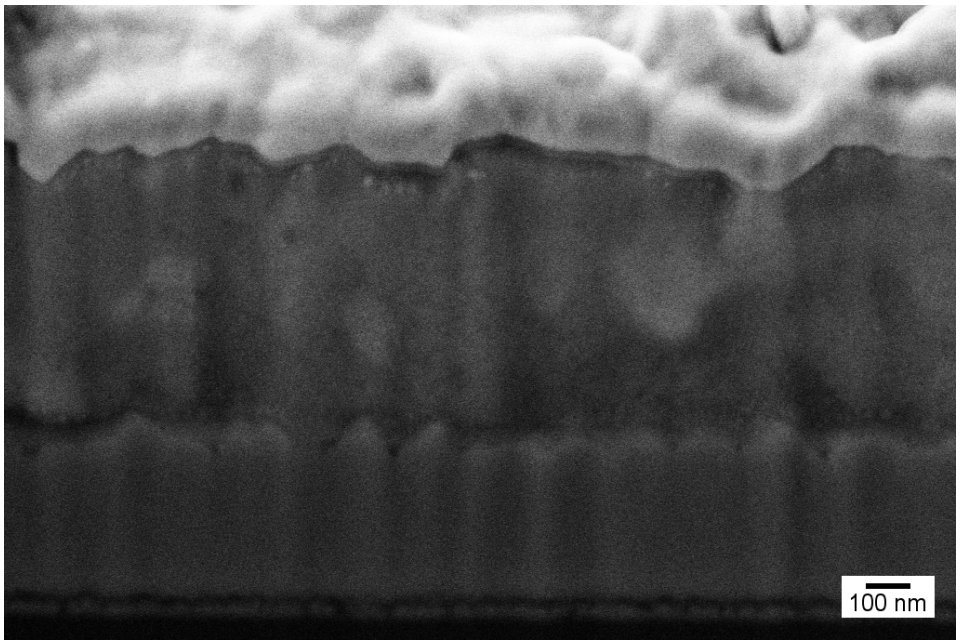

b

Figure 4.32: Cross-Section SEM images of full SC structure with Drop-Cast as the deposition method for HTL a); close-up of Perovskite-HTL interface b).

Table 4.20: Performance values for the samples in figure 4.34

SC Devices	Voc(V)	Jsc(mA/cm^2)	FF	Rsh(kΩ)	Rs(kΩ)	PCE(%)
Cholorobenzene	0.488	10.50	0.197	0.53	0.8	1.01
Diethyl Ether	0.674	9.75	0.211	0.59	1.57	1.39

Figure 4.33: Perovskite film after HTL deposition using Aqueous CuSCN solution.

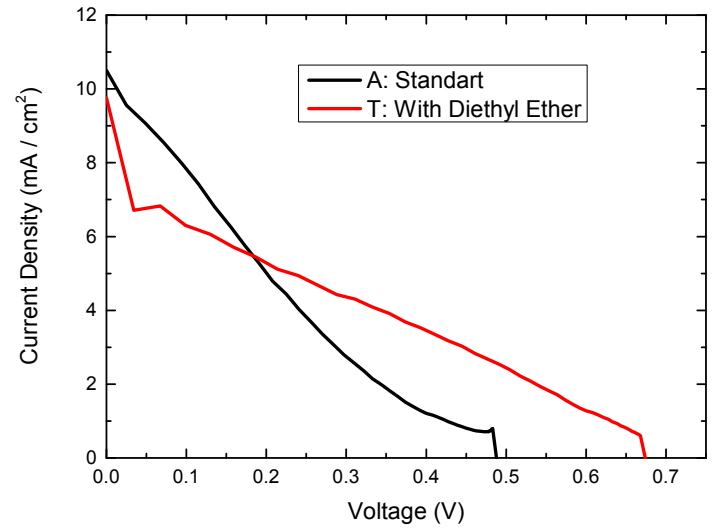

a

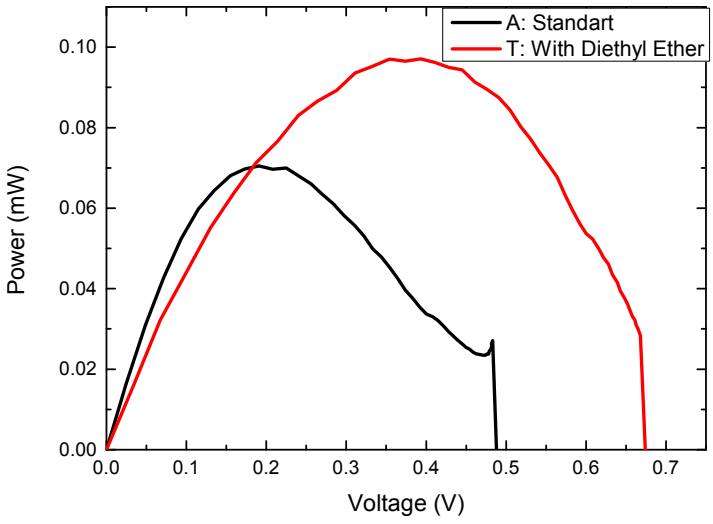

b

Figure 4.34: I-V a) and P-V b) measurements of best SC devices with different anti-solvents. Perovskite films produced over compact TiO_2, using 1 M solution annealed for 15 minutes at 100° C; CuSCN deposited as HTL on top.

except current density. To understand the reason behind this improvement, XRD measurements were performed on two different samples using these two anti-solvent agents. Figure 4.35 coupled with the corresponding peak parameters in tables 4.21 and 4.22, make it clear that using Diethyl Ether results in better quality of the Perovskite films, most likely due to its increased ability to dissolve water (1.5% for diethyl-ether vs 0.04% in chlorobenzene)[64].

Once again, using the new anti-solvent agent had the specific purpose of tackling the low FF of the devices. Analyzing the numbers in table 4.23, becomes clear that using this anti-solvent brings benefits regarding the FF parameter of these devices, as intended and expected.

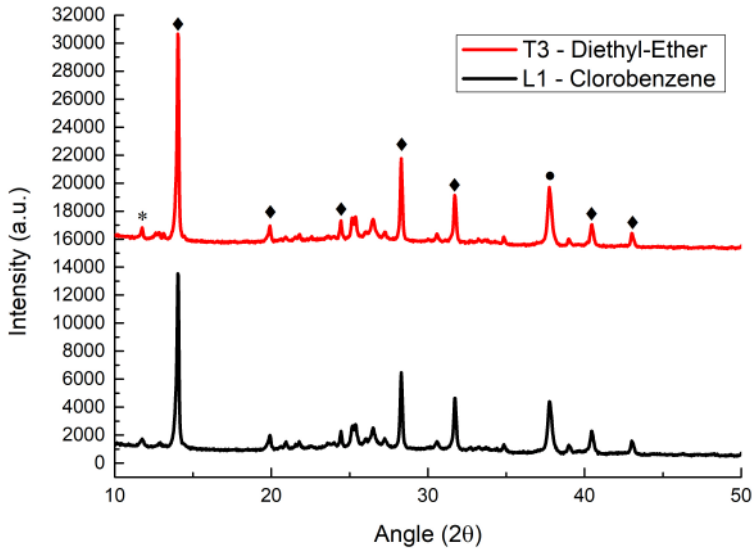

Figure 4.35: XRD diffractograms of Perovskite films deposited with different anti-solvent agents. Peaks corresponding to the tetragonal phase of $MAPbI_3$, marked with full rhombus, the PbI_2 peak, marked with an asterisk and also peaks regarding the CuSCN and FTO layer (marked with cardinal and full circle, respectively).

Table 4.21: Perovskite peak parameters of the diffractogram in 4.35, chlorobenzene sample.

Peak(◦)	Intensity (a.u.)	FWHM (◦)
14.03	12216.7	0.154
28.3	5189.3	0.170

Table 4.22: Perovskite peak parameters of the diffractogram in 4.35, Diethyl Ether sample.

Peak(◦)	Intensity (a.u.)	FWHM (◦)
14.03	14443.5	0.136
28.3	5551.3	0.164

Table 4.23: FF values taken from the batch devoted to testing the Drop-Cast deposition method, obtained using three samples for each sample type.

SC Devices	Highest FF	Lowest FF	Average FF
Chlorobenzene	0.204	0.066	0.119
Diethyl Ether	0.220	0.097	0.160

4.3.5 Improving Fill Factor

As already stated previously, the low FF was the main issue to tackle in these devices. The previous two studies, both proved effective in increasing the FF of the devices while also improving the overall performance.

Separately, both Drop-Cast deposition method and the new anti-solvent agent (Diethyl Ether), when compared with the "standard"device, presented better results, so it was only natural to fabricate a device using both, in order to achieve the highest performance possible.

As can be seen from the I-V and P-V measurements of figure 4.36 coupled with the performance values of table 4.24, the device using both the Drop-Cast deposition method and Diethyl Ehter as anti-solvent agent, is the best performing device to date.

For this batch it was also tested anti-solvent dropping in the early seconds of spin, with unsuccessful results. This is most likely due to the fact that the first step of the spin acts mostly as a "film spreader", uniformly spreading the film on the entire substrate, and as such, it is a low rpm step, meaning most of the solvents are still present. Adding another liquid, disrupts the flow of the Perovskite solution on the substrate causing it to "leave"the substrate prior to the solute deposition. The substrates (prior to gold contact deposition) are represented in figure 4.37, where the difference in film due to different anti-solvent agents and different dropping times can be observed. To note is the fact that, although the anti-solvent Diethyl Ether appears to produce better performing devices, a clear difficulty in obtaining uniform and smooth films was observed during the fabrication. This increased difficulty, when comparing with chlorobenzene, is most likely related with its vapor pressure and viscosity [65, 66]. In figure 4.38 it is depicted a full SC resulting from this batch.

Table 4.24: Performance values for the samples in figure 4.36

SC Devices	Voc(V)	Jsc(mA/cm^2)	FF	Rsh(kΩ)	Rs(kΩ)	PCE(%)
Cholorobenzene	0.682	13.59	0.271	0.99	0.56	2.51
D-Ether - at 5 seconds	0.142	2.61	0.109	0.35	1.40	0.04
D-Ether - last 10 seconds	0.701	15.11	0.250	0.68	0.55	2.65

4.3.6 Humidity Influence on device performance

There seems to be a discrepancy between batches that share the same, or very similar devices. The only parameter that was not controlled inside the laboratory was the humidity

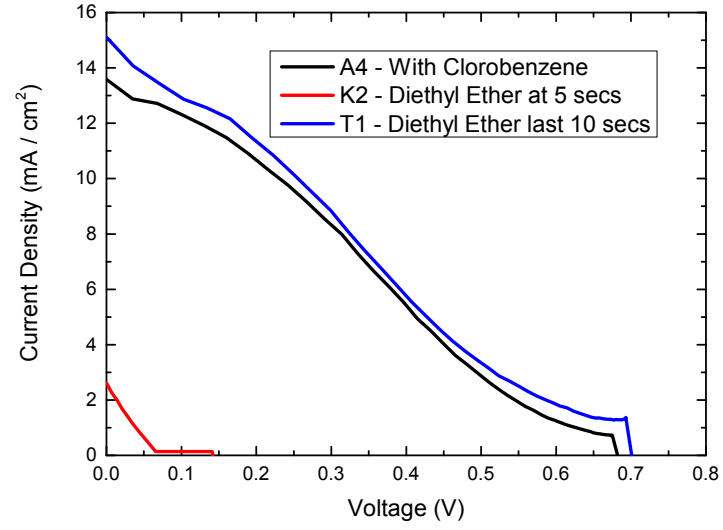

a

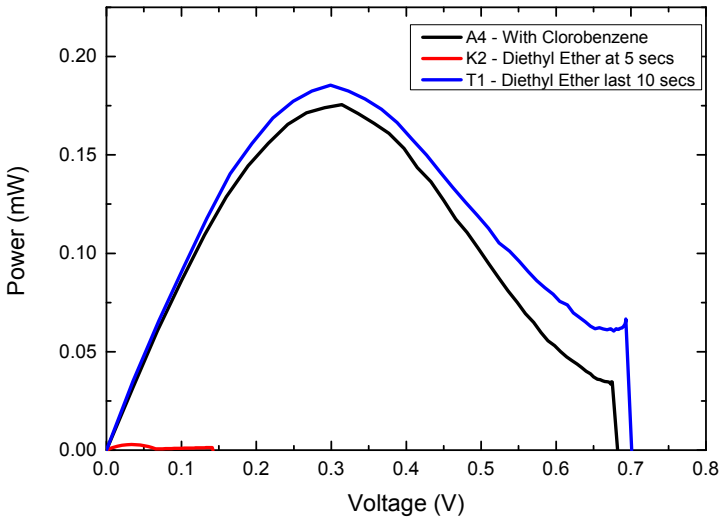

b

Figure 4.36: I-V a) and P-V b) measurements of best SC devices with different anti-solvents. Perovskite films produced over compact TiO_2, using 1 M solution annealed for 15 minutes at 100° C; CuSCN deposited as HTL on top using Drop-Cast method.

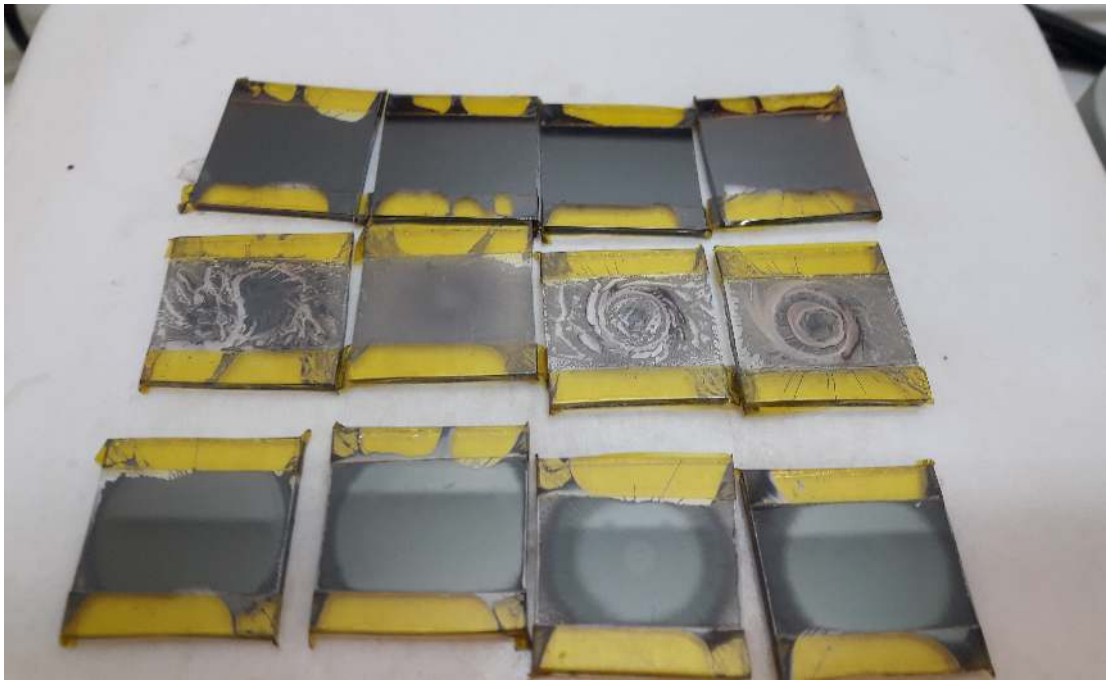

Figure 4.37: Substrates prior to gold contact deposition. 1st row: with Chlorobenzene in last 10 seconds; 2nd row: with Diethyl Ether in first 5 seconds; 3rd row: with Diethyl Ether in last 10 seconds. The Kapton masks (yellow stripes on the top and bottom of each substrate) are removed before the gold deposition step.

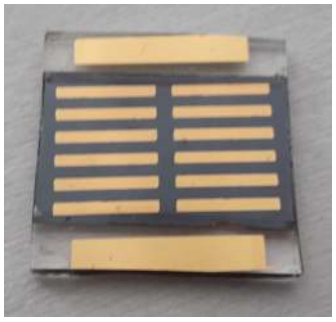

Figure 4.38: Full Solar Cell device, prior to I-V and P-V measurements.

level. Coincidentally, the best performing devices during this Optimization study (2.09% and 2.65% PCE) were fabricated on the days with the lowest registered humidity levels, 47% and 44%, respectively (blue circles in figure 4.39).

It has been reported previously that Perovskite films, plus air and humidity exposure is an ideal combination, mainly due to the MAI hydrophilicity [28, 67]. J.Troughton *et al.* reported an average of 4% and 6% PCE for very similar devices fabricated in a 50% humidity level environment, using chlorobenzene and diethyl ether as anti-solvent agents, respectively [64].

Although a significant improvement, regarding the devices from the previous work [34], has been achieved, considering the average humidity level for the duration of this work, the already obtained results and the consequent discrepancies between the same

or very similar samples (only fabricated in different days) make more sense when the humidity factor is taken into account.

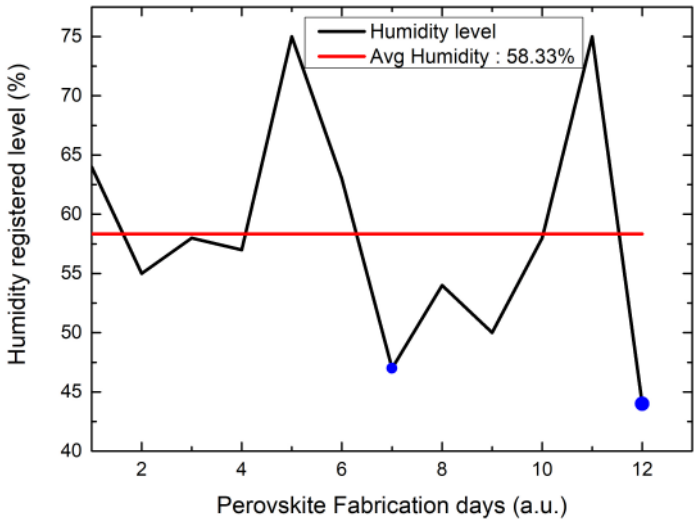

Figure 4.39: Humidity levels on Perovskite film fabrication days.

In order to minimize the humidity factor, it was tested annealing the Perovskite film on a desiccator, as opposed to the traditional hot-plate.

The obtained XRD diffractograms of the samples annealed in a hot-plate or on a desiccator, are represented in figure 4.40.

Table 4.25: Perovskite peak parameters of the diffractogram in 4.40, hot-plate sample.

Peak(◦)	Intensity (a.u.)	FWHM (◦)
14.03	22641.3	0.138
28.3	9117.9	0.160

Table 4.26: Perovskite peak parameters of the diffractogram in 4.40, desiccator sample.

Peak(◦)	Intensity (a.u.)	FWHM (◦)
14.03	49244.1	0.134
28.3	20746.1	0.153

Although the devices are still exposed to ambient conditions prior to the annealing step (after leaving the spinner), and before the HTL deposition step, using the desiccator for annealing the Perovskite films has an advantage over the traditional hot-plate annealing in regards to film quality, improving it substantially, as confirmed from the values of tables 4.25 and 4.26.

Considering this results, a new batch of SC devices was made in order to confirm the humidity influence. The resulting I-V and P-V measurements are represented in figure

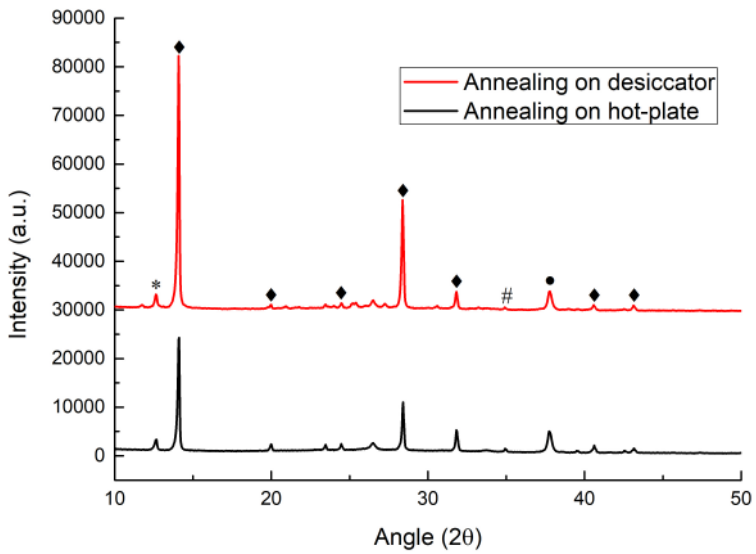

Figure 4.40: XRD diffractograms of Perovskite films annealed in hot-plate and desiccator. Peaks corresponding to the tetragonal phase of $MAPbI_3$, marked with full rhombus, the PbI_2 peak, marked with an asterisk and also peaks regarding the CuSCN and FTO layer (marked with cardinal and full circle, respectively).

4.41, with the corresponding performance values for each device in table 4.27. Coupled with the different annealing setups, a new anti-solvent agent was tested (Ethyl acetate), as this as been reported to help produce good performing devices under high humidity environments, which has been attributed to its increased ability to dissolve water (3.3%), which is more than twice as much for diethyl ether (1.5%) [64].

Table 4.27: Performance values for the samples in figure 4.41

SC Devices	Voc(V)	Jsc(mA/cm^2)	FF	Rsh(kΩ)	Rs(kΩ)	PCE(%)
D-Ether in hot-plate	0.561	9.94	0.144	0.44	1.33	0.805
D-Ether in desiccator	0.685	6.24	0.234	1.08	1.95	1.001
E-acetate in hot-plate	0.729	8.31	0.175	0.77	2.14	1.058

The results from figure 4.41 show a noticeable difference in device performance, corroborating the previous assumption that the humidity level during the fabrication process of the Perovskite films, actually plays a key role in film quality, and by extent, device performance. This batch was fabricated on a especially high humidity level of 71%, which is most likely the cause for the lower performance obtained, when compared with previous devices.

Comparing the devices with Perovskite films annealed in different setups, although the device with the Perovskite film annealed in the hot-plate presents higher current density, the device that was submitted to a Perovskite annealing on a desiccator shows better overall performance, indicating that it was possible to reduce humidity degradation

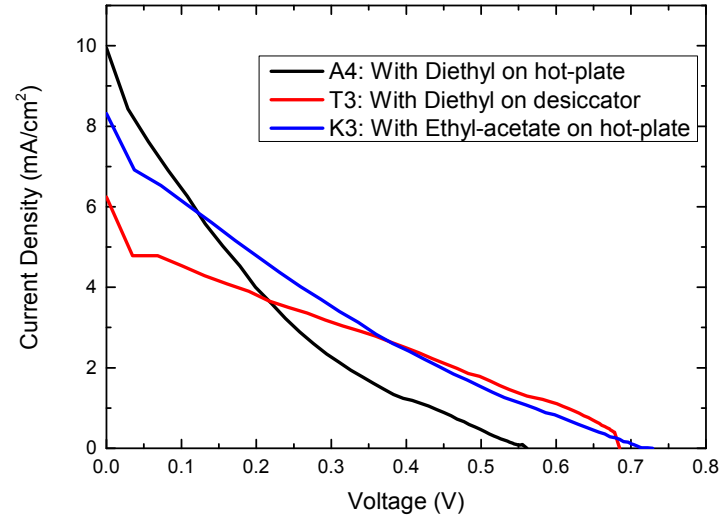

a

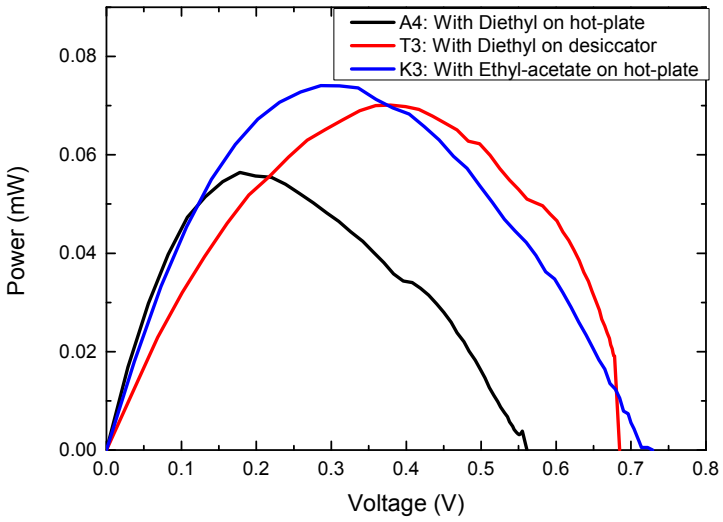

b

Figure 4.41: I-V a) and P-V b) measurements of best SC devices annealing in different setups and with different anti-solvents. Perovskite films produced over compact TiO_2, using 1 M solution annealed for 15 minutes at 100° C; CuSCN deposited as HTL on top using Drop-Cast method.

during the crystallization of the Perovskite film, which in turn results in better quality films and devices.

As already mentioned, as well as devices with different annealing setups, it was also tested a different anti-solvent agent during the fabrication of the Perovskite films. This device actually surpasses, if only by a small amount, the device with the Perovskite film annealed in a desiccator. These results indicate that the use of Ethyl Acetate versus Diethyl Ether results in reduced interaction with humidity. The reduced humidity degradation stems from the higher ability of Ethyl Acetate to dissolve water, meaning that upon deposition of this agent, during the spinning step, humidity within the proximity of the substrate will mix with this agent, instead of reacting with the intermediate complex (PbI_2-MAI-DMSO) of the Perovskite film.

To help corroborate these results, XRD measurements were performed on each sample type and are visible in figure 4.42, with the corresponding values of interest in tables 4.28, 4.29 and 4.30.

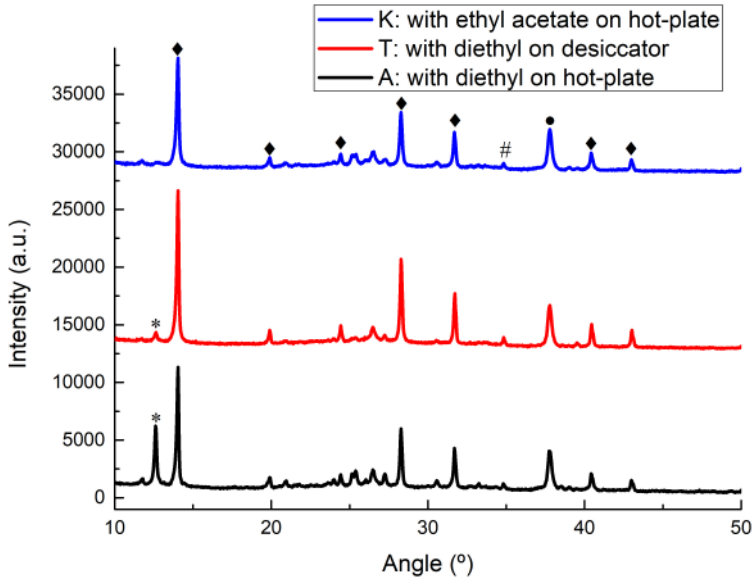

Figure 4.42: XRD diffractograms of Perovskite films annealed in hot-plate (with Diethyl Ether or Ethyl Acetate) and in a desiccator. Peaks corresponding to the tetragonal phase of $MAPbI_3$, marked with full rhombus, the PbI_2 peak, marked with an asterisk and also peaks regarding the CuSCN and FTO layer (marked with cardinal and full circle, respectively).

Table 4.28: Perovskite peak parameters of the diffractogram in 4.42, hot-plate sample with Diethyl Ether.

Peak(◦)	Intensity (a.u.)	FWHM (◦)
14.03	9825.9	0.157
28.3	4799.9	0.171

Table 4.29: Perovskite peak parameters of the diffractogram in 4.42, desiccator sample.

Peak(◦)	Intensity (a.u.)	FWHM (◦)
14.03	12662.5	0.153
28.3	6854.8	0.169

Table 4.30: Perovskite peak parameters of the diffractogram in 4.42, hot-plate sample with Ethyl acetate.

Peak(◦)	Intensity (a.u.)	FWHM (◦)
14.03	9104.6	0.157
28.3	4454.7	0.186

The XRD diffractograms demonstrates that the device with a Perovskite film annealed on a desiccator, possesses improved film quality, as this sample shows the higher and more narrow peaks of the three samples. The sample with the Perovskite film fabricated using Diethyl Ether as anti-solvent agent and annealed in the hot-plate exhibits a considerably high PbI_2 peak, indicating a higher degree of organic degradation when compared with the other samples.

These XRD results also point towards the fact that indeed fabrication environment, more specifically humidity levels, play a fundamental role in Perovskite films quality and SC device performance.

4.3.7 Conclusions

The results presented in this section demonstrated a significant improvement regarding device performance, which is attributed to the higher bulk densities and quality of the Perovskite layer. This enhancement is most likely due to the aging of the precursor solution, coupled with lower annealing time.

These results also demonstrate the sensitivity of the fabrication process, especially for the Perovskite film, demonstrating the challenges regarding good film quality and device performance.

The improved contact procedure also played a key role in the optimization of these devices, as demonstrated by the ability to measure every sample in a batch, as oppose to what had been happening with previous batches.

In this section it is possible to understand that HTL deposition, even though it has been improved slightly, still holds demands, when using this specific material (CuSCN).

One of the key goals to achieve is low fabrication cost, meaning that fabrication of good devices must be possible out of high vacuum and extremely controlled fabrication sites. Therefore, fabrication conditions were also evaluated, namely the humidity level, and it was proven to have been affecting device performance, as is expected on more less controlled fabrication environments. Despite this proven humidity influence, it was still possible to obtain higher performance with the devices, giving more hope for future

studies.

Chapter 5

Conclusions and Future work

As previously mentioned, one of the main goals for this work, was to keep fabrication costs as low as possible, since low fabrication cost is a critical step to achieve when considering such devices for future commercialization. In this regard, a possible substitute for MAI was investigated, MACl, which is considerably cheaper. Various fabrication parameters were tested, focusing mostly on solvent-engineering, and the best fabrication parameters, within the tested parameters, are present in 4.2.7. Although it has been reported that using solution-processed techniques with a precursor solution using MACl can produce good quality films with good device efficiency [31, 36], the same cannot be reported in the present document. Despite that, MACl should not be dismissed as a replacement for MAI in Perovskite precursor solutions, as it was proven that using this material, it is possible to obtain the $MAPbI_3$ phase, as confirmed from the XRD diffractogram. Using the reported best fabrication parameters as a starting point, further tests should be conducted in order to find, under the same experimental setup, the best parameters for the fabrication of Perovskite thin films and SC's, using this solution.

The main objective for this work was to improve the solar devices fabricated until this stage using the same fabrication setup, meaning: low-cost fabrication techniques under "uncontrolled"ambient conditions.

One the major steps of device optimization was related to the gold contacts, as the previous contact method was thought to be damaging device performance. As demonstrated, the contact procedure greatly influenced device performance. The solution that was found (after testing different methods), tackles the main issue of the contacts, which is the fact that damage to the solar device is possible due to the measuring tips during electrical characterization. It can be said that the final version of the contact procedure was the correct one, as no noticeable film damage is observed (as with other reported procedures), and using this contact procedure, to my understanding, resulted in the ability

to measure all samples of a batch, which never happened until that point.

A major issue, that was reported as playing a big role in the low performance of devices fabricated until this stage, was the low bulk density of the Perovskite layer, which could have diminishing light absorption, increase charge recombination and allow direct contact between HTL and ETL [34]. The resulting devices presented very low FF and current densities 4.24.

Solution aging and reduced annealing time (so as to also reduce ambient air exposure time) proved extremely effective in increasing the bulk density of the Perovskite layer, achieving bulk concentrations above 95% (value estimated based on the cross-section images obtained).

The low FF, high series resistance, and low-shunt resistance was thought to also stem from bad layer interfaces and efforts were made to improve this specific problem.

Using a mesoporous layer to act as scaffold for the Perovskite film is reported to improve the ETL-Perovskite interface. Although most devices in the literature possess mesoscopic structure, the addition of a mesoporous layer actually yielded devices with lower performance, which was attributed to the increased thin film thickness (in both ETL and Perovskite layer). Considering this, the ultra thin compact layer of TiO_2 hybridized with mesoporous TiO_2, reported by I. Jeong *et al.*, should be considered as a possible ETL in future devices, as it reportedly produces a TiO_2 blocking layer under 5 nanometers in thickness [42].

Perovskite thin film quality is, unquestionably, a critical goal for good performing SC devices. In this department, during fabrication of some of the devices, it was observed that the HTL precursor solution was damaging the Perovskite film. To reduce Perovskite degradation via HTL deposition, a different deposition method, reported by N. Arora *et al.*, here designated as Drop-Cast method, was used with success, as confirmed by the cross-section images and increased device performance (figures 4.31 and 4.32). To my understanding, this method although improving, it does not counteract the degradation completely, which is why further research should be dedicated in order to completely minimize this HTL-deposition induced degradation. Inverting the device structure could be a possible way to deal with HTL-induce degradation, but a new ETL with low-temperature processing needs, is essential for an inverted device architecture.

Coincidentally, the TiO_2 high temperature needs are the main reason why this device was not tested on a flexible substrate. Solving this issue would allow this device to be fabricated onto a flexible substrate, as all other layers do not require high processing temperatures.

As an effort to further increase device efficiency by increasing the Fill-Factor, another anti-solvent agent was tested, yielding successful results, attributed to increased film quality. That was also the time it was first thought, that the humidity level could have been affecting device performance, by tampering with the Perovskite's film quality.

Due to the discrepancy of performance between batches on very similar and sometimes identical devices, and the fact that the best performing devices were fabricated

on the lowest registered humidity days, the humidity influence was tested and indeed confirmed to tamper the quality of the Perovskite film.

Considering the hydrophilic nature of the organic component of Perovskite, further research should be conducted to reduce humidity degradation during Perovskite film deposition and annealing, without resorting to high vacuum environments and other rather expensive/non-practical methods.

In the future, it should be considered the removal of the "human factor", at least during Perovskite film deposition, as it was observed that film formation and quality are highly influenced by the anti-solvent deposition step, in terms of dispensed volume, timing, distance to substrate, and relative position to the center of the substrate, portraying this as an extremely sensitive procedure that should be optimized with the help of engineering.

Overall, the device optimization can be considered a success, as the top reported PCE in the previous work was 0.4% [34], which has now been increased to 2.65%, more than six times the previous efficiency, presenting a current density of 15.11 mA/cm^2 and a V_{oc} of 0.701 (as confirmed with figure 4.36 and table 4.24). The fabrication conditions for the Perovskite layer of the best device are summarized in tables 5.1 and 5.2. The HTL deposition was made using the Drop-Cast method already mentioned.

Although these fabrication conditions yielded the best performing device during this work, it is believed that the use of Ethyl acetate as anti-solvent can further improve device performance, as it demonstrated superior ability to reduce humidity induced Perovskite degradation, during film fabrication. Using the $TiCl_4$ precursor solution for ETL deposition, might also add benefits to the device fabrication.

Table 5.1: Fabrication parameters for the Perovskite solution used for the best performing device.

Concentration	**Solvent ratio (DMF:DMSO)**	**Stir Temperature**	**Stir Time**
1M	4:1	70º	24 hours

Table 5.2: Deposition parameters for the Perovskite layer used for the best performing device.

Dispersed volume	**2 stage spin parameters**	**Anti-Solvent**	**Disperse timing**	**Annealing parameters**
120µl	1000 rpm - 10 seconds 6000 rpm - 20 seconds	Diethyl Ether 100µl	After 20 seconds	100º C for 15 minutes

Bibliography

[1] Z. Yu and L. Sun. "Recent Progress on Hole-Transporting Materials for Emerging Organometal Halide Perovskite Solar Cells." In: *Advanced Energy Materials* 5.12 (2015). DOI: 10.1002/aenm.201500213.

[2] M. Ye, X. Hong, F. Zhang, and X. Liu. "Recent advancements in perovskite solar cells: flexibility, stability and large scale." In: *Journal of Materials Chemistry A* 4.18 (2016), pp. 6755–6771. DOI: 10.1039/C5TA09661H.

[3] H. S. Jung and N.-G. Park. "Perovskite Solar Cells: From Materials to Devices." In: *Small* 11.1 (2015), pp. 10–25. DOI: 10.1002/smll.201402767.

[4] A. Kojima, K. Teshima, Y. Shirai, and T. Miyasaka. "Organometal Halide Perovskites as Visible-Light Sensitizers for Photovoltaic Cells." In: *Journal of the American Chemical Society* 131.17 (2009), pp. 6050–6051. DOI: 10.1021/ja809598r.

[5] H.-S. Kim, C.-R. Lee, J.-H. Im, K.-B. Lee, T. Moehl, A. Marchioro, S.-J. Moon, R. Humphry-Baker, J.-H. Yum, J. E. Moser, M. Grätzel, and N.-G. Park. "Lead Iodide Perovskite Sensitized All-Solid-State Submicron Thin Film Mesoscopic Solar Cell with Efficiency Exceeding 9%." In: *Scientific Reports* 2.1 (2012), p. 591. DOI: 10.1038/srep00591.

[6] S. I. Seok, M. Grätzel, and N.-G. Park. "Methodologies toward Highly Efficient Perovskite Solar Cells." In: *Small* 14.20 (2018), p. 1704177. DOI: 10.1002/smll.201704177.

[7] NREL Efficiency Chart. *NREL Efficiency Chart*. 2016. URL: https://www.nrel.gov/pv/assets/images/efficiency-chart.png (visited on 05/02/2018).

[8] A. Polman, M. Knight, E. C. Garnett, B. Ehrler, and W. C. Sinke. "Photovoltaic materials: Present efficiencies and future challenges." In: *Science* 352.6283 (2016), aad4424–aad4424. DOI: 10.1126/science.aad4424.

[9] C. Wehrenfennig, G. E. Eperon, M. B. Johnston, H. J. Snaith, and L. M. Herz. "High Charge Carrier Mobilities and Lifetimes in Organolead Trihalide Perovskites." In: *Advanced Materials* 26.10 (2014), pp. 1584–1589. DOI: 10.1002/adma.201305172.

[10] S. D. Stranks, G. E. Eperon, G. Grancini, C. Menelaou, M. J. P. Alcocer, T. Leijtens, L. M. Herz, A. Petrozza, and H. J. Snaith. "Electron-Hole Diffusion Lengths Exceeding 1 Micrometer in an Organometal Trihalide Perovskite Absorber." In: *Science* 342.6156 (2013), pp. 341–344. DOI: 10.1126/science.1243982.

[11] M. H. Kumar, N. Yantara, S. Dharani, M. Graetzel, S. Mhaisalkar, P. P. Boix, and N. Mathews. "Flexible, low-temperature, solution processed ZnO-based perovskite solid state solar cells." In: *Chemical Communications* 49.94 (2013), p. 11089. DOI: 10.1039/c3cc46534a.

[12] S. S. Shin, W. S. Yang, J. H. Noh, J. H. Suk, N. J. Jeon, J. H. Park, J. S. Kim, W. M. Seong, and S. I. Seok. "High-performance flexible perovskite solar cells exploiting Zn2SnO4 prepared in solution below 100 °C." In: *Nature Communications* 6.1 (2015), p. 7410. DOI: 10.1038/ncomms8410.

[13] B. Dou, E. M. Miller, J. A. Christians, E. M. Sanehira, T. R. Klein, F. S. Barnes, S. E. Shaheen, S. M. Garner, S. Ghosh, A. Mallick, D. Basak, and M. F.A. M. van Hest. "High-Performance Flexible Perovskite Solar Cells on Ultrathin Glass: Implications of the TCO." In: *The Journal of Physical Chemistry Letters* 8.19 (2017), pp. 4960–4966. DOI: 10.1021/acs.jpclett.7b02128.

[14] J. Hanania, K. Stenhouse, Yyelland. Brodie, and J. Donev. *Photovoltaic effect - Energy Education*. 2017. URL: http://energyeducation.ca/encyclopedia/Photovoltaic{_}effect{\#}cite{_}note-3 (visited on 01/07/2018).

[15] S. Almosni, A. Delamarre, Z. Jehl, D. Suchet, L. Cojocaru, M. Giteau, B. Behaghel, A. Julian, C. Ibrahim, L. Tatry, H. Wang, T. Kubo, S. Uchida, H. Segawa, N. Miyashita, R. Tamaki, Y. Shoji, K. Yoshida, N. Ahsan, K. Watanabe, T. Inoue, M. Sugiyama, Y. Nakano, T. Hamamura, T. Toupance, C. Olivier, S. Chambon, L. Vignau, C. Geffroy, E. Cloutet, G. Hadziioannou, N. Cavassilas, P. Rale, A. Cattoni, S. Collin, F. Gibelli, M. Paire, L. Lombez, D. Aureau, M. Bouttemy, A. Etcheberry, Y. Okada, and J.-F. Guillemoles. "Material challenges for solar cells in the twenty-first century: directions in emerging technologies." In: *Science and Technology of Advanced Materials* 19.1 (2018), pp. 336–369. DOI: 10.1080/14686996.2018.1433439.

[16] H. A. Atwater and A. Polman. "Plasmonics for improved photovoltaic devices." In: *Nature Materials* 9.3 (2010), pp. 205–213. DOI: 10.1038/nmat2629.

[17] M. T. Neukom. "Charge Carrier Dynamics of Methylammonium Lead-Iodide Perovskite Solar Cells." In: January (2016). arXiv: 1611.06425.

[18] M. Grätzel. "The light and shade of perovskite solar cells." In: *Nature Materials* 13.9 (2014), pp. 838–842. DOI: 10.1038/nmat4065.

[19] M. Xiao, F. Huang, W. Huang, Y. Dkhissi, Y. Zhu, J. Etheridge, A. Gray-Weale, U. Bach, Y.-B. Cheng, and L. Spiccia. "A Fast Deposition-Crystallization Procedure for Highly Efficient Lead Iodide Perovskite Thin-Film Solar Cells." In: *Angewandte Chemie* 126.37 (2014), pp. 10056–10061. DOI: 10.1002/ange.201405334.

[20] M. Saliba, T. Matsui, J.-Y. Seo, K. Domanski, J.-P. Correa-Baena, M. K. Nazeeruddin, S. M. Zakeeruddin, W. Tress, A. Abate, A. Hagfeldt, and M. Grätzel. "Cesium-containing triple cation perovskite solar cells: improved stability, reproducibility and high efficiency." In: *Energy & Environmental Science* 9.6 (2016), pp. 1989–1997. DOI: 10.1039/C5EE03874J.

[21] N. J. Jeon, J. H. Noh, Y. C. Kim, W. S. Yang, S. Ryu, and S. I. Seok. "Solvent engineering for high-performance inorganic–organic hybrid perovskite solar cells." In: *Nature Materials* 13.9 (2014), pp. 897–903. DOI: 10.1038/nmat4014.

[22] C.-H. Chiang, Z.-L. Tseng, and C.-G. Wu. "Planar heterojunction perovskite/PC 71 BM solar cells with enhanced open-circuit voltage via a (2/1)-step spin-coating process." In: *J. Mater. Chem. A* 2.38 (2014), pp. 15897–15903. DOI: 10.1039/C4TA03674C.

[23] J. Burschka, N. Pellet, S.-J. Moon, R. Humphry-Baker, P. Gao, M. K. Nazeeruddin, and M. Grätzel. "Sequential deposition as a route to high-performance perovskite-sensitized solar cells." In: *Nature* 499.7458 (2013), pp. 316–319. DOI: 10.1038/nature12340.

[24] A. T. Mallajosyula, K. Fernando, S. Bhatt, A. Singh, B. W. Alphenaar, J.-C. Blancon, W. Nie, G. Gupta, and A. D. Mohite. "Large-area hysteresis-free perovskite solar cells via temperature controlled doctor blading under ambient environment." In: *Applied Materials Today* 3 (2016), pp. 96–102. DOI: 10.1016/j.apmt.2016.03.002.

[25] Q. Chen, H. Zhou, Z. Hong, S. Luo, H.-S. Duan, H.-H. Wang, Y. Liu, G. Li, and Y. Yang. "Planar Heterojunction Perovskite Solar Cells via Vapor-Assisted Solution Process." In: *Journal of the American Chemical Society* 136.2 (2014), pp. 622–625. DOI: 10.1021/ja411509g.

[26] B. R. Sutherland, S. Hoogland, M. M. Adachi, P. Kanjanaboos, C. T. O. Wong, J. J. McDowell, J. Xu, O. Voznyy, Z. Ning, A. J. Houtepen, and E. H. Sargent. "Perovskite Thin Films via Atomic Layer Deposition." In: *Advanced Materials* 27.1 (2015), pp. 53–58. DOI: 10.1002/adma.201403965.

[27] Z. Wei, H. Chen, K. Yan, and S. Yang. "Inkjet Printing and Instant Chemical Transformation of a CH 3 NH 3 PbI 3 /Nanocarbon Electrode and Interface for Planar Perovskite Solar Cells." In: *Angewandte Chemie* 126.48 (2014), pp. 13455–13459. DOI: 10.1002/ange.201408638.

[28] N.-G. Park, M. Grätzel, and M. Tsutomu. *Organic-Inorganic Halide Perovskite Photovoltaics*. Ed. by N.-G. Park, M. Grätzel, and T. Miyasaka. Cham: Springer International Publishing, 2016, pp. 1–366. ISBN: 978-3-319-35112-4. DOI: 10.1007/978-3-319-35114-8.

[29] G. E. Eperon, V. M. Burlakov, P. Docampo, A. Goriely, and H. J. Snaith. "Morphological Control for High Performance, Solution-Processed Planar Heterojunction Perovskite Solar Cells." In: *Advanced Functional Materials* 24.1 (2014), pp. 151–157. DOI: 10.1002/adfm.201302090.

[30] A. Dualeh, N. Tétreault, T. Moehl, P. Gao, M. K. Nazeeruddin, and M. Grätzel. "Effect of Annealing Temperature on Film Morphology of Organic-Inorganic Hybrid Pervoskite Solid-State Solar Cells." In: *Advanced Functional Materials* 24.21 (2014), pp. 3250–3258. DOI: 10.1002/adfm.201304022.

[31] W. Nie, H. Tsai, R. Asadpour, J.-C. Blancon, A. J. Neukirch, G. Gupta, J. J. Crochet, M. Chhowalla, S. Tretiak, M. A. Alam, H.-L. Wang, and A. D. Mohite. "High-efficiency solution-processed perovskite solar cells with millimeter-scale grains." In: *Science* 347.6221 (2015), pp. 522–525. DOI: 10.1126/science.aaa0472.

[32] Z. Xiao, C. Bi, Y. Shao, Q. Dong, Q. Wang, Y. Yuan, C. Wang, Y. Gao, and J. Huang. "Efficient, high yield perovskite photovoltaic devices grown by interdiffusion of solution-processed precursor stacking layers." In: *Energy Environ. Sci.* 7.8 (2014), pp. 2619–2623. DOI: 10.1039/C4EE01138D.

[33] J.-H. Im, I.-H. Jang, N. Pellet, M. Grätzel, and N.-G. Park. "Growth of CH3NH3PbI3 cuboids with controlled size for high-efficiency perovskite solar cells." In: *Nature Nanotechnology* 9.11 (2014), pp. 927–932. DOI: 10.1038/nnano.2014.181.

[34] A. G. Fonseca. "Perovskite Solar Cells: Developing a Simple, Fast and Low-Cost Fabrication Technology." Master Thesis. Universidade Nova de Lisboa, 2017.

[35] B. Cai, W.-H. Zhang, and J. Qiu. "Solvent engineering of spin-coating solutions for planar-structured high-efficiency perovskite solar cells." In: *Chinese Journal of Catalysis* 36.8 (2015), pp. 1183–1190. DOI: 10.1016/S1872-2067(15)60929-9.

[36] H. Tsai, W. Nie, Y.-H. Lin, J. C. Blancon, S. Tretiak, J. Even, G. Gupta, P. M. Ajayan, and A. D. Mohite. "Effect of Precursor Solution Aging on the Crystallinity and Photovoltaic Performance of Perovskite Solar Cells." In: *Advanced Energy Materials* 7.11 (2017), p. 1602159. DOI: 10.1002/aenm.201602159.

[37] X. Tong, F. Lin, J. Wu, and Z. M. Wang. "High Performance Perovskite Solar Cells." In: *Advanced Science* 3.5 (2016), p. 1500201. DOI: 10.1002/advs.201500201.

[38] I. Mesquita, L. Andrade, and A. Mendes. "Perovskite solar cells: Materials, configurations and stability." In: *Renewable and Sustainable Energy Reviews* 82.May (2018), pp. 2471–2489. DOI: 10.1016/j.rser.2017.09.011.

[39] K. Zhao, R. Munir, B. Yan, Y. Yang, T. Kim, and A. Amassian. "Solution-processed inorganic copper(I) thiocyanate (CuSCN) hole transporting layers for efficient p–i–n perovskite solar cells." In: *Journal of Materials Chemistry A* 3.41 (2015), pp. 20554–20559. DOI: 10.1039/C5TA04028K.

[40] V. Zardetto, B. L. Williams, A. Perrotta, F. Di Giacomo, M. A. Verheijen, R. Andriessen, W. M. M. Kessels, and M. Creatore. "Atomic layer deposition for perovskite solar cells: research status, opportunities and challenges." In: *Sustainable Energy & Fuels* 1.1 (2017), pp. 30–55. DOI: 10.1039/C6SE00076B.

[41] M. Abdi-Jalebi, M. I. Dar, A. Sadhanala, S. P. Senanayak, F. Giordano, S. M. Zakeeruddin, M. Grätzel, and R. H. Friend. "Impact of a Mesoporous Titania–Perovskite Interface on the Performance of Hybrid Organic–Inorganic Perovskite Solar Cells." In: *The Journal of Physical Chemistry Letters* 7.16 (2016), pp. 3264–3269. DOI: 10.1021/acs.jpclett.6b01617.

[42] I. Jeong, Y. H. Park, S. Bae, M. Park, H. Jeong, P. Lee, and M. J. Ko. "Solution-Processed Ultrathin TiO 2 Compact Layer Hybridized with Mesoporous TiO 2 for High-Performance Perovskite Solar Cells." In: *ACS Applied Materials & Interfaces* 9.42 (2017), pp. 36865–36874. DOI: 10.1021/acsami.7b11901.

[43] N. Arora, M. I. Dar, A. Hinderhofer, N. Pellet, F. Schreiber, S. M. Zakeeruddin, and M. Grätzel. "Perovskite solar cells with CuSCN hole extraction layers yield stabilized efficiencies greater than 20%." In: *Science* 358.6364 (2017), pp. 768–771. DOI: 10.1126/science.aam5655.

[44] N. Wijeyasinghe, A. Regoutz, F. Eisner, T. Du, L. Tsetseris, Y.-H. Lin, H. Faber, P. Pattanasattayavong, J. Li, F. Yan, M. A. McLachlan, D. J. Payne, M. Heeney, and T. D. Anthopoulos. "Copper(I) Thiocyanate (CuSCN) Hole-Transport Layers Processed from Aqueous Precursor Solutions and Their Application in Thin-Film Transistors and Highly Efficient Organic and Organometal Halide Perovskite Solar Cells." In: *Advanced Functional Materials* 27.35 (2017), p. 1701818. DOI: 10.1002/adfm.201701818.

[45] M. Jung, Y. C. Kim, N. J. Jeon, W. S. Yang, J. Seo, J. H. Noh, and S. Il Seok. "Thermal Stability of CuSCN Hole Conductor-Based Perovskite Solar Cells." In: *ChemSusChem* 9.18 (2016), pp. 2592–2596. DOI: 10.1002/cssc.201600957.

[46] University of Louisville. *Spin Coating Theory*. Louisville, 2013. URL: http://www.brewerscience.com/spin-coating-theory.

[47] B. G. Higgins. "Evaporative Convection in Spin Coating Evaporative Convection in Spin Coating." In: March 2014 (2018). URL: https://www.researchgate.net/publication/261133233{_}Evaporative{_}Convection{_}in{_}Spin{_}Coating.

[48] S. Ahmadi, N. Asim, M. A. Alghoul, F. Y. Hammadi, K. Saeedfar, N. A. Ludin, S. H. Zaidi, and K. Sopian. "The Role of Physical Techniques on the Preparation of Photoanodes for Dye Sensitized Solar Cells." In: *International Journal of Photoenergy* 2014.February (2014), pp. 1–19. DOI: 10.1155/2014/198734.

[49] *Electron Beam Evaporation Angstrom Engineering*. URL: https://angstromengineering.com/tech/electron-beam-evaporation/ (visited on 04/09/2018).

[50] Thomas Heinig. *Scanning Electron Microscopy (SEM) - Helmholtz-Zentrum Dresden-Rossendorf, HZDR*. 2013. URL: https://serc.carleton.edu/research{_}education/geochemsheets/techniques/SEM.html (visited on 07/10/2017).

[51] H. Ma and U. Schollwo. "Electron - Electron Interactions." In: (2009), pp. 1360–1367. URL: https://serc.carleton.edu/research{_}education/geochemsheets/electroninteractions.html.

[52] B. L. Dutrow and C. M. Clark. *X-ray Powder Diffraction (XRD)*. 2017. URL: https://serc.carleton.edu/research{_}education/geochemsheets/techniques/XRD.html (visited on 07/12/2017).

[53] M. A. A. Eskandari and M. Jafari. *Atherosclerotic Cardiovascular Disease*. Ed. by K. Pesek. 2011. URL: http://www.microscopy.ethz.ch/bragg.htm (visited on 07/12/2017).

[54] *FTO Glass/FTO-Coated Glass (Unpatterned) - Ossila*. URL: https://www.ossila.com/products/fto-glass-unpatterned{\#}FTO-Glass-Etch (visited on 09/22/2017).

[55] P. Vivo, A. Ojanperä, J.-H. Smått, S. Sandén, S. G. Hashmi, K. Kaunisto, P. Ihalainen, M. T. Masood, R. Österbacka, P. D. Lund, and H. Lemmetyinen. "Influence of TiO 2 compact layer precursor on the performance of perovskite solar cells." In: *Organic Electronics* 41 (2017), pp. 287–293. DOI: 10.1016/j.orgel.2016.11.017.

[56] Fridman. "RCA-1 Silicon Wafer Cleaning." In: *Film* 2 (1960), pp. 2–4.

[57] M. Bachman. "RCA-2 Silicon Wafer Cleaning." In: *UCI Integrated Nanosystems Research Facility* 2 (2002), pp. 1–3.

[58] W. Wang, Z. Zhang, Y. Cai, J. Chen, J. Wang, R. Huang, X. Lu, X. Gao, L. Shui, S. Wu, and J.-M. Liu. "Enhanced performance of CH3NH3PbI3x Cl x perovskite solar cells by CH3NH3I modification of TiO2-perovskite layer interface." In: *Nanoscale Research Letters* 11.1 (2016), p. 316. DOI: 10.1186/s11671-016-1540-4.

[59] L. Fan, Y. Ding, J. Luo, B. Shi, X. Yao, C. Wei, D. Zhang, G. Wang, Y. Sheng, Y. Chen, A. Hagfeldt, Y. Zhao, and X. Zhang. "Elucidating the role of chlorine in perovskite solar cells." In: *Journal of Materials Chemistry A* 5.16 (2017), pp. 7423–7432. DOI: 10.1039/C7TA00973A.

[60] N. K. Elumalai and A. Uddin. "Hysteresis in organic-inorganic hybrid perovskite solar cells." In: *Solar Energy Materials and Solar Cells* 157.August (2016), pp. 476–509. DOI: 10.1016/j.solmat.2016.06.025.

[61] H.-S. Kim and N.-G. Park. "Parameters Affecting I – V Hysteresis of CH 3 NH 3 PbI 3 Perovskite Solar Cells: Effects of Perovskite Crystal Size and Mesoporous TiO 2 Layer." In: *The Journal of Physical Chemistry Letters* 5.17 (2014), pp. 2927–2934. DOI: 10.1021/jz501392m.

[62] *Sources of Peak Broadening*. URL: http://pd.chem.ucl.ac.uk/pdnn/peaks/broad.htm (visited on 04/17/2018).

[63] Y. Gao, L. Yang, F. Wang, Y. Sui, Y. Sun, M. Wei, J. Cao, and H. Liu. "Anti-solvent surface engineering via diethyl ether to enhance the photovoltaic conversion efficiency of perovskite solar cells to 18.76%." In: *Superlattices and Microstructures* 113 (2018), pp. 761–768. DOI: 10.1016/j.spmi.2017.12.015.

[64] J. Troughton, K. Hooper, and T. M. Watson. "Humidity resistant fabrication of CH 3 NH 3 PbI 3 perovskite solar cells and modules." In: *Nano Energy* 39.June (2017), pp. 60–68. DOI: 10.1016/j.nanoen.2017.06.039.

[65] A. Santilio, G. Ziemacki, P. Stefanelli, and R. Dommarco. *Evaluation of nitrobenzenes and chlorobenzenes levels in samples of sediments from Italy: A rapid and simple method by automatic extractor and GC/MS ion trap*. 2008. URL: http://www.tandfonline.com/doi/abs/10.1080/10934520701796150 (visited on 05/11/2018).

[66] U.S National Library of Medicine. *Ether | (C2H5)2O PubChem*. 2017. URL: https://pubchem.ncbi.nlm.nih.gov/compound/diethyl{_}ether{\#}section=Top (visited on 05/05/2018).

[67] B. Conings, J. Drijkoningen, N. Gauquelin, A. Babayigit, J. D'Haen, L. D'Olieslaeger, A. Ethirajan, J. Verbeeck, J. Manca, E. Mosconi, F. D. Angelis, and H.-G. Boyen. "Intrinsic Thermal Instability of Methylammonium Lead Trihalide Perovskite." In: *Advanced Energy Materials* 5.15 (2015), p. 1500477. DOI: 10.1002/aenm.201500477.

[68] *Part II - Photovoltaic Cell I-V Characterization Theory and LabVIEW Analysis Code - National Instruments*. URL: http://www.ni.com/white-paper/7230/en/{\#}top (visited on 04/08/2018).

Appendix A

Solar Cell Performance

This appendix serves the purpose of understanding the procedure necessary to evaluate Solar Cell performance. Figure A.1 represents a very ideal I-V and P-V curves for a Solar device, together with the importance parameters to determine device performance.

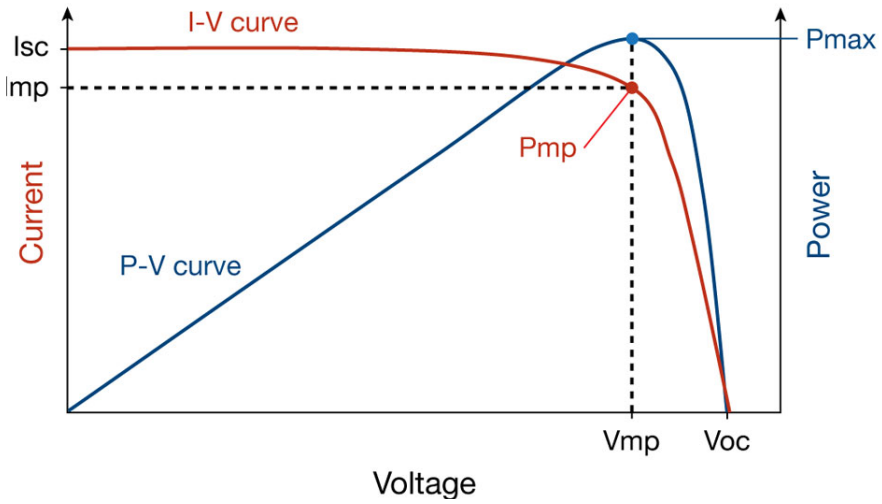

Figure A.1: Typical I-V and P-V measures of a solar device, with respective important parameters. [SC-curve]

To determine device performance, obtaining some parameters is needed to reach a universally accepted way of understanding device performance. The SC performance can be translated in a single number called PCE (Power Conversion Efficiency). To reach a PCE number however, some parameters are needed, as illustrated in figure A.1 and are as follows:

- Isc: Short-circuit current. Corresponds to the current measured at null voltage;

- Voc: Open-circuit voltage. Corresponds to the voltage measured at null current;
- FF: Fill-Factor. Represents the proximity of the measured I-V curve to the theoretical perfect I-V curve (square) and is obtained through equation A.1;
- Imp: Maximum Power current. Obtained via crossing the Vmp with the measured I-V curve, as illustrated in figure A.1;
- Vmp Maximum Power voltage. Obtained at the P-V maximum, as illustrated by figure A.1;
- Rs and Rsh: Series and Shunt resistance, respectively. Obtained by inverting the I-V slope on specific regions, demonstrated in A.1;
- Pmax: Maximum generated Power. Can be obtained by finding the maximum on P-V curve or by equation A.2;
- PCE: Power Conversion Efficiency. Is obtained with equation A.3 and is represented in percentage.

$$FF = \frac{Imp \times Vmp}{Isc \times Voc} \tag{A.1}$$

$$Pmax = Imp \times Vmp \tag{A.2}$$

$$PCE = \frac{Pmax}{Plight} \times 100 \tag{A.3}$$

Typically, most of the parameters are provided by the software analyzing the device. In this case, all the parameters were provided by software with the exception of the P_{light}, which is device dependent, and was calculated accordingly for each device.

Figure A.2 demonstrates the influence that the two types of resistance can have on device performance, mainly influencing the Fill-Factor of the device.

Ideally, Shunt resistance should be as high as possible, to avoid providing an alternative path to the current, while Series resistance should be as low as possible resulting in minimized pre-load voltage drop [68]. These resistance have also the ability to affect Voc and Jsc, if their numbers are too far from the ideal ones.

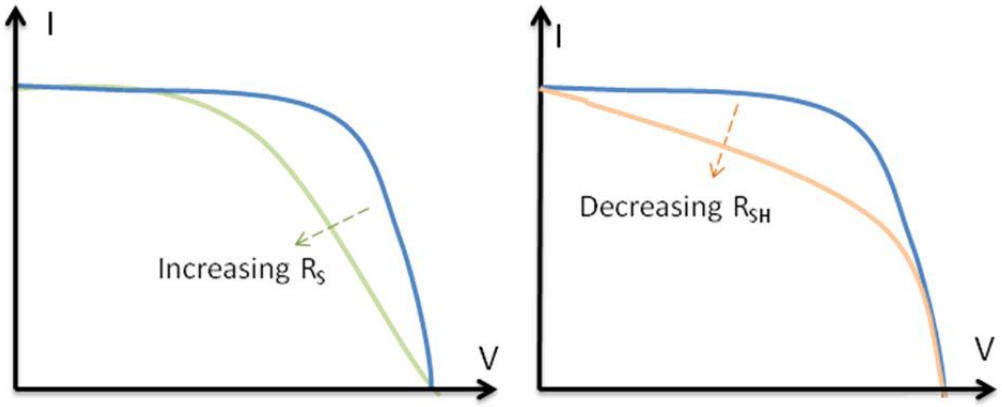

Figure A.2: Specific influence of series(Rs) and shunt resistance(Rsh), on I-V measurements of Solar Cell devices [68].

APPENDIX B

Materials and solution preparation

Table B.1: List of reagents used throughout this work

Materials	Abreviation	Purity(%)	CAS number	Company
Absolute Ethanol	EtOH	99.99	64-17-5	Fisher Chemical
Aqueous Ammonia	-	25	1336-21-6	Merck
Chlorobenzene	-	99	180-90-7	SIGMA ALDRICH
Colloidal TiO_2 Paste (22 nm)	-	-	-	SIGMA ALDRICH
Copper(I) Thiocyanate	CuSCN	96	1111-67-7	Alfa Aesar
Di-n-propyl Sulfide	-	98	111-47-7	Alfa Aesar
Diethyl Ether	-	99.7	60-29-7	MERCK
Dimethylformamide	DMF	99.8	68-12-2	Panreac
Dimethyl Sulfoxide	DMSO	99.9	67-68-5	Fisher Chemical
Hidrochloric Acid	HCl	37	7647-01-0	SIGMA ALDRICH
Lead Iodide	PbI_2	99	10101-36-0	SIGMA ALDRICH
Methylammonium Chloride	MACl	99	539-51-1	Acros Organic
Methylammonium Iodide	MAI	98	14965-49-2	SIGMA ALDRICH
Titanium (IV) Isopropoxide	TTIP	97	546-68-9	SIGMA ALDRICH
Titanium(IV) Chloride	$TiCl_4$	99.9	7550-45-0	Acros Organic
Toluene	-	99	108-88-3	Merck
Zinc powder	-	-	9029-97-4	José M.Vaz Pereira

ETL Solution Preparation

Compact TTIP compact solution

- Add 180 µl of TTIP to 1.25 ml of absolute ethanol - solution 1;
- Add 18 µl of HCL to 1.25 ml of absolute ethanol - solution 2;
- Add solution 2 to solution 1, , while solution 1 stirs at ambient temperature;
- Stir for 15-20 minutes.

Compact $TiCl_4$ solution: Add 440 µl of ice-cooled $TiCl_4$ to 2 ml of ice-cooled DI water. Leave to stir for at least one hour at room temperature.

Mesoporous TiO_2 solution: Add 150 mg of TiO_2 paste to 1 ml of absolute ethanol. Leave to stir for 20 minutes at room temperature.

Perovskite Solution Preparation

MACl Perovskite solution

- Add amount of PbI_2 and MACl powders, according to the desired concentration to use (table B.2);
- Add corresponding solvents: pure DMF, pure DMSO, mix of DMF:DMSO, according to the desired solution;
- Seal container and leave to stir at 70° C for 24 hours.

MAI Perovskite solution

- Add amount of PbI_2 and MAI powders, according to the desired concentration to use (table B.3);
- Add corresponding solvents: pure DMF, pure DMSO, mix of DMF:DMSO, according to the desired solution;
- Seal container and leave to stir at 70° C for 24 hours.

HTL Solution Preparation

Aqueous CuSCN solution

- Add 15 mg CuSCN to 1 ml of aqueous ammonia;
- Stir for one hour at 50° C;
- Stir over night at room temperature.

Table B.2: Reagent molarity for the different MACL precursor solution used in this work - quantities for 1 ml solutions.

Desired concentration	**PbI_2 (mmol)**	**MACl(mmol)**
0.217M	0.217	0.217
0.434M	0.434	0.434
0.642M	0.642	0.642
0.868M	0.868	0.868
1.085M	1.085	1.085

Table B.3: Reagent molarity for the different MAI precursor solution used in this work - quantities for 1 ml solutions.

Desired concentration	**PbI_2 (mmol)**	**MAI(mmol)**
1 M	1	1
1.5 M	1.5	1.5

CuSCN Di-n-propyl sulfide solution

- Add 15 mg of CuSCN to 1 ml of di-n-propyl sulfide;
- Stir at room temperature for at least 48 hours.

Appendix C

Optical Analysis

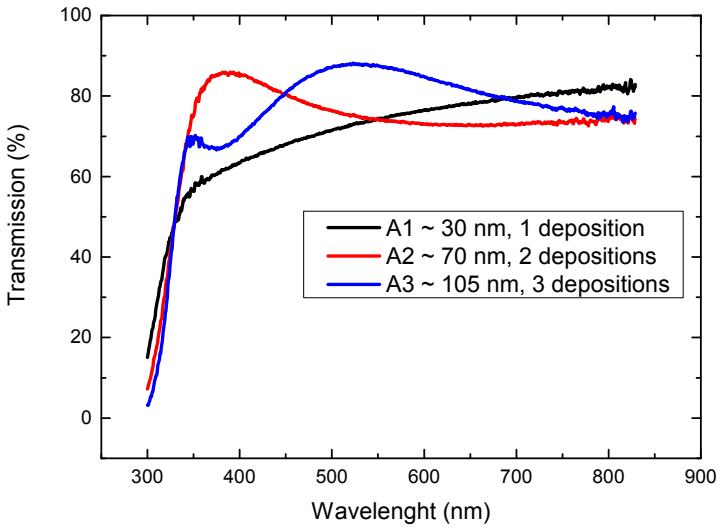

Figure C.1: Relation between number of depositions and thickness of c-TiO_2 layer; Thickness estimation done by fitting experimental curves with simulated ones using TMM method software.

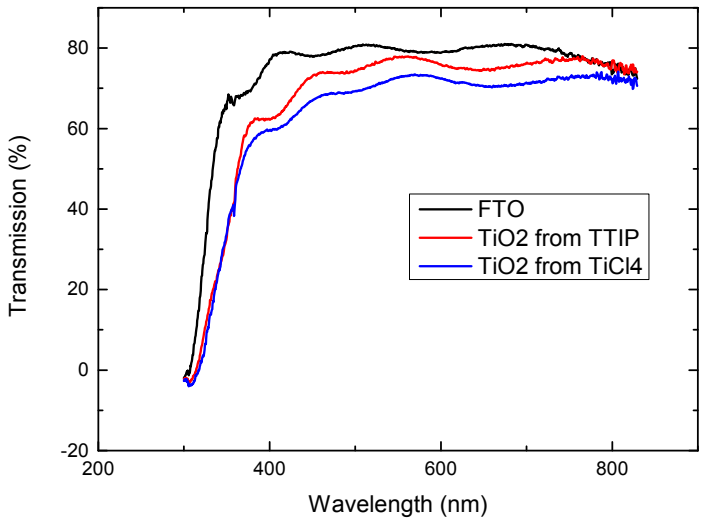

Figure C.2: Transmission of FTO coated glass, with the addition of either c-TiO_2 using TTIP solution or c-TiO_2 using $TiCl_4$ solution.

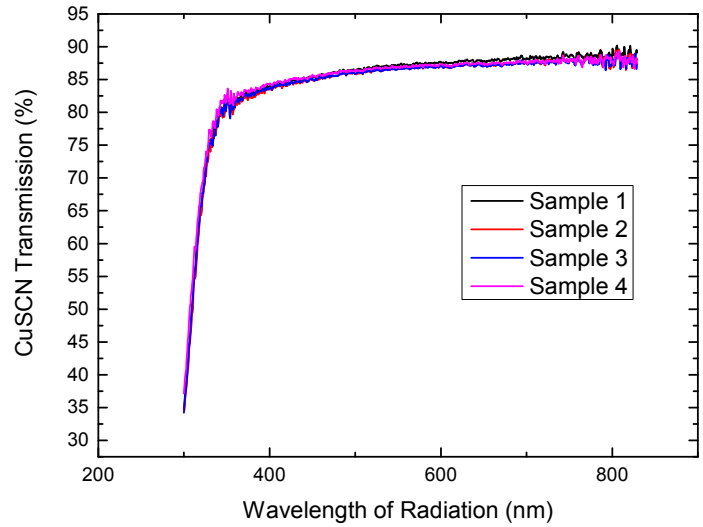

Figure C.3: Transmission of CuSCN layer deposited on glass of four different samples, using the same fabrication conditions, showing the reproducibility of the coating method.

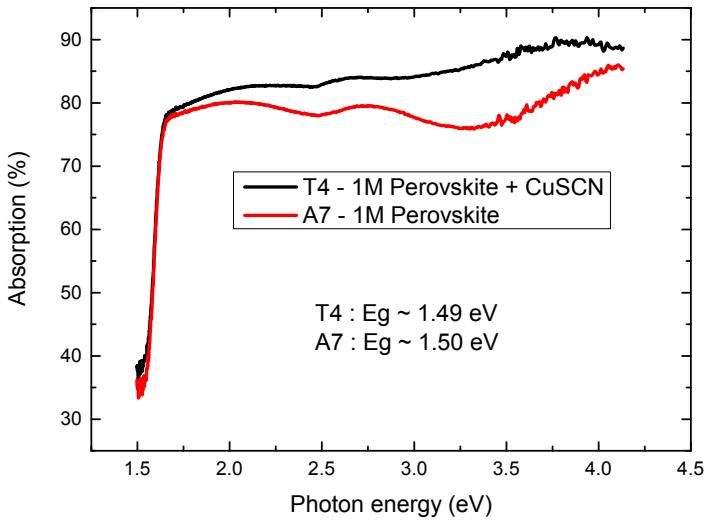

Figure C.4: Influence of CuSCN deposition on Absorbance spectra of Perovskite layer.